New insights into the FLS2 trafficking and signaling pathway revealing a role for late defense responses in *Arabidopsis* immunity

Inaugural-Dissertation

zur

Erlangung des Doktorgrades

der Mathematisch-Naturwissenschaftlichen Fakultät

der Universität zu Köln

vorgelegt von

Thomas Spallek

aus Germersheim

Köln, September 2011

Die vorliegende Arbeit wurde am Max-Planck-Institut für Pflanzenzüchtungsforschung in Köln in der Abteilung für Molekulare Phytopathologie (Direktor: Prof. Dr. P. Schulze-Lefert) angefertigt.

MAX-PLANCK-GESELLSCHAFT

Max Planck Institute for Plant Breeding Research

Berichterstatter: Prof. Dr. Paul Schulze-Lefert

Prof. Dr. Marcel Bucher

Dr. Matthieu Joosten

Prüfungsvorsitzender: Prof. Dr. Martin Hülskamp

Tag der Disputation: 10.11.2011

PUBLICATIONS

Spallek T, Robatzek S, Göhre V (2009)
How microbes utilize host ubiquitination.

Cellular Microbiology **11:** 1425-1434. Review.

Göhre V, **Spallek T,** Häweker H, Mersmann S, Mentzel T, Boller T, de Torres M, Mansfield JW, Robatzek S (2008)
Plant Pattern-Recognition Receptor FLS2 Is Directed for Degradation by the Bacterial Ubiquitin Ligase AvrPtoB.

Current Biology **18:** 1824-1832.

TABLE OF CONTENTS

ABBREVIATIONS

°C	degree Celsius
μ	micro
∅	diameter
α	anti
A. thaliana	*Arabidopsis thaliana*
A. tumefaciens	*Agrobacterium tumefaciens*
AA	amino acid
ABA	abscisic acid
ACO	1-aminocyclopropane-1-carboxylate oxidase
ADP	adenin diphosphate
AP	alkaline phosphatase
APS	ammonium persulfate
ARA	*Arabidopsis* Rab-like GTPase
Arabidopsis	*Arabidopsis thaliana*
ATP	adenosine triphosphate
BF	bright field
BSA	bovine serum albumin
Cam^R	chloramphenicol resistance
CBB	Coomassie Brilliant Blue
cDNA	complementary DNA
CFP	cyan fluorescent protein
cfu	colony forming units
Chr	chromosome
cm	centimeter
Col-0	Colambia-0
CTAB	Cetyltrimethylammonium bromide
ddH$_2$0	double-distilled water
DMSO	dimethyl sulfoxide
DNA	deoxyribonucleic acid
dNTP	deoxyribonucleotide triphosphate
dpi	days post infection
DTT	dithiothreitol
E. coli	*Escherichia coli*
e.g.	exempli gratia
EDS	ENHANCED DISEASE SUSCEPTIBILITY
EDTA	ethylenediaminetetraacetic acid
EE	early endosomes
engl.	englisch
ER	endoplasmatic reticulum
ESCRT	Endosomal Sorting Complex Required for Transport
et al.	et alii
F$_1$	first filial generation after crossing two different parental lines
F$_2$	second filial generation after crossing two different parental lines

F$_3$	third filial generation after crossing two different parental lines
FC	fold change
fli	flg22-Insensitive
FLS2	FLAGELLIN SENSITIVE 2
FLS2CD	cytosolic domain of FLS2
FW	fresh weight
g	gram
Gent^R	Gentamycin resistance
GFP	green fluorescent protein
GST	Glutathione S transferase
GTP	guanosine triphosphate
GW	Gateway
Hpa	*Hyaloperonospora arabidopsidis*
hpi	hours post infection
IPTG	Isopropyl β-D-1-thiogalactopyranoside
K	lysine
kb	kilo base pair
kDa	kilo Dalton
l	Liter
Le	*Lycopersicon esculentum*
L*er*	Landsberg *erecta*
m	milli
m	meter
M	molar
M$_5$	fifth filial generation after mutagenesis
mA	Milli Ampere
Mb	mega base pairs
MEKK	MAP KINASE KINASE KINASE
min	minutes
MKK	MAP KINASE KINASE
MS	Murashige and Skoog
ms	milli seconds
MS/MS	tandem mass spectrometry
MVB	Multivesicular body
NaCl	sodium chloride
N. benthamiana	*Nicotiana benthamiana*
Nb	*Nicotiana benthamiana*
nm	nano meter
NTA	mitrilotriacetic acid
N-Terminus	amino terminus
o/n	over night
OD$_{600}$	optical density measured at 600 nm
Os	*Oryza sativa*
p	promotor fragment
P	probability value
p35S	promoter of Cauliflower mosaic virus promoter 35S

PAGE	polyacrylamide gel electrophoresis
PCR	polymerase chain reaction
pERK	phosphorylated Extracellular signal- Regulated Kinase
pH	negative logarithm of proton concentration
PM	plasma membrane
PMSF	phenylmethanesulfonyl fluoride
PRR	Pattern Recognition Receptor
Pto DC3000	*Pseudomonas syringe* pv. *syringae* DC3000
pv.	pathovar
PVDF	polyvinylidene fluoride
qPCR	quantitative PCR
R	arginine
Ref	reference
Re-seq	re-sequencing
RFP	red fluorescent protein
Rif^R	Rifampicilin resistance
RLK	Receptor Like Kinase
RLP	Receptor Like Protein
RNA	ribonucleic acid
RT-PCR	real-time polymerase chain reaction
SD	standard deviation
SDM	site directed mutagenesis
SDS	sodium dodecyl sulfate
sec	seconds
SNP	short nucleotide polymorphisms
SYP	SYNTAXIN OF PLANTS
T_1	first filial generation after transformation
T_2	second filial generation after transformation
TBE	Tris-Borate-EDTA
TBS-t	Tris-Buffered Saline and tween 20
TEMED	N,N,N',N'-Tetramethylethylenediamine
TGN	Trans-Golgi Network
U	Unit
Ub	Ubiquitin
UTR	untranslated region
UV	ultra violet
V	Volt
v/v	volume of solute per volume of solvent
vs.	versus
w/v	weight of solute per volume of solvent
Ws	Wassilewskija
wt	wild-type
x	fold
YFP	yellow fluorescent protein
λ	lambda
χ	chi

SUMMARY

Pathogen-associated molecular pattern (PAMP) triggered immunity (PTI) enables plants to efficiently defend themselves against most pathogens. PTI is initiated by plasma membrane pattern recognition receptors like Flagellin Sensitive 2 (FLS2), which detects flg22 peptides derived from bacterial flagellin. Flg22 triggers cellular trafficking of FLS2 to endosomal compartments and several defense responses, including early responses such as closure of stomatal apertures or gene activation and late responses such as seedling growth arrest or callose deposition.

Cellular trafficking is often regulated by ubiquitination. In order to find factors modulating FLS2 endosomal trafficking, we used the *Pseudomonas syringe* pv. *tomato (Pto)* DC3000 effector AvrPtoB to identify residues in FLS2, which are ubiquitinated by AvrPtoB. Using tandem mass-spectrometry we identified one ubiquitination site in the juxtamembrane domain of FLS2. FLS2 mutated in all juxtamembrane located lysines showed reduced ubiquitination *in vitro*, enhanced resistance to *Pto* DC3000 and increased FLS2 endosome numbers upon flg22 treatment. Ubiquitinated plasma membrane proteins are targeted to late endosomal compartments by the Endosomal Sorting Complex Required for Transport (ESCRT) in yeast and animals. Using confocal microscopy we observed flg22-dependent co-localization of FLS2 with ESCRT-1 positive vesicles. Furthermore, ESCRT-1 mutants *vps28-2* and *vps37-1* showed reduced flg22-triggered defense gene activation, loss of flg22-dependent stomatal closure and decreased numbers of FLS2 endosomes. Both mutants showed higher susceptibility to biotrophic pathogens, indicating a role of ESCRT-1 components in plant immunity.

A second approach aimed to genetically dissect flg22 responses by analyzing a previously isolated *flagellin insensitive 1* (*fli1*) mutant. *Fli1* mutants were similar susceptible to *Pto* DC3000 than *fls2-17* receptor mutants. Increased susceptibility of *fli1* to *Pto* DC3000 correlated with higher expression of sugar starvation responsive genes during infections and reduced late flg22 responses. Early flg22 responses and transcriptional profiles three hours post infection resembled wild-type plants, suggesting a positive role of late PAMP responses in plant immunity. Genetic analysis showed that *fli1* is recessive inherited and co-segregated with markers on the upper arm of chromosome 5. Sequence differences in *fli1* predicted by whole genome sequence analysis were, however, shared with L*er* wild-type plants, leaving the designation of *fli1* to one gene open.

In conclusion, these data provide good evidences for a role of late FLS2 endosomal trafficking and late flg22-repsonses as critical components of plant immunity against *Pto* DC3000.

ZUSAMMENFASSUNG

Die Erkennung von Pathogenen wird über diverse Wirtsrezeptoren gewährleistet. Diese so genannten Mustererkennungsrezeptoren (engl. Pattern Recognition Receptors, PRR) erkennen pathogen-assoziierte molekulare Muster (engl. Pathogen Associated Molecular Pattern, PAMP). In *Arabidopsis thaliana* wird flg22, ein konservierter Bestandteil des bakteriellen Flagellums, von FLS2 (Flagellin Sensitive 2) Rezeptoren erkannt. Flg22 Perzeption führt zur Endozytose von FLS2 und zur Initiierung von früheren und späten PAMP Antworten. Frühe PAMP Antworten sind zum Beispiel die transkriptionelle Aktivierung von Genen und das Schließen von Stomataöffnungen. Späte Antworten dagegen beinhalten Kalloseablagerungen und die Reduktion des Keimlingswachstums.

Endozytose und endosomaler Transport wird oft über Ubiquitinierung reguliert. FLS2 wird von endogenen Ubiquitinligasen und AvrPtoB, einem Effektorportein aus *Pseudomonas syringae* pv. *tomato* (*Pto*) DC3000, ubiquitiniert. Unsere Experimente zeigen, dass FLS2 an mindestens zwei unterschiedlichen Positionen von AvrPtoB *in vitro* ubiquitiniert wurde. Eine Position konnte dabei mittels Massenspektrometrie einem Lysin in der Juxtamembranregion von FLS2 zugeordnet werden. FLS2 Varianten, in denen mögliche Ubiquitinierungsstellen mutiert wurden, zeigten eine reduzierte Ubiquitinierung durch AvrPtoB *in vitro*, eine erhöhte Resistenz gegenüber *Pto* DC3000, sowie eine erhöhte Anzahl von FLS2 Endosomen im Vergleich zu untersuchten Wildtypkonstrukten.

Studien in Hefe und tierischen Zellen zeigen, dass ubiquitinierte Plasmamembranproteine über den endosomalen Sortierung Komplex für Transport (ESCRT) zu spätendosomalen Kompartimenten transportiert werden. Mittels konfokaler Mikroskopie beobachteten wir, dass in transgenen *Arabidopsis* Pflanzen, FLS2 Endosomen mit ESCRT-1 Vesikeln partiell kolokalisieren. Darüberhinaus zeigten ESCRT-1 Mutanten *vps28-2* und *vps37-1* reduzierte flg22 induzierte Genaktivierung, Verlust von flg22 vermittelter Schließung der Stomataöffnungen, und eine geringere Anzahl an FLS2 Endosomen als Wildtyppflanzen. Beide Mutanten zeigten zudem eine erhöhte Anfälligkeit gegenüber biotropher Pathogene, was auf eine Rolle von ESCRT-1 Proteinen in der Pflanzenimmunität hindeutet.

In einer zweiten Studie, wurde die Rolle später flg22 Antworten genetisch untersucht. Dabei wurde eine zuvor isolierte *flagellin insensitive 1* (*fli1*) Mutante genauer analysiert. *Fli1* Mutanten zeigten eine ähnliche erhöhte Anfälligkeit gegenüber *Pto* DC3000 wie *fls2-17* Rezeptormutanten. Transkriptionsanalysen zeigten, dass *fli1* Mutanten besonders in späten Infektionsphasen deutlich anders als Wildtyppflanzen reagieren. So wurde einer erhöhten Expression von Gene gefunden, denen eine Rolle im Zuckermangel zugeschrieben wird. Auch andere späte Immunantworten waren in *fli1* Mutanten deutlich verändert. Es wurden deutlich weniger flg22 induzierte Kalloseablagerungen und eine geringere flg22 Sensitivität in Keimlingswachstumsexperimenten gefunden. Frühe transkriptionelle Antworten dagegen glichen denen in Wildtyppflanzen. Auch in frühen PAMP Antworten unterschieden sich *fli1* Mutanten nicht signifikant von Wildtyppflanzen. Zusammenfassend deuten unsere Daten daraufhin, dass späte PAMP Antworten eine wichtige Rolle

in der pflanzlichen Immunität spielen. Genetische Analysen zeigten, dass *fli1* rezessiv vererbt wird und mit Markern auf dem oberen Arm von Chromosom 5 kosegregiert. Sequenzunterschiede in *fli1*, ermittelt durch Genomsequenzierung, wurden jedoch auch in Wildtyppflanzen gefunden, so dass *fli1* keinem Gen zu geordnet werden konnte.

1. INTRODUCTION

1.1. THE PLANT IMMUNE SYSTEM

The plant immune system is based on two layers of active defense responses (Jones and Dangl, 2006). The first layer senses pathogen-associated molecular patterns (PAMPs, also referred to as MAMPs for microbe-associated molecular patterns). PAMPs are conserved across large classes of microbial species, *e.g.* bacterial flagellin or fungal chitin, and detected by cognate pattern recognition receptors (PRRs). The second layer of plant immunity employs recognition of Avirulence gene products from one particular pathogen strain. In this case, recognition occurs often intracellular, when pathogen-derived Avirulence gene products or effectors, are injected into host cells. Effector proteins interact either directly or indirectly with their corresponding plant resistance proteins. Following pathogen recognition defense signaling is initiated, leading to several defense responses and subcellular re-organization (Boller and Felix, 2009; Frey and Robatzek, 2009).

1.2. DEFENSE SIGNALING

Plant PRRs can be grouped based on their modular structure into two major classes: Receptor-like kinases (RLKs) include rice Xa21 (Song et al., 1995), FLAGELLIN SENSITIVE 2 (FLS2) (Gómez-Gómez and Boller, 2000), ELONGATION FACTOR-TU RECEPTOR (EFR) (Zipfel et al., 2006), or CHITIN ELICITOR RECEPTOR KINASE1 (CERK1) (Miya et al., 2007). RLKs are built-up by a ligand binding extracellular domain, a single transmembrane domain and an intracellular kinase. Transmembrane domains of RLKs are flanked by regulatory juxtamembrane regions, which can modulate protein-protein interactions and kinase activity (Chen et al., 2010c; Chen et al., 2010b).

The second class of PRRs lacks an intracellular kinase domain: Receptor-like proteins (RLPs) include Chitin Elicitor-Binding Protein (CEBiP) or tomato LeEIX2 (Kaku et al., 2006). LeEIX2 recognizes fungal ETHYLENE-INDUCED-XYLANASE (EIX) (Ron and Avni, 2004) and shows high homology to tomato Cf disease resistance proteins (Ron and Avni, 2004). Cf proteins confer resistance to certain

Cladosporium fulvum strains by detecting their cognate Avr protein (Stergiopoulos and de Wit, 2009).

Arabidopsis FLS2 is a major model to study PRR function (Boller and Felix, 2009). FLS2 directly binds a conserved 22 amino acid peptide (flg22) of bacterial flagellin (Gómez-Gómez and Boller, 2000). *FLS2* is wide-spread in plant genomes with orthologues found in tomato, *Nicotiana benthamiana* and rice (Hann and Rathjen, 2007; Robatzek et al., 2007; Takai et al., 2008). In contrast to FLS2, EFR is restricted to *Brassicaceae* and binds elf18, a conserved peptide derived from bacterial elongation factor Tu (Kunze et al., 2004; Zipfel et al., 2006).

FLS2 and EFR require the BRI1-ASSOCIATED-KINASE1 (BAK1) for efficient activation of downstream responses (Chinchilla et al., 2007). BAK1 belongs to the family of SOMATIC-EMBRYOGENESIS RECEPTOR-LIKE KINASES (SERK1-5) and interacts with brassinosteroid receptor, BRASSINOSTEROID INSENSITIVE, BRI1 (Li et al., 2002). SERK1-5 share partially redundant functions in brassinosteroid signaling (Albrecht et al., 2008) and were recently also identified in active PRR complexes (Roux et al., 2011). FLS2 and EFR associate with BAK1 (SERK3) seconds after ligand binding (Chinchilla et al., 2007; Schulze et al., 2010). The resulting protein complex triggers trans-phosphorylation events, which are essential for proper PAMP signaling (Chinchilla et al., 2007; Schulze et al., 2010; Schwessinger et al., 2011). Following the formation of this receptor complex cytosolic BOTRYTIS-INDUCED KINASE 1 (BIK1) dissociates from FLS2 to activate downstream responses (Zhang et al., 2010). Within in seconds or minutes after initiation of PRR signaling several cellular responses can be measured, including ion fluxes across the plasma membrane (Jeworutzki et al., 2010), generation of reactive oxygen species (ROS) (Gómez-Gómez and Boller, 2000), activation of mitogen-activated protein kinases (MAPKs) (Asai et al., 2002) and activation of calcium-dependent protein kinases (CDPKs) (Boudsocq et al., 2010). These responses are followed by transcriptional reprogramming of more than 1000 flg22 and elf18 responsive genes (Zipfel et al., 2004).

This first wave of detected immune responses is collectively referred to as early PAMP responses (Boller and Felix, 2009). By contrast, late responses appear hours or days after PAMP stimulus and include callose deposition, and inhibition of seedling growth (Boller and Felix, 2009). Callose synthases PMR4 (POWDERY MILDEW RESISTANT 4, also referred to as GLUCAN SYNTHASE-LIKE 5, GSL5) is the major source of flg22-induced callose in *Arabidopsis* (Clay et al., 2009). Analyses of *pmr4-1* loss of function mutants are hampered by elevated salicylic acid (SA), resulting in enhanced resistance to biotrophic pathogens (Nishimura et al., 2003). The relevance of callose deposition in

restricting bacterial growth is under debate (Boller and Felix, 2009) and alternative roles of callose in detoxification of antimicrobial compounds are discussed (Luna et al., 2011). If PAMP perception continues over days, *Arabidopsis* seedlings reduce growth and display severe stress symptoms (Boller and Felix, 2009). PAMP-induced hormones like ethylene, jasmonic acid or SA account only marginally for flg22-induced growth inhibition (Tsuda et al., 2009). Alternatively, down-regulation of auxin signaling by flg22 induced micro RNAs and gibberellin signaling via DELLA protein is linked to flg22-induced growth phenotypes (Navarro et al., 2006; Navarro et al., 2008). To date, most identified components of PTI signaling affect early PAMP responses, whereas genetic control of late response and PAMP-triggered immunity remains largely unknown.

The contribution of one single PRR to plant immunity is often difficult to estimate. *Fls2* mutants for example are only immuno-compromised in the pre-invasive infection phase, when pathogenic *Pseudomonas syringae* pv. *tomato* DC3000 (*Pto* DC3000) are spray-inoculated, but not during the post-invasive phase, when bacteria are infiltrated into the leaf tissue (Zipfel et al., 2004). Flg22-induced stomatal closure is discussed to account for FLS2's predominate role in pre-invasive immunity (Zhang and Zhou, 2010). In contrast to eukaryotic plant pathogens, bacteria are unable to actively penetrate the plant epidermis. To access the nutrient-rich apoplastic space, they rely on natural openings like stomata or wounds. Flg22 induces stomatal closure within one hour of PAMP perception (Melotto et al., 2006) and requires PAMP-induced ROS signaling via Respiratory burst oxidase homolog D (RbohD)*,* (Mersmann et al., 2010), MAPK signaling (Gudesblat et al., 2009) and several components which are shared with abscisic acid (ABA) - mediated stomatal closure (Melotto et al., 2006). Plant pathogens in turn evolved strategies to re-open stomata, for example with the help of the jasmonate mimic coronatine (Melotto et al., 2006).

Besides the phytotoxin coronatine, several of the 28 type-three secreted effectors encoded by *Pto* DC3000 genome target PTI components (Cunnac et al., 2009): AvrPto and HopF2 interfere with PRR complex formation (Shan et al., 2008; Xiang et al., 2011), whereas AvrPtoB directly interacts with FLS2 (Göhre et al., 2008). AvrPtoB structurally mimics eukaryotic ubiquitin ligases (Rosebrock et al., 2007). Ubiquitin ligases covalently attach ubiquitin moieties to lysine residues of substrate proteins, a common post-translational protein modification in eukaryotes. AvrPtoB ubiquitinates several plant kinases including FLS2 and CERK1 and promotes thereby their degradation (Rosebrock et al., 2007; Göhre et al., 2008; Gimenez-Ibanez et al., 2009). FLS2 ubiquitination was recently also shown by two

endogenous PLANT U-BOX PROTEINS (PUBs), PUB12 and PUB13 (Lu et al., 2011). Even though enhanced FLS2 turn-over by ubiquitination through PUB12, 13 or AvrPtoB appears analogous and requires flg22 activation *in vivo*, both interactions differ in their mode of action. Whereas PUB12 and PUB13 are recruited by BAK1, AvrPtoB binds directly to FLS2 to facilitate FLS2 ubiquitination and degradation.

In conclusion, the progression of an infection is balanced between efficient activation of host immunity and deactivation by invading pathogens. This explains, why flg22 pre-treatment renders *Arabidopsis* plants more resistant to *Pto* DC3000 even in the post-invasive infection phase, a phenomenon termed flg22-induced resistance, (Zipfel et al., 2004). It also explains, why PTI component *FLS2* is the major quantitative trait locus (QTL) for *Arabidopsis* non-host resistance to *Pseudomonas syringae* pv. *phaseolicola* 1448A (Forsyth et al., 2010). Vice versa, adapted pathogens partially loss their virulence, when exposed to PRRs of non-host plants as shown by expression of *Arabidopsis* EFR in *Solanaceas* or transgenic citrus expressing rice *Xa21* (Mendes et al., 2009; Lacombe et al., 2010)*.

Table 1 summarizes key components in PTI signaling on the basis of FLS2-flg22 pathway, including steps which are targeted by *Pto* DC3000 effectors.

Table 1   Illustration of key steps in the flg22-FLS2 signaling pathway

| | sec | < 5 min | < 15 min | < 1hour | 2 hours | 12 hours | > 1day |
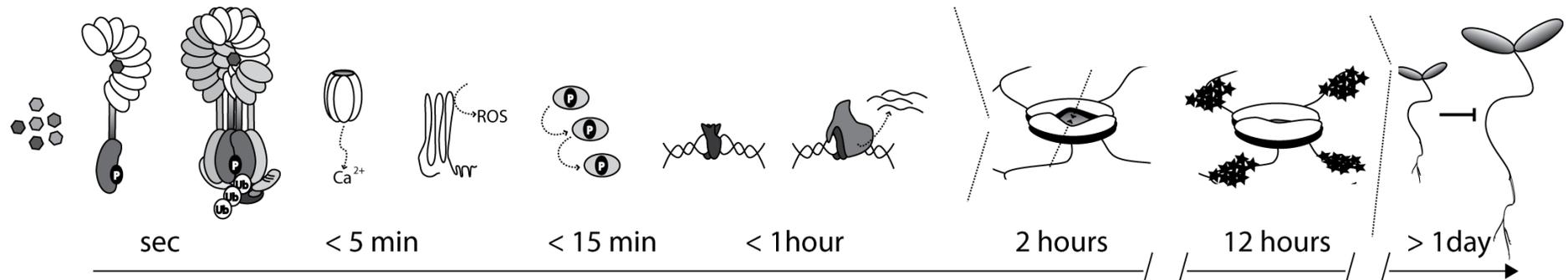
PAMP	PRR	Complex	Ca²⁺	NADPH oxidase	MAPK[b] / CDPK	Transcription Factors[c]	Induced genes	Stomatal closure	Callose deposition	Seedling growth arrest
flg22	FLS2	BAK1 SERK1,2,4 BIK1, PUB12,13	?[a]	RbohD	MEKK1 MKK1,2 MKK4,5 MPK3,4,6 CDPK4,5,6,11	Several WRKYs	> 1000	RbohD MPK3 COI1	PMR4	miRNA DELLA
Pto DC3000 effectors targeting PTI steps:										
	AvrPtoB	AvrPto HopF2			HopAI1			Coronatine		

[a] Channels conducting flg22-induced calcium (Ca²⁺) influxes are currently not known, but inhibitor studies suggest a role ionotropic glutamate receptor -like channels (Kwaaitaal et al., 2011).

[b] Two MAPK cascades are activated by flg22 (Rodriguez et al., 2010). HopAI1 inactivates MAPK3 and MAPK6 by removing phosphor groups (P) from activated MAPKs (Zhang et al., 2007a).

[c] WRKY transcriptions play a major role in regulating transcriptional defense responses (Rushton et al., 2010).

1.3. CELLULAR DEFENSE

Plant immunity involves the interplay of different subcellular compartments and vesicle transport pathways (Frey and Robatzek, 2009; Wang and Dong, 2011). PRRs for example need to be secreted from the endoplasmic reticulum (ER) via golgi compartments to the plasma membrane to perceive PAMPs. The importance of secretory and ER quality control pathway in PRR function was discovered in forward genetic screens for mutants impaired in elf18 signaling (Nekrasov et al., 2009; Saijo et al., 2009). Interestingly, identified mutants were only slightly or not at all affected in flg22 and chitin responses, illustrating specific requirements for ER quality control proteins in different PRR maturation processes (Nekrasov et al., 2009; Saijo et al., 2009). EFR protein accumulation and functions are thereby differently compromised in ER quality control mutants. *Radial swelling 3 (rsw3, glucosidase 2)* mutants show for example only slight reduction in elf18 binding and maintain wildtype-like early PAMP responses and callose depositions upon elf18 treatment, but fail to maintain wildtype-like defense gene expression and elf18-induced immunity during infections with *Pto* DC3000 (Lu et al., 2009).

Post-golgi vesicle trafficking plays a major role in plant defense against non-host pathogens. Resistance of *Arabidopsis thaliana* against barley powdery mildew fungus *Blumeria gramminins hordie* (*Bgh)* is mediated by a protein complex consisting of the syntaxin PENETRATION 1 (PEN1, AtSYP121), SNAP33 (SOLUBLE N-ETHYLMALEIMIDE-SENSITIVE FACTOR ADAPTOR PROTEIN 33) and VESICLE-ASSOCIATED MEMBRANE PROTEIN (VAMP) 721/722 (Collins et al., 2003; Kwon et al., 2008). The PEN1-SNAP33-VAMP721/722 complex accumulates at fungal penetration sites and mediates exocytosis of cell-wall enhancing compounds (Kwon et al., 2008). SYP132 of *N. benthamiana* is essential for secretion the of PATHOGEN-RELATED protein 1 (PR1) and required for resistance to non-host *Pto* DC3000 (Heese et al., 2001). Alternatively to golgi-derived vesicles, PEN2 and PEN3 dependent secretion of anti-microbial compounds employs trafficking of peroxisomes to fungal infection sites (Lipka et al., 2005; Stein et al., 2006; Bednarek et al., 2009).

The trans-golgi network (TGN) serves not only as secretory compartment, but also partially merges with plasma membrane derived early endocytic vesicles in plants (Richter et al., 2009; Viotti et al., 2010). The TGN – early endosome compartment is highly dynamic and sorts vesicles back to the plasma membrane or to late endosomes (Viotti et al., 2010). Endomembrane systems are classified by associated proteins like Rab GTPase, which regulate vesicle formation, mobility and fusion (Stenmark and Olkkonen, 2001). Whereas Rab5 related proteins define early endosomes in animals, it also associated with late endosomes in plants or yeasts (Robinson et al., 2008; Ebine et al., 2011). Early endosome are the first endomembrane compartment of internalized plasma membrane proteins. Endocytosis of several plant plasma membrane proteins was shown, including auxin carrier proteins, metal transporters, BRI1, but also for PRRs like FLS2 and LeEIX2 (Russinova et al., 2004; Dhonukshe et al., 2007; Kasai et al., 2010; Barberon et al., 2011).

Endocytosed plasma membrane proteins are often marked by ubiquitination (Sorkin and von Zastrow, 2009). Different types of ubiquitination have been reported. Attachment of one single ubiquitin (Ub) to lysines of substrate proteins is referred to as mono-ubiquitination. Mono-ubiquitination and poly-ubiquitin chains linked via lysine 63 of ubiquitin (Ub^{K63}) are often associated with endocytic trafficking and protein-protein interactions. By contrast, Ub^{K48}-linked poly-ubiquitination leads mainly to proteasomal degradation of substrate proteins (Mukhopadhyay and Riezman, 2007). *In planta* ubiquitination of two metal transporters was recently described (Kasai et al., 2010; Barberon et al., 2011). Controversially, ubiquitination is essential for internalization of IRON-REGULATED TRANSPORTER 1 (IRT1)(Barberon et al., 2011), but not for boron transporter REQUIRES HIGH BORON 1 (BOR1)(Kasai et al., 2010). Instead BOR1 ubiquitination is required for late endosomal trafficking to lytic vacuoles. Although FLS2 is ubiquitinated in an flg22-dependent manner (Lu et al., 2011), the implementation of ubiquitination in FLS2 endocytosis remains elusive. Inhibitor studies suggest that ubiquitination is required for receptor internalization (Robatzek et al., 2006). In addition, a $FLS2^{\Delta PEST}$ variant is incapable to undergo endocytosis, but maintains a wild type-like ROS burst after flg22 treatment (Salomon and Robatzek, 2006). PEST-sequences act as ubiquitination and phosphorylation signals in yeast and plants (Rogers et al., 1986; Camborde et al., 2010). Notably, $FLS2^{\Delta PEST}$ mutant variants do not escape ubiquitination by PUB12, 13 and AvrPtoB *in vitro,* which could point at an ubiquitination independent role of the FLS2 PEST domain in regulating endocytosis (Göhre et al., 2008; Lu et al., 2011).

After internalization BOR1 endosomes mature to late endosomes and co-localize with ARA6 and ARA7 (Takano et al., 2005; Ebine et al., 2011). Late endosomes are characterized by the presence of small internal vesicles, and are therefore also referred to as multivesicular bodies (MVBs) (Robinson et al., 2008). MVBs terminate in lytic plant vacuoles in plants and yeasts or fuse with lysosomes in animals (Stenmark and Olkkonen, 2001; Richter et al., 2009).
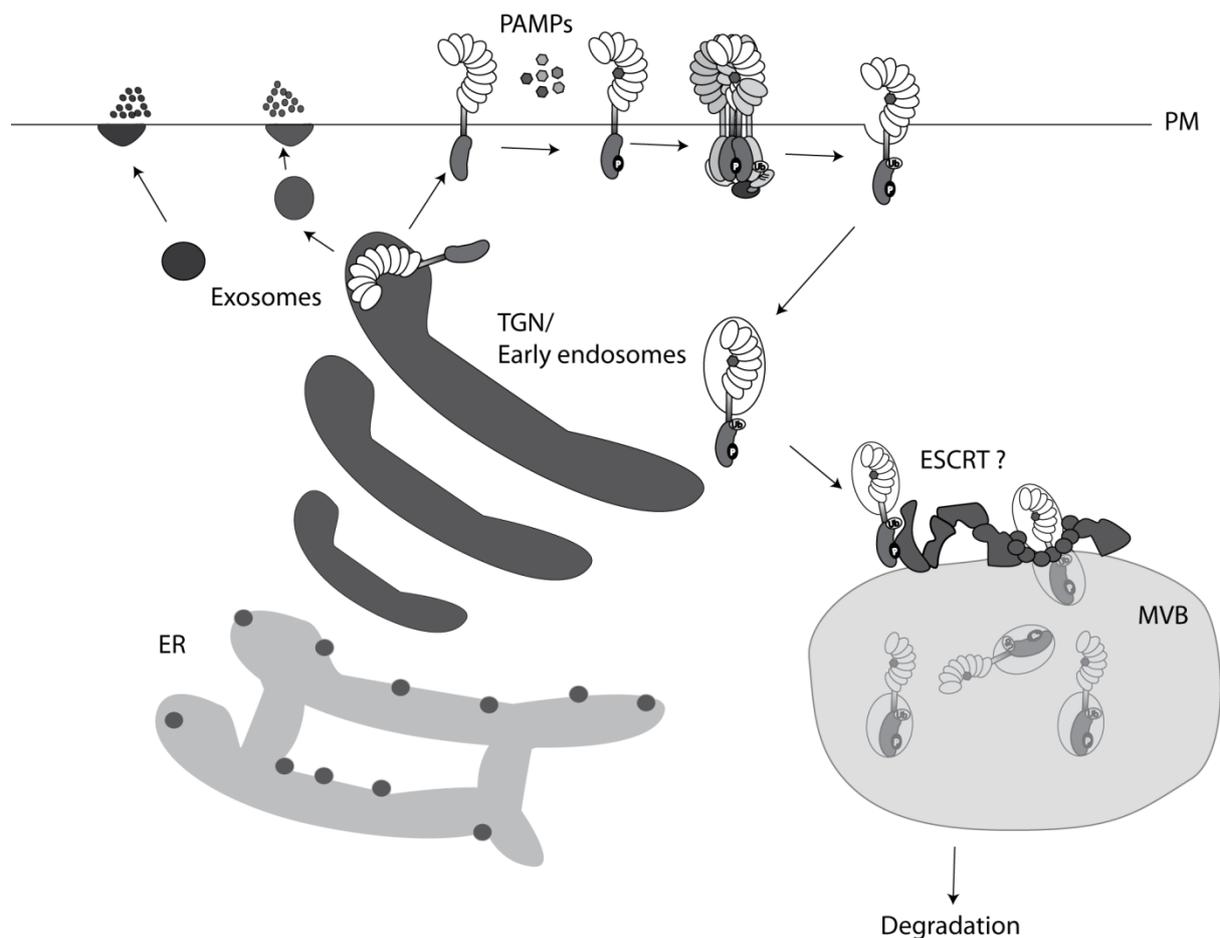
Figure 1 **Vesicle trafficking in plant immunity.** PRR transport form the ER via the TGN to the plasma membrane (PM) is required for PRR function. PAMPs mediate PRR endocytosis from PM to TGN - early endosomal compartments, followed by maturation to late endosomes, MVBs, and receptor degradation. TGN dirved vesicles are recruited to fungal penetration sites in order to release cell wall enhancing compounds. Anti-microbial defense products are alternatively exocytosed from TGN-indepenent compartments.

The presence of the Endosomal Complex Required for Transport (ESCRT) is a hallmark of MVBs. ESCRT proteins are directly involved in MVB biogenesis by mediating vesicle invagination and cargo recognition (Hurley and Hanson, 2010). The ESCRT machinery consists of three sub-complexes,

ESCRT-1-3, which are conserved in all eukaryotes (Figure 2) (Field and Dacks, 2009). Whereas ESCRT-1 initiates cargo recruitment, ESCRT-2 and ESCRT-3 are mainly involved in membrane scission (Hurley and Hanson, 2010). ESCRT-1 is composed of three different proteins: VACULAR PROTEIN SORTING 23 (VPS23) mediates ubiquitin binding, VPS28 bridges ESCRT complex 1 to complex 2 and VPS37 interacts with acidic membrane lipids (Hurley and Hanson, 2010). *Arabidopsis* carries at least two *VPS23* homologous (*ELC*, and *ELC-like*), two copies of *VPS28* (*VPS28-1* and *VPS28-2*) and two copies of *VPS37* (*VPS37-1* and *VPS37-2*) (Spitzer et al., 2006). ESCRT-3 accessory proteins CHARGED MULTIVESICULAR BODY PROTEIN1 (CHMP1) and CHMP2 were previously reported to target auxin carriers PIN-FORMED 1 (PIN1), PIN2 and AUXIN RESISTANT 1 (AUX1) to MVBs and to be essential for embryo and seedling development (Spitzer et al., 2009). It is currently not known, if ESCRT proteins also participate in PRR trafficking.
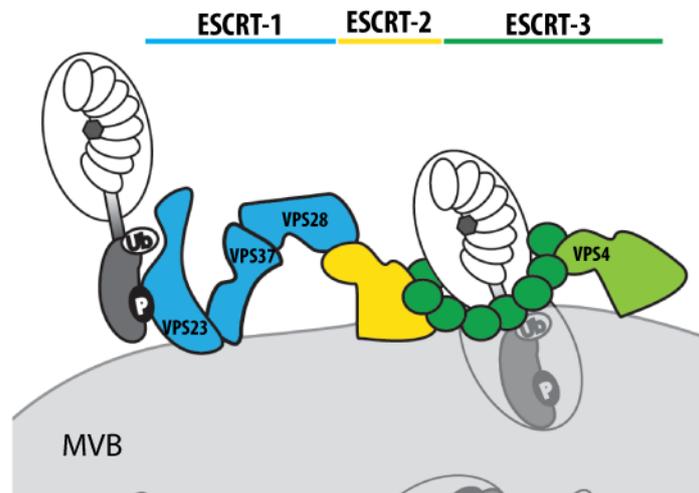
Figure 2   The ESCRT machinery consists of three major sub-complexes. ESCRT complex 1 (blue), 2 (yellow) and 3 (green) constitute together the ESCRT machinery, which is essential for MVB biogenesis. ESCRT-1 consists of VPS23 (ELC in *Arabidopsis*), VPS37 and VPS28 and recruits early endosomes via interaction with ubiquitinated cargos to MVBs. Vesicle fusion is mediated by ESCRT-2 and ESCRT-3. VPS4 disassembles ESCRT complexes after endosomal sorting.

The complexity of endocytic pathways and its integration in different signaling networks known from animals (Sorkin and von Zastrow, 2009) is likely to find its equivalent in plant cells. Many key components along endocytic trafficking pathways are conserved between animals and plants, others seem to be plant specific (Robinson et al., 2008). Although several plant receptors are endocytosed, a detailed understanding of their cellular routes and possible connections to signaling is still pending and focus of current and future research (Frey and Robatzek, 2009; Hicks and Raikhel, 2010).

1.4. AIM OF MY THESIS

PAMP-triggered immunity comprises plasma membrane-derived signaling, endocytic trafficking and a series of cellular immune responses. To which extent these cell responses are linked is not well understood. My work aims to dissect spatio-temporal flg22 signaling and to contribute new insights to the two following questions:

1. What controls FLS2 endocytic trafficking?

2. Which genes regulate temporal flg22 responses?

To address the first question, conserved features of endocytosis known from animals were exploited: Receptor ubiquitination and the Endosomal Sorting Complex Required for Transport (ESCRT) of ubiquitinated cargos. The second question is addressed by analysis of a late PAMP response-defective mutant, which was previously identified in a forward genetic screen for flagellin insensitivity (Salomon, 2009).

2. MATERIALS AND METHODS

2.1. MATERIALS

2.1.1. Plant material and growth conditions

Arabidopsis thaliana plants used in this study are listed in Table 2. Unless otherwise indicated, plants were grown on soil (Arabidopsis mix, John Ines Centre, Norwich) or sterile on Murashige and Skoog medium (recipe in Table 6) under 10 hours or 16 hours of light at 20 - 22°C and 65 % humidity. Seeds were stratified in dark at 4°C for two days in 0.1 % (w/v) agarose or directly on agar plates. *Nicotiana benthamiana* plants were grown under 16 hours of light at approximately 24°C with a relative humidity of 45 - 65 %.

Table 2   **Description of plant material presented in this study.**

Lines [a]	Accession	Description	Reference
Col-0	Col-0	wild-type (wt) reference line	J. Dangl [b]
eds1	L*er*	*eds1-2* loss-of-function mutant	(Aarts et al., 1998)
fli1	L*er*	gamma-irradiation mutant	(Salomon, 2009)
fli2	L*er*	gamma-irradiation mutant	(Salomon, 2009)
fli3	L*er*	gamma-irradiation mutant	(Salomon, 2009)
fli4	L*er*	gamma-irradiation mutant	(Salomon, 2009)
fli5	L*er*	gamma-irradiation mutant	(Salomon, 2009)
fli6	L*er*	gamma-irradiation mutant	(Salomon, 2009)
fls2	Col-0	homozygous SAIL_691C4 T-DNA insertion line for *FLS2*	(Zipfel et al., 2004)
fls2 FLS2-GFP (*fls2 pFLS2::FLS2:GFP*)	Col-0	*fls2* plant expressing *FLS2::GFP* driven by 1 kb of native promoter	present study
FLS2-GFP$^{3K->R}$ (*fls2 pFLS2:: FLS2$^{KKK854, 857, 861RRR}$:GFP*)	Col-0	*fls2* plant expressing *FLS2$^{KKK854, 857, 861RRR}$:GFP* driven by 1 kb of native promoter	present study
fls2-17	L*er*	*fls2^{G1064R}* substitution mutant	(Gómez-Gómez and Boller, 2000)
L*er*	L*er*	wild-type reference line	NASC [c]
pFLS2::FLS2:GFP	Col-0	Col-0 plant expressing *FLS2::GFP* driven by 1 kb of native promoter	(Robatzek et al., 2006)
FLS2-GFP RFP-VPS28-2 (*pFLS2::FLS2:GFP 35S::RFP:VPS28-2*)	Col-0	*pFLS2::FLS2:GFP* plant transformed with *RFP:VPS28-2* driven by the *35S* promoter sequence	present study
vps28-2	Col-0	homozygous SALK_040274 T-DNA line for *VPS28-2*	S. Schellmann, University of Cologne
vps28-2 FLS2-GFP (*vps28-2 pFLS2::FLS2:GFP*)	Col-0	*vps28-2* mutants transgenic for *pFLS2::FLS2:GFP*, obtained by crossing.	Present study
vps37-1	Col-0	homozygous SAIL_97_H04 T-DNA line for *VPS37-1*	S. Schellmann, University of Cologne
vps37-1 FLS2-GFP (*vps37-1 pFLS2::FLS2:GFP*)	Col-0	*Vps37-1* mutants transgenic for *pFLS2::FLS2:GFP*, obtained by crossing.	present study
Ws-2	Ws-2	wild-type reference line, natural fls2 null mutant	K. Feldmann , University of Arizona, Tucson, AZ

[a] Names written in bold are used abbreviation in this work.

[b] University of North Carolina, Chapel Hill, NC, USA; [c] Nottingham Arabidopsis Stock Centre

2.1.2. Bacterial strains

E. coli DH5α, *E. coli* Rosetta and *Agrobacterium tumefaciens* and were used for cloning and heterologous gene expression, respectively. Plant pathogenic *Pseudomonas syringe* pv. *tomato* DC3000 and its non-virulent *hrcC* mutant (Yuan and He, 1996) were tested on selected *Arabidopsis* mutants to investigate potential immune deficiencies. All strains with corresponding antibiotic resistances and growth conditions are listed in Table 3.

Table 3   Use of pathogenic and non-pathogenic bacterial strains

Strain	Used for	Resistance	Media
Escherichia coli DH5α	Cloning	none	L-medium
Escherichia coli Rosetta	heterologous gene expression	Cam^R	L-medium
Agrobacterium tumefaciens GV3101	heterologous gene expression	Rif^R + Gent^R	L-medium
Pseudomonas syringe pv. *tomato* DC3000	Pathogenicity test	Rif^R	NYBA, King's B
Pseudomonas syringe pv. *tomato* DC3000 *hrcC* (Yuan and He, 1996)	Pathogenicity test	Rif^R	NYBA, King's B

2.1.3. Oomycete strains

Waco 9 isolate of *Hyaloperonospora arabidopsidis (Hpa)* was used in infection assays and microscopy. Isolates were maintained as previously described in Toer et al., 2002 (Toer et al., 2002). Both strains originated from stocks maintained by Professor Dr. Jonathan Jones, Norwich.

2.1.4. Plasmids

Plasmids were constructed by either classical cloning with appropriate restriction enzymes or using Gateway technology (Invitrogen, UK). Table 4 describes used vectors.

Table 4   **Vector used to generate transgenic plants or for heterologous gene expression.**

Name	Insert	Backbone	type of vector	Reference
35S::CFP:ELC	cds of *ELC*	pAM-PAT-GW (Weinl et al., 2005)	binary vector	present study
35S::YFP:VPS28-2	cds of *VPS28-2*	pEARLY104 (Earley et al., 2006)	binary vector,	present study
35S::RFP:VPS37-1	cds of *VPS37-1*	pGWB555 (Nakagawa et al., 2007)	binary vector	present study
pFLS2::FLS2:GFP	*pFLS2::FLS2:GFP*	pGREEN	binary vector	(Robatzek et al., 2006)
pFLS2::FLS2KjmR:GFP	*pFLS2::FLS2$^{KKK854, 857, 861RRR}$:GFP*	pGREEN	binary vector	present study
FLS2CD-His	cds of FLS2CD	pET42	*E. coli* expression	(Göhre et al., 2008)
FLS2CD$^{KKK854, 857, 861RRR}$-His	cds of *FLS2CD$^{KKK854, 857, 861RRR}$:GFP*	pET42	*E. coli* expression	present study
GST-AvrPtoB	*AvrPtoB*	pGEX-2TM-GW	*E. coli* expression	(Göhre et al., 2008)
UBC9-His	*cds UBC9*	pET42	*E. coli* expression	(Göhre et al., 2008)

2.1.5. Oligonucleotides

Oligonucleotides were synthesized by Sigma-Aldrich (St. Louis, MI, USA), diluted with ddH$_2$0 to 100 µM stock solutions and 10 µM working solution. Table 5 lists used oligonucleotides and their corresponding targets.

Table 5 **Overview of cloning, genotyping and qPCR primers with corresponding targets and sequences**

name	forward sequence	reverse sequence	used for	target
elc GW	GGGGACAAGTTTGTACAAAAAAGCAGGCTTA ATGGTTCCCCCGCCGTCTAATC	GGGGACCACTTTGTACAAGAAAGCTGG GTATCATGAATGTAACCTACCTGCGATG	Gateway Cloning	*ELC*, AT3G12400
vps28-2 GW	GGGGACAAGTTTGTACAAAAAAGCAGGCTTA ATGATGGAGGTCAAATTATGGAACGAC	GGGGACCACTTTGTACAAGAAAGCTGG GTATTAATTACCAGCTTTAGGCAAAGCT GCC	Gateway Cloning	*VPS28-2*, At4g05000
vps37-1 GW	GGGGACAAGTTTGTACAAAAAAGCAGGCTTA ATGTTCAATTTCTGGGGATC	GGGGACCACTTTGTACAAGAAAGCTGG GTATCAAATGTTTGACGTTTTAGC	Gateway Cloning	*VPS37-1*,At3g53120
elc	ATGGTTCCCCCGCCGTCTAATC	TCATGAATGTAACCTACCTGCGATG	genotyping	*ELC*, AT3G12400
RFP	GCGCTTCAAGGTGCGCATGG	GTCTTGTAGGCGCCGGGCAG	genotyping	*RFP*
SAIL_LBa1	GCCTTTTCAGAAATGGATAAATAGCCTTGCTT CC		genotyping	Sail tDNA
SALK_LBa1	TGGTTCACGTAGTGGGCCATCG		genotyping	Salk tDNA
vps28-2	ATGATGGAGGTCAAATTATGGAACGAC	TTAATTACCAGCTTTAGGCAAAGCTGCC	genotyping	*VPS28-2*, At4g05000
vps37-1	ATGTTCAATTTCTGGGGATC	TCAAATGTTTGACGTTTTAGC	genotyping	*VPS37-1*,At3g53120
CTR1	CCACTTGTTTCTCTCTCTAG	TATCAACAGAAACGCACCGAG	map-based cloning	Chr 5, 0.98 Mb
5-AB010070-0918	CTCTGTTGGGGCAAAACC	GATGCTGGAGAGTAGCTTAG	map-based cloning	Chr 5, 2.48 Mb
5-AL133421-0927	TTATGCCCATTTGAAACC	TGAAACTTTGGGCCTCAG	map-based cloning	Chr 5, 2.50 Mb
5-AL360334-1190	TGGGATTACATAGGTACCG	TGTCCAAATAATGAAATATC	map-based cloning	Chr 5, 3.21 Mb
5-AL365234	GGGGACATTTAGGTGGTATC	CATCGCCGCCAATACCTC	map-based cloning	Chr 5, 3.42 Mb
5-AL391149-1762	GTAACGTATGCATGGTTTG	AAGTTTTGGTTAGATTACAC	map-based cloning	Chr 5, 4.75 Mb
ciw8	TAGTGAAACCTTTCTCAGAT	TTATGTTTTCTTCAATCAGTT	map-based cloning	Chr 5, 7.49 Mb
ACO2	ACAACCCGGGAAGCGATGCG	TGCAGAAGCATTCTTCATTGCTGCG	qPCR	*ACO2*, At1g62380
Actin2	GGTAACATTGTGCTCAGTGGTGG	AACGACCTTAATCTTCATGCTGC	qPCR	*ACT2*, At3g18780
AT3G60140	ACTACACGGCTCGCTTCGCT	GCCCCTTTCTTCCCCAGGTCC	qPCR	*DIN2*,AT3G60140
FLS2qPCR	ACTCTCCTCCAGGGGCTAAGGAT	AGCTAACAGCTCTCCAGGGATGG	qPCR	*FLS2*, AT5G46330
FRK1	ACGGCTCTTGTTGAACACTAC	CTTTAATCTTCCTCATGGCATC	qPCR	*FRK1,* At2g19190
PsaA	AGCCCAAACAATGGATTCAA	GGCACAAGCATCTCAGGTAA	qPCR	*PsaA*, ATCG00350
PsbD	TCCACTAGGTCAATCTGGTTGGTTC	GGCGACTCCCATCATATGAAATG	qPCR	*PsbD*, ATCG00270
AT3G06500	CGGGGCTAATGCCAGCGAGT	ACCACAAACCAGAGTCAACAGGGC	qPCR	AT3G06500
WRKY22	GATCATCTAGCGGTGGGAGA	TATTCCTCCGGTGGTAGTGG	qPCR	*WRKY22*, At4g01250
FLS2seq1	ATGAAGTTACTCTCAAAGAC		sequencing	*FLS2*, AT5G46330
FLS2seq2	CTGAGGAAATCTGCAAAACC		sequencing	*FLS2*, AT5G46330
FLS2seq3	GATTCCTCGAGAAATCGGGA		sequencing	*FLS2*, AT5G46330
FLS2seq4	GATTTCTCGAGGAATCGGTC		sequencing	*FLS2*, AT5G46330
FLS2seq5	AGCCGATGTATTCAGCTTCGGGAT		sequencing	*FLS2*, AT5G46330
FLS2seq6	GGTGAACAGCTCCTCGCCCTT		sequencing	*FLS2*, AT5G46330
GFPseq1	ACAAGTTCAGCGTGTCCGGCG		sequencing	*GFP*
GFPseq2	CGCGCTTCTCGTTGGGGTCTTT		sequencing	*GFP*
FLS2K854R	GTTCATTGTGATCTGAGGCCAGCTAATATACT CC	GGAGTATATTAGCTGGCCTCAGATCAC AATGAAC	SDM	*FLS2*, AT5G46330
FLS2K857R	CAGCTCTGCGTCTGAGGAGATTTGAACCAAAA G	CTTTTGGTTCAAATCTCCTCAGACGCAG AGCTG	SDM	*FLS2*, AT5G46330
FLS2K861R	GAGATTTGAACCAAGAGAGTTGGAGCAAGCA ACAG	CTGTTGCTTGCTCCAACTCTCTTGGTTCA AATCTC	SDM	*FLS2*, AT5G46330

2.1.6. Chemicals

If not stated otherwise, standard chemicals were purchased from Sigma-Aldrich (St. Louis, MI, USA), Merck (Whitehouse Station, NJ, USA), Invitrogen (Carlsbad, CA, USA), VWR (Radnor, PA, USA) or Helena Bioscience (Gateshead, UK). EZBiolab Inc. (Westfield, IN, USA) synthesized the flg22 peptide used in this study and previous work (Göhre et al., 2008).

2.1.7. Enzymes

Genotyping PCRs were performed with Taq DNA polymerase from New England Biolabs (Ipswich MA, USA). DNA amplification for cloning purposes was done the Expand High Fidelity PCR system (Roche Diagnostics Co., UK). RT-PCRs were carried out with Superscript II (Invitrogen Carlsbad, CA, USA), and SybrGreen master mix (Sigma-Aldrich, St. Louis, MI, USA). Restriction enzymes were commonly purchased from New England Biolabs (Ipswich MA, USA), Gateway Cloning Enzymes from Invitrogen (Carlsbad, CA, USA).

2.1.8. Antibodies

Anti (α)-FLS2 antibodies were raised in rabbits and purified by Eurogentec (Seraing, Liège, Belgium)**.** 1:5000 deletions in 1 % (v/w) milk powder (Premier International Food, St Albans, UK) TBS-t (10 mM Tris-HCl, pH 7.4, 14 mM NaCl, 2.5 mM KCl , 0.05 % (v/w) Tween 20) were sufficient for specific detection of FLS2 as described in Göhre et al., 2008 (Göhre et al., 2008). αPhospho-p44/42 MAPK (α-pERK, rabbit polyclonal antibody from Cell Signaling, Boston, MA, USA) were diluted 1:1000 in 5 % BSA (w/v) TBS-t. In both cases goat α-rabbit IgG coupled to alkaline phosphatase (Sigma-Aldrich (St. Louis, MI, USA) was used as secondary antibody. GFP as probed with αGFP from Roche Applied Science (Penzberg, Germany) 1:1000 dilutions, followed by goat α-mouse IgG- alkaline phosphatase (Sigma-Aldrich, St. Louis, MI, USA) detection. Ubiquitin conjugated were detected by αUbiquitin (mouse monoclonal, P4D1, Santa Cruz Biotechnology, Santa Cruz, CA, USA) in deletions of 1:2000.

2.1.9. Growth media and antibiotics

Growth media were autoclaved for 20 min at 121°C, cooled down to approximately 50°C before adding antibiotics. Detailed recipes are listed in Table 6 and final concentrations of antibiotics in Table 7.

Table 6   Growth media recipes

Name	Species	Recipe	
L-Medium	*E.coli* and *A.tumefaciens*	10 g/l	bacto-peptone
		5 g/l	yeast extract
		5 g/l	NaCl
		1 % (w/v)	bacto-agar (optional, (Duchefa, Haarlem, Netherlands)
		pH 7.2	
King's B-Medium	*Pseudomonas*	20 g/l	bacto-peptone
		1.5g/l	heptahydrated magnesium sulfate
		1.5g/l	potassium hydrogen phosphate
		10 % (v/v)	glycerol
		1 % (w/v)	bacto-agar (optional)
		pH 7.2	
NYG-Medium	*Pseudomonas*	5.0 g/l	bacto-peptone
		3 g/l	yeast extract
		20 % (v/v)	glycerol
		1.5 % (w/v)	bacto-agar (optional)
		pH 7.2	
MS (Murashige and Skoog)	*Arabidopsis thaliana*	4.4 g/l	MS powder
		10.0 g/l	Sucrose
		pH 5.8	

Table 7   Used antibiotics

Name	Abbreviation	Final Concentration [µg/ml]	
Carbenicillin	Carb	100	in ddH$_2$0
Chloramphenicol	Cam	35	in Ethanol
Gentamicin	Gent	30	in ddH$_2$0
Hygrommycin	Hygr	30	in ddH$_2$0
Kanamycin	Kan	50	in ddH$_2$0
Phosphinothricin	PPT	15	in ddH$_2$0
Rifampicin	Rif	50	in DMSO
Spectinomycin	Spec	100	in ddH$_2$0

2.2. METHODS

2.2.1. Seed sterilization

Arabidopsis thaliana seeds were sterilized for 10 min in 70 % (v/v) ethanol 0.05 % (v/v) SDS, followed by three short washings with 98 % (v/v) ethanol. Seeds were then dried on sterile Whatman paper before sowing on MS agar plates.

2.2.2. Generation of *Arabidopsis thaliana* F_1, F_2 and F_3 progeny

Plants were crossed according to Weigel and Glazbrook (Weigel and Glazebrook, 2002). Basically, flowers with well-developed stigma were emasculated and pollinated with one single donor stamen. Developing siliques were then carefully wrapped in paper envelopes and harvest once they turned yellow. The resulting F_1 generation was tested for heterozygosity by PCR and allowed to self-pollinate to generate F_2 progeny. With the exception of *fli1* F_2 families used for map-based cloning, F_2 individuals were screened for the aimed genotypes and propagated to the next generation for further analyzes.

2.2.3. Stable transformation of *Arabidopsis thaliana*

Arabidopsis plants were stably transformed using floral dip method (Clough and Bent, 1998). Flowering plants were dipped for 30 sec in a 0.8 OD_{600}-dense solutions of *Agrobacteria* (5 % sucrose, 0.025 % Silwet L-77 (Lehle Seeds, Round Rock, TX, USA), kept in a dark environment for 24 hours and further propagated under standard long-day plant growth conditions. Successfully transformed seeds were recovered in the following T_1 generation on selective MS agar plates or by spraying BASTA (Duchefa, Haarlem, Netherlands) three-times on 4-5 –week-old plants at weekly intervals.

2.2.4. Transient transformation of *Nicotiana benthamiana*

Agrobacteria were grown over night (o/n) at 28°C in L-medium containing the appropriate antibiotics, centrifuged for 5 min at 5000 x g and washed once with 10 mM $MgCl_2$. A final OD_{600} = 0.1 of agrobacterial suspensions were then infiltrated underneath the lower epidermis of three to four week-old *N. benthamiana* leaves using a 1 ml needless syringe. Microscopically analysis followed two to three days post infiltration.

2.2.5. Pathogen infections

2.2.5.1. *Pseudomonas syringae patho-phenotyping*

Arabidopsis plants were grown for two weeks on Jiffy pellets (Jiffy Products International AS, Grorud, Norway) under controlled environment and 10 hours of photoperiod before inoculation. To prepare the inoculum, *Pseudomonas* was streaked out on King's B plates with appropriate antibiotics from glycerol stocks (30 % (v/v) glycerol, -80°C) and incubated for two days at 28°C. Single colonies were then transferred to 50 ml NYG broth containing 50 µg/ml of Rifampicin and grown under constant shaking for 12 to 13 hours. Bacterial cultures were then centrifuged for 15 min at 1000 g (RC8, Sorvall, Thermo Fisher Scientific, Waltham, MA, USA) resuspended in 5 ml 10 mM $MgCl_2$ and adjusted to a final density of OD_{600} = 0.02. 0.04 % Silwet (Lehle Seeds, Round Rock, TX, USA) was added before spraying the inoculum with an airbrush system (model AS18-2, Ningbo Haosheng Pneumatic Machinery Ningbo, China) on each seedling for approximately 2 seconds. Inoculated plants were kept under elevated humidity for 2.5 hours and disease symptoms were assessed 5 days post infection. Disease symptoms were grouped into four classes, where class 0 showed no symptoms, class 1 mild symptoms on maximal one leaf, class 2 infected plants had at least two infected leaves but showed no necrosis and class 3 with plants displaying severe disease symptoms including beginning necrotic lesions. Plants were randomly distributed on different trays.

2.2.5.2. *Pseudomonas syringae growth quantification*

Bacterial growth curves assays followed the infection procedure described above (2.2.5.2), but using four-week-old plants. To quantify bacterial replication, two leaf disks ($\varnothing$ = 0.5 cm) from two different surface-sterilized leaves (30 sec in 70 % (v/v) ethanol, followed by 30 sec in sterile ddH$_2$O) and at least four plants per genotype were sampled 4 days after inoculation. Leaf disks were grinded in 10 mM MgCl$_2$ with an electric drill (Heidolph, Schwabach, Germany), diluted 1:10 serially and plated on selective NYG agar plates. Two dates after incubation at 28°C colonies forming units were counted and statistically analyzed.

2.2.5.3. *Flg22-induced resistance to Pseudomonas syringae*

According to the protocol published by Zipfel et al., 2004 (Zipfel et al., 2004), four-week-old plants were either pre-infiltrated with ddH$_2$O or 1 µM flg22 using a needle-less syringe. 24 hours later the same leaves were syringe-inoculated with *Pseudomonas syringe* pv. *tomato* DC3000 (OD$_{600}$ = 0.001). Bacterial growth was quantified as described above.

2.2.5.4. *Hyaloperonospora arabidopsidis (Hpa) spore counting*

*Hpa s*pore suspensions of 5 x 10^4 spores/ml were spray-inoculated onto 14-day-old seedling and incubated at high humidity at 18°C. 6 days post-inoculation, spores of 12 seedlings per genotype (in pools of 3) were washed from infected leaves by vortexing in 1 ml ddH$_2$O and quantified in relation to seedling fresh weight. Spores were counted with an improved Neubauer haemocytometer (Brand, Wertheim, Germany).

2.2.6. Plant assays

2.2.6.1.   Measurements of root growth

Response to salt stress was studied according to Achard et al., 2006 (Achard et al., 2006). Seedlings were grown sterile on MS plates for 5-7 days and then transferred to MS plates containing 0, 50 mM or 100 mM NaCl. Plates were orientated vertically, and primary root growth of at least 20 individuals measured 3 days later. Glucose stress was applied similar to Zhou et al., 1998 (Zhou et al., 1998). Seven-day-old seedlings grown on MS plate were exposed for additional seven days to 0 %, 4 % (w/v) and 6 % (w/v) glucose. Primary root growth of at least 20 seedlings was measured and statistically analyzed. Root growth arrest upon flg22 stress was examined on seedlings grown in dark on vertical MS plates supplemented with 0, 100 nM or 500 nM flg22. At least 20 individual primary roots were measured per genotype and experiment.

2.2.6.2.   Flg22-induced callose deposition

Flg22-induced callose deposition was stained as described in (Lu et al., 2009). Briefly, ten-day-old seedlings were transferred to liquid MS media with and without 1 µM flg22, destained after 24 hours in acetic acid - ethanol (1:3) for four hours, washed twice with ddH_2O, and incubated o/n in aniline blue solution (150 mM KH_2PO_4, 0.01 % (w/v) aniline blue, pH 9.5). Stained callose was then visualized ultraviolet epifluorescence microscopy (Zeiss Axiophot, Carl Zeiss AG, Oberkochen, Germany).

2.2.6.3.   Measurements of stomatal apertures

According to Mersmann et al., 2010 (Mersmann et al.) *Arabidopsis* seedlings were transferred after one week growth on solid MS plates to liquid MS media. One week later MS media was exchanged with 5 µM flg22 or ddH_2O respectively. Mild vacuum was applied for 10 min and after 2 hours of recovery seedlings were mounted on glass slides. Stomatal apertures were imaged with a Zeiss

Axiophot microscope (Carl Zeiss AG, Oberkochen, Germany). In total at least 20 stomata were measured per genotype and condition. High-throughput stomatal apparatus measurements (> 100 stomata) were conducted with a fully automated confocal imaging system Opera (Perkin Elmer, Germany) and subsequent computational analyzes (Dr. Gildas Bourdais, The Sainsbury Laboratory, Norwich).

2.2.6.4. *Measurements of reactive oxygen production (ROS)*

16 leaf discs ($\varnothing$ = 0.5 cm) per genotype of four-week-old plants were incubated o/n in ddH$_2$O. Water was then exchanged with 100 µl of 20 µM luminol (Sigma-Aldrich (St. Louis, MI, USA), 1 µg horseradish peroxidase (Sigma-Aldrich, St. Louis, MI, USA) and 100 nM flg22. Light emission was read with a Varioskan Flash multiplate reader (Thermo Fisher Scientific, Waltham, MA, USA) for 35 min.

2.2.7. Molecular biological methods

2.2.7.1. *Isolation of genomic plant DNA*

A modified version of the Edward's DNA extraction protocol (Sambrook and William Russell, 2001) was used to extract genomic DNA. Approximately 10-20 mg a leaf tissue was grinded in 180 µl Edward's buffer (200 mM Tris-HCl, pH 7.5, 250 mM, NaCl, 25 mM EDTA, 0.5 % SDS (v/v)), centrifuged at maximum speed for 5 min (table centrifuge 5415D, Eppendorf, Hamburg Germany) and 120 µl of supernatant transferred into a fresh tube. One volume of isopropanol was added to precipitate DNA and centrifuged at maximum speed for 5 min. The supernatant was discarded and the pellet was washed once with 70 % (v/v) ethanol. Air-dried DNA pellets were dissolved in 100 µl sterilized ddH$_2$O and 3 µl used in 50 µl PCR reactions.

To extract high quality DNA for re-sequencing potential SNPs 10-20 mg leaf tissue was grinded in 200 µl of CTAB extraction buffer (1 % CTAB (w/v), 100 mM Tris-HCl, pH 7.5, 1 M NaCl, 50 mM EDTA, 5 % N-Sarcosylate (v/v)), incubated for 10 min at 65°C followed by 5 minutes at room temperature. 200 µL of 24:1 (v/v) chloroform-isoamylacohol was added, and centrifuged at 15000 g for 5 minutes at

4°C (table centrifuge 5415R, Eppendorf, Hamburg Germany). The upper phase was transferred into a new tube and one volume of cold (-20°C) isopropanol was added. Tubes were inverted 3 times and centrifuged at 15,000 g for one minute at 4°C. The precipitated DNA was washed once with 70 % (v/v) ethanol, air-dried and resuspended 100 μl sterilized ddH$_2$O.

2.2.7.2. Isolation of plasmid DNA and PCR products

Plasmid DNA was purified with QIAprep Spin Miniprep Kit (Qiagen, Hilden, Germany) and PCR product were isolated with QIAquick PCR purification and gel extraction kits (Qiagen, Hilden, Germany) according to manufacturer's recommendations.

2.2.7.3. PCR protocols

Standard PCR

Standard DNA amplification, which did not require sequence accuracy and used mainly for genotyping, was performed with 0.2 mM dNTPs (Promega, Fitchburg, WI, USA), 0.2 μM of each primer, 15 mM MgCl$_2$ and 1 U Taq polymerase (New England Biolabs) in Peltier Thermal Cycler PTC-225 (GMI Inc., Ramsey, USA). 4 min of initial denaturation at 96°C proceeded 20-30 cycles of denaturation at 96°C, 30 sec of primer annealing at 55°C to 60°C, and 1 min per 1 kb DNA amplification at 72°C. A final elongation step at 72°C for 3 min was added at the end of the protocol.

High Fidelity PCR and site-directed mutagenesis

In cases where sequence accuracy was necessary (*e.g.* cloning of genes or introducing mutation, Expand High Fidelity PCR system (Roche Applied Science, Penzberg, Germany) was used according to manufactory's instructions. The same thermal profile was used as in standard PCRs with the exception of 68°C instead of 72°C and 2 sec per kb during elongation steps. The Expand High Fidelity PCR system was also used for site-directed mutagenesis according to the protocol and primer design described for QuikChange Site-Directed Mutagenesis Kit (Startagene, Santa Clara, CA, USA).

Visualizing PCR products

20 µl PCR product was mixed with 5 µl of DNA-loading dye (5 M Betain, 0.05 % (w/v) Orange G, Sigma-Aldrich (St. Louis, MI, USA) and separated on 1 -2 % agarose gels (Melford Laboratories, Ipswich, UK) by electrophoresis (80-110 V, Biorad, UK). Agarose gels were prepared by boiling agarose in TBE buffer (45 mM Tris, 45 mM boric acid, 1 mM EDTA, pH 8.3). 1 µl/ml ethidium bromide (Sigma-Aldrich St. Louis, MI, USA) was added before pouring gels and visualized by UV excitation (ChemiDOC XRS, Bio-Rad Laboratories, Hercules, CA, USA). 2-log DNA ladder (New England Biolabs) was used as a reference.

2.2.7.4.   Sanger-Sequencing

Sanger method (Sanger et al., 1977) was used to verify DNA sequences. Reactions were carried out in final volumes of 10 µl containing 80-100 ng template DNA, 1 µM primer, 0.05 % (v/v) DTT, 1 µl 5x sequencing buffer and 1 µl Big Dye Terminator Ready Reaction Mix (Perkin Elmer, Waltham, MA, USA). The PCR program started with an initial denaturation step at 96°C for 1 min, followed by 35 cycles of denaturation at 96°C for 10 sec, annealing at 50°C for 5 sec and elongation at 60°C for 4 min. Read analysis was carried out with Dye-Deoxy Terminator Cycle Sequencer (Perkin Elmer, Waltham, MA, USA) in the The Genome Analysis Centre (TGAC, Norwich, UK).

2.2.7.5.   Illumina-Sequencing

76 bp paired-end reads generated by Illumina Solexa GA2 platform (Illumina, Cambridge, UK) was used for whole-genome sequencing. High-purity DNA was isolated with protocol adapted from McKinney et al., 1995 (McKinney et al., 1995). 2 g fresh weight of two-week-old *fli1* mutants was grinded in liquid nitrogen, incubated at 37°C for 30 minutes in 10 ml extraction buffer (50 mM Tris-HCl, pH 8.0, 200 mM NaCl, 2 mM EDTA, 0.5 % SDS (v/v), 100 mg/ml Proteinase K, Invitrogen (Carlsbad, CA, USA). 10 ml of saturated phenol-chloroform-isoamyl alcohol was added, and centrifuged (SS-34 rotor, Beckman Thermo Fisher Scientific, Waltham, MA, USA) at 16,000 g for 10 minutes (10°C). The top layer was transferred into a new tube and mixed with 10 ml of chloroform-

isoamyl alcohol (24:1). After centrifugation at 16,000g for 10 minutes (10 °C) the upper layer was transferred into a new tube and mixed with 900 μl of 3M sodium acetate (pH 5) and 2.5 volumes ethanol (98 % (v/v)). Precipitated DNA was pelleted for 20 minutes at 8,000g (10 °C), washed twice with 70 % (v/v) ethanol, air dried and resuspended 200 μl of TE buffer (20 mM Tris-HCl, pH 7.5, 1 mM EDTA). DNA was stored at 4°C. Library preparation and sequencing was carried out by Jodie Pike, followed by bioinformatics analysis in collaboration with Dr. Dan MacLean (The Sainsbury Laboratory, Norwich, UK). In brief, paired reads were removed prior to alignment if either of the pair contained an ambiguous nucleotide (I.E an 'N' was called). Illumina scaled quality scores (ASCII offset 64) were converted to Sanger scaled quality scores (ASCII offset 33) using the equations found in Cock PJ, Fields CJ, Goto N, Heuer ML, Rice PM. The Sanger FASTQ file format for sequences with quality scores, and the Solexa/Illumina FASTQ variants. Nucleotide distributions and Quality score distributions after filtering were calculated using the FASTQ Information tool in the FASTX-Toolkit version 0.0.13 (http://hannonlab.cshl.edu/fastx_toolkit/). Quality score distributions revealed that the reads had median quality scores of at least 25 across the length of the reads so no further pre-filtering was carried out. Paired reads were mapped to the TAIR10 Arabidopsis thaliana reference sequence using BWA version 0.5.8c. The TAIR 10 Fasta sequence was indexed with the 'index' command and paired reads mapped with 'sampe'. Resulting SAM format files were filtered to remove reads that appeared to be optical or PCR duplicates and converted to BAM format using SAMTools version 0.0.12a. In order to identify candidate SNPs, positions polymorphic to the reference genome were identified using the bcftools software in the SAMTools 0.0.12a package. Pileups were generated using SAMTools mpileup as 'mpileup -Q 13 -q 20 -C 50 -uf' (-Q = minimum base quality for a read nucleotide to be included in the pileup; -q = minimum mapping quality for a read to be included in the pileup; -C = filter to remove effects of reads with very large number of mismatches). Pileups were converted to bcf format with the bcftools 'view' command and SNPs called using 'vcfutils.pl -D 100 -d 10' (-D = maximum coverage depth for SNP calling; -d = minimum coverage depth for SNP calling). Candidate SNPs were removed from the list if they appeared in candidate lists generated in an identical pipeline from L*er*-FYVE, *fel2*, *fel4* or *fel9* mutants (Salomon, 2009) or if they appeared in the list of Landsberg Erecta 1 / Colombia 0 SNPs generated by the 1001 genomes project (Assembly dated 26-04-2011). SNP positions within genes (including UTRs, CDS, Exon and Intron) as described in the TAIR 10 annotation were marked with information as to which gene contained the SNP and whether it caused a synonymous or non-synonymous mutation in the gene using a custom Perl script. All bioinformatic analyzes were carried out in The Sainsbury Laboratory's compute cluster, a 22 node cluster composed of IBM blade server machines with AMD 64 processors running Debian GNU/Linux version 5.0.8 'Lenny' and with 4Gb to 32Gb RAM.

2.2.7.6. DNA restriction and Gateway cloning

DNA was digested with restriction enzymes according to the manufacturer's recommended conditions. Plasmid DNA was cut for at least one hours at the appropriate temperature.

Gateway cloning was done as described by Invitrogen (Carlsbad, CA, USA). Where necessary, pDONR vectors were cut with NsiI (New England Biolabs, Ipswich MA, USA) to remove the Kanamycin resistance cassette in pDONRs.

2.2.7.7. RNA isolation and cDNA synthesis

10 to 14 day-old plants were grinded in liquid nitrogen with mortar and pestle. Total plant RNA of approximately 50 mg of frozen plant powder was extracted with RNeasy Plant Mini Kit (Qiagen, Hilden, Germany) and treated for 30 min with DNAse (Promega, Fitchburg, WI, USA). DNAse was heat inactivated for 10 min at 65°C and total RNA quantified with a Nanodrop spectrophotometer (Thermo Fisher Scientific, Waltham, MA, USA).

1 µg of total RNA were used for cDNA synthesis with SuperScript II reverse transcriptase according to manufacturer's directions (Invitrogen, Carlsbad, CA, USA). In brief, 11 µl RNA (in total 1 µg) was pre-incubated for 10 min at 65°C with 1 µl 10 mM dNTPs and 1 µl of 500 µg/ml oligo(dT)$_{15}$, chilled on ice and added to 4 µl 5 x reaction buffer, 2 µl 2 µl DTT (0.1 M), 0.5 µl RNaseOUT (40 U/µl, Invitrogen, Carlsbad, CA, USA) and 1 unit of SuperScript II. After 50 min at 42°C, RT-Taq was heat-inactivated for 15 min at 70°C. cDNA was diluted 1:50 with ddH$_2$O and stored at -20°C.

2.2.7.8. Quantitative real-time (RT) PCR

Reactions were carried out in white 96 well plates with optical lids (Thermo Fisher Scientific, Waltham, MA, USA). Each reaction contained 1 µl cDNA, 1 µl or each primer (10 µM), 7 µl ddH$_2$O and 10 µl of SYBR Green Jump Start (Sigma-Aldrich (St. Louis, MI, USA). Each primer pair and cDNA combination was analyzed in triplicates by C1000 Thermal Cycler (Bio-Rad Laboratories, Hercules,

CA, USA) with the following program: 95°C for 4 min, 40 cycles of 10 sec at 94°C, 15 sec at 62°C, 30 sec at 72°C, followed by reading SYBR Green emission. The program terminated with a last elongation step at 72°C and melting curve measurements form 65°C to 95°C in 0.5°C steps. The data were analyzed by Bio-Rad CFX qPCR software.

2.2.7.9. Whole genome transcript array

For every genotype and condition five pools of each seven seedlings were sampled. The infection was done on two-week old seedlings as described previously with following modifications: An OD_{600} of 0.1 (corresponds to approximately 10^8 cfu) was used instead of 0.02, and instead of 0.04 % Silwet, 0.02 % was used. Infected plants were covered with lids for 3 hours instead of 2.5 hours. Adaptations became necessary to maintain similar disease progressions after changing growth cabinets used in later experiments. Samples were collected 3 hours after infection of *Pto* DC3000 spray inoculated plants and 24 hours after infection from inoculated and control plants by cutting and freezing aerial parts in liquid nitrogen. RNA was extracted as previously described and stored at -80°C. Quality assessment, Affymetrix Ath1 chip (Santa Clara, CA, USA) hybridization and read-out was done by Dr. Bruno Huettel (MPIPZ, ADIS, Cologne, Germany). Transcript abundances were calculated from three microarray chips per conditions and genotype.

2.2.7.10. Total protein extraction from plants

Harvested plant material was frozen in liquid nitrogen and stored at -80°C or directly grinded with mortar and pestle in liquid nitrogen. 15 - 25 mg plant powder was transferred into a 1.5 ml Eppendorf tube and 100 µl/mg protein extraction buffer (26 mM Tris-base, 17 % (v/v) glycerol, 2 % SDS (v/v), 0.005 % (w/v) Bromphenol Blue, 3 % (w/v) DDT , 3 mM PMSF, 1 x plant protease inhibitor (Sigma-Aldrich, St. Louis, MI, USA)), 1 mM benzamidine) was added. Samples were vortexed briefly and boiled instantly at 95°C for 5 min (Thermomixer, Eppendorf, Hamburg Germany).

2.2.7.11. SDS-PAGE and Coomassie staining

15 µl of protein samples were loaded on 10 mm spaced acryl-amid gels. Separating gels contained 7 % – 12 % (v/v) final concentration of acrylamid (Severn Biotech Worcestershire, UK) in 0.375 M Tris-HCl, pH 8.8, 0.1 % (v/v) SDS, 0.0005 % (v/v) APS, 0.0016 % (v/v) TEMED. Sacking gels consisted of 4.5 % acrylamid in 0.5 M Tris-HCl (pH 6.8), 0.04 % SDS (v/w), 0.001 % APS (w/v), 0.002 % (v/w) TEMED final concentrations. Proteins were separated by electrophoresis (Mini-PROTEAN , Bio-Rad Laboratories, Hercules, CA, USA) at 20 mA per gel in SDS-running buffer (25 mM Tris-HCl, 250 mM glycin and 0.1 % (v/v) SDS). As reference 6.5 µl of pre-stained protein standard (Precision Plus, Bio-Rad Laboratories, Hercules, CA, USA) was loaded on the same gels. If visualization and fixations of proteins was required, gels were stained with 0.25 % (w/v) Coomassie brilliant blue, 10 % (v/v) acidic acid, 50 % (v/v) methanol, for 10 min, destained for 15 min in 10 % (v/v) acidic acid, 50 % (v/v) methanol, followed by 30 min in 10 % (v/v) acidic acid, 10 % (vv) methanol.

2.2.7.12. Western Blot

Protein gels were blotted on PVDF membrane (Imobilon, EMD Millipore, Billerica, MA, USA) with Bio-Rad Trans-Blot Semi-Dry blotting system. The protocol was previously described in Göhre *et al.* 2008 (Göhre et al., 2008). In summary, membranes were activated with methanol for 2 min and incubated for at least 20 min in anode buffer 2 (300 mM Tris-Base, 20 % (v/v) methanol. Gels were shortly rinsed in cathode buffer (25 mM Tris, 40 mM ε-amino-n-carpic acid, 20 % methanol and transferred on activated membranes, piled on one layer of extra-thick blotting paper soaked in anode buffer 1 (25 mM Tris, 20 % methanol), followed by a second blotting paper soaked in anode buffer 2. The stack was covered by a third blotting paper, which was rinsed in cathode buffer. Proteins were transferred for 90 min at 25 V.

2.2.7.13. Immunodetection of proteins

Western blots were blocked with 5 % (w/v) milk powder (Premier International Food, St Albans, UK) in TBS-t (10 mM Tris-HCl, pH 7.4, 14 mM NaCl, 2.5 mM KCl, 0.05 % (v/v) Tween 20) for at least one hour at room temperature or alternatively at 4°C o/n. Hybridization with primary antibodies was done o/n at 4°C. Membranes were then washed three times for 10 min with TBS-t and incubated for 1 h at room temperature in 1:30,000 dilutions of alkaline-phosphatase coupled secondary antibodies (in 1 % (w/v) milk powder TBS-t). Three 10 min washing steps with TBS-t and one with alkaline phosphate buffer (100 mM Tris-HCl pH 9, 100 mM NaCl, 5 mM $MgCl_2$) followed. CDP-Star (Roche Applied Science (Penzberg, Germany) was used as an alkaline-phosphate substrate and emission captured on medical X-ray films (Fuji, Tokyo, Japan).

PVDF membranes were stained for 5 min in 0.25 % (w/v) Coomassie-brilliant blue in 10 % (v/v) acidic acid, 50 % (v/v) methanol and destaining for 10 min in 10 % (v/v) acidic acid, 50 % (v/v).

2.2.7.14. *Heterologous gene expression and protein purification*

Recombinant proteins were expressed in *E. coli* Rosetta cells by inducing expression with 0.2 mM IPTG for one hour. Cells were then harvested by centrifugation for 15 min, 2000 g, 4°C and stored at -20°C. According to Göhre et al, 2008 (Göhre et al., 2008), bacteria were lysed by sonication in STE buffer (10 mM Tris-HCl, pH 8, 150 mM NaCl, 1 mM EDTA, 100 µg/ml lysozyme, bacterial protease inhibitors (Sigma-Aldrich, St. Louis, MI, USA), centrifuged at maximal speed for 10 min at 4°C and bound to magnetic GST or NiNTA beads (Promega, Fitchburg, WI, USA) for 30 min at 4°C. Beads were washed three times with TBS buffer (10 mM Tris-HCl, pH 7.4, 14 mM NaCl, 2.5 mM KCl). His-tagged proteins were eluted with 100 mM immidazol for 5, 20, 60 min. The first elution was discarded and only latter ones used for in vitro assays.

2.2.7.15. *In vitro ubiquitination assay*

Ubiquitination assays were conducted as previously described (Göhre et al., 2008). In brief, purified substrate proteins were mixed with 33 ng/µl yeast E1 (Calbiochem, Merck, Whitehouse Station, NJ, USA), Ubiquitin variants (Calbiochem) 0.25 µg/µl UbcH5 (Calbiochem) or recombinant Ubc9-His and purified GST-bound AvrPtoB from *E.coli*. Reactions were carried out in ubiquitination buffer (50 mM Tris-HCl, pH 7.5,2 mM MgCl$_2$, 4 mM ATP, 1 mM DTT) for 2 hours at 30°C and analyzed on Western blots. For identification of FLS2 ubiquitination sites, ubiquitinated FLS2CD was re-purified from the assay using magnetic NiNTA beads as described above and concentrated with centrifugal filters with a cut-off of 30 kDa (Millipore, Billerica, MA, USA). Tandem mass-spectrometry and spectra analysis were done in collaboration with Dr. Thomas Colby (MPIPZ, Cologne, Germany).

2.2.8. Cell biological methods

2.2.8.1. Confocal microscopy

Four to five-week-old *Nicotiana benthamiana* leaf disks or cotyledons of ten-day-old sterile grown *Arabidopsis* seedlings were examined. Unless otherwise indicated *in vivo* confocal microscopy of fluorophor-labeled proteins was done with a Leica SP5 confocal microscope (Leica Microsystems, Wetzlar, Germany). Images were recorded using HCX PL APO CS 63.0 x 1.20 water objective, four scans per line, and zoom factor 4. Differential labeled proteins within one specimen were scanned sequentially. An argon laser source was used to excite CFP at λ = 458 nm, and GFP with λ = 488 nm. Emitting CFP was detected at λ = 500nm - 535nm, and GFP between λ = 515 nm - 555 nm, respectively. RFP was excited with a diode-pumped solid-state laser at λ = 561 nm and emission captured between λ = 570 – 630 nm. Chlorophyll fluorescence was monitored between λ = 730 nm – 800 nm. Data analyzes were done with Leica LAS AF software (Leica Microsystems, Wetzlar, Germany) and ImageJ (open source imaging tool from National Institutes of Health, Bethesda, MA, USA).

2.2.8.2. Automated confocal microscopy

High-content confocal imaging was performed according to Salomon *et. al*, 2010 (Salomon et al., 2010) using the Opera platform (Perkin Elmer, Waltham, MA, USA). Cotyledons of two-week-old plants grown on soil were placed on an imaging stamp, which was then inverted on top of a 96-well sensoplate with glass bottom (Greiner Bio-One GmbH, Essen, Germany). In all experiments a water-immersion 40x-objective was used. FLS2-GFP endosome levels were monitored 35 min after incubation in 10 µM flg22 solution using a λ = 488 nm laser excitation, λ = 540/75 nm detection and an exposure time of 80 ms. 21 focal planes were merged on 5 fields of each cotyledon. Two plates each containing 12 control and 48 flg22-treated samples were measured per experiment. Experiments were done in triplicates.

Co-localization studies were performed by sequential scanning of RFP (λ = 521 nm excitation, λ = 521/630 nm detection, exposure time 120 ms) and GFP (λ = 488 nm excitation, λ = 540/75 nm detection, exposure time 120 ms).

2.2.9. Data processing and statistical analysis

DNA sequence analysis, including primer design, Clustal W alignments and Sanger-Sequencing assemblies were done with Vector NTI Advanced version 11 (Invitrogen, Carlsbad, CA, USA). Specificity of primers was tested *in silico* by blast search analysis on the NCBI database (National Centre for Biotechnology, Bethesda, MA, USA). DNA sequences were retrieved from NCBI or Phytozome (Joint Genome Institute, University of California Regents, Oakland, CA, USA). Mapping primers were obtained from the Arabidopsis Mapping Platform (AMP, Peking University, Beijing, China).

Affymetrix data were processed with the open source data analyzing software R version 2.9.2 (R Foundation for Statistical Computing, Vienna, Austria) using freely accessible Affymetrix analyzes tools (Parmigiani et al., 2003) and further investigated in Microsoft Office Excel 2007 (Microsoft, Redmond, Washington, USA) and MeV 4.6.0 (Saeed et al., 2003) for hierarchical clustering. Assemblies of Illumina reads on reference genomes were visualized with Savant genome browser (Fiume et al., 2010).

R was used for statistical analysis of variance (ANOVA) in biological data, followed by multiple-comparison testing with Tukey's honest significance test. Significant differences were observed when P values were below 0.05.

Endosome levels were quantified with Acapella 2.0 (Perkin Elmer, Waltham, MA, USA) as previously described in Salomon et al., 2010 (Salomon et al., 2010) and statically analyzed using R.

ImageJ, Adobe Photoshop and Adobe Illustrator (Adobe Systems, San Jose, CA, USA) were used for illustration proposes as well as Cn3D 4.3 (NCBI, (Wang et al., 2000)) for protein structure representation.

3. RESULTS

3.1. UBIQUITINATION-PATTERN INFLUENCES FLS2 FUNCTION

To find new factors regulating FLS2 endosomal trafficking, we focused on previously reported FLS2 ubiquitination (Göhre et al., 2008; Lu et al., 2011). To study FLS2 ubiquitination in more detail, we used *Pto* DC3000 effector AvrPtoB instead of *Arabidopsis* PUB12, 13 for two reasons: Firstly, the role of PUB12 and PUB13 in FLS2 ubiquitination was not identified, when our work was initiated. Secondly, the direct interaction between FLS2 and AvrPtoB allowed us to analyze FLS2 ubiquitination in a cell-free environment. We have previously reported that *Pto* DC3000 effector AvrPtoB catalyzes ubiquitination of FLS2, but the type of ubiquitination remained unknown (Göhre et al., 2008). We therefore surveyed different ubiquitin mutant variants for their ability to from AvrPtoB mediated FLS2-ubiqutin products *in vitro* (Figure 3). Purified recombinant cytosolic domains of FLS2 (FLS2CD) were analyzed on Western blots either in the presence or in the absence of AvrPtoB, ubiquitin activating enzyme E1, ubiquitin conjugating enzyme E2, and wt ubiquitin, ubiquitin mutated at lysine 63 (Ub^{K63R}), ubiquitin mutated at lysine 48 (Ub^{K48R}), or ubiquitin mutated at all lysine residues (Ub^{noK}). Non-ubiquitinated FLS2CD was detected as major band with an expected size of about 42 kDa in the absence of AvrPtoB (Figure 3). Additional bands separated by the approximately 10 kDa, the size of one single ubiquitin moiety, emerged above this band in the presence of AvrPtoB independent of the ubiquitin variant used. Bands of corresponding sizes were also detected by anti-Ubiquitin antibodies, indicating the observed shift in molecular weight was caused by covalent attachments of ubiquitin molecules. Due to cross-reacting bands detected by anti-FLS2 antibodies in a range between 75 kDa and 200 kDa, we were not able to clearly resolve FLS2-Ub conjugates in a higher order than triple ubiquitinated FLS2CD (FLS2CD-Ub3). Higher molecular weight ubiquitin conjugates could however be analyzed by anti-Ubiquitin antibodies. Ubiquitination was most pronounced with Ub^{K48R}, but also detectable with Ub^{K63R} variants and wt Ub. In each case strong anti-Ubiquitin antibody signals were detected for proteins above 75 kDa, presumably resulting from a mixture of ubiquitinated AvrPtoB and FLS2CD. By contrast, Ub^{noK} –containing reaction mixtures generated severely fewer ubiquitinated proteins. Only two bands at the size of approximately 50 and 60 kDa were labeled at a similar size with anti-FLS2 and anti-Ubiquitin antibodies. Because Ub^{noK} variants are not able to form poly-ubiquitin chains, we concluded that AvrPtoB ubiquitinated FLS2CD at least at two independent residues *in vitro*.
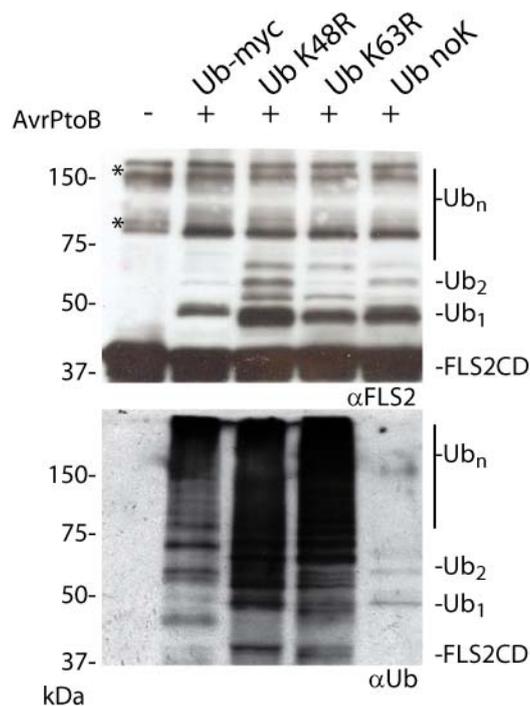
Figure 3   **AvrPtoB ubiquitinates cytosolic domains of FLS2 at two independent sites.** Purified recombinant proteins of histidin-tagged FLS2 cytoplasmic domain (FLS2CD) alone (-) or mixed with GST-AvrPtoB, and Ubc9-His (E2), yeast E1, and indicated ubiquitin variants (+) were analyzed by Western blots using anti-FLS2 antibodies (upper panel) or anti-Ubiquitin antibodies (lower panel). Cross-reacting bands are marked by asterisks.

In order to identify FLS2 ubiquitination sites, we used Ub^{noK} variants and increased the reaction volume to generate sufficient amounts of FLS2CD-Ub conjugates, suitable for tandem mass spectrometry (MS/MS) analyzes. FLS2CD and ubiquitinated forms were re-purified from the assay and concentrated. Purified and un-purified fractions of FLS2CD-Ub as well FLS2CD alone were analyzed on Coomassie stained SDS gels and by Western blots (Figure 4 A). In contrast to one single FLS2CD band of 42 kDa, several additional Coomassie stained bands of higher molecular weight appeared in AvrPtoB ubiquitination reaction mixtures. Re-purification of FLS2CD removed most of the bands except two, which run about 10 and 20 kDa above un-ubiquitinated FLS2CD proteins. Both additional bands were detected with anti-FLS2 and anti-Ubiquitin antibodies. Compared to un-purified fractions, far less ubiquitinated proteins were labeled, indicating efficient enrichment of FLS2-ubiquitin conjugates. Purified fractions were further processed by MS/MS analysis (in collaboration with Dr. Thomas Colby, MPIPZ, Cologne, Germany). MS/MS data revealed a di-glycine modification resulting from trypsin digestion of ubiquitinated K854 in the N-terminal part of FLS2CD (Suppl. table 1). K854 is flanked by to two neighboring lysines on position 857 and 861 (Figure 4 B). All three lysine residues are located in the juxtamembrane region of FLS2. K861 is also present in the

33

juxtamembrane of tomato FLS2 (Figure 4 B). In addition, comparison with the crystal structure of human Ephrin type-A receptor 3 (Epha3) proposed a potential surface exposure of K861 (Figure 4 B). K854, K856 and K861 were substituted with arginine residues and equal amounts of FLS2CD and FLSCD^{K854,856,861R} were tested for *in vitro* ubiquitination by AvrPtoB (Figure 4 C). In the presence of AvrPtoB, E2, E1 and Ub^{noK} FLS2CD proteins of higher molecular weight were detected on Western blots, which corresponded to the expected size of mono- and di-ubiquitnated FLS2CD conjugates observed previously (Figure 3). FLSCD^{K854,856,861R} variants showed less intense bands at comparable sizes and no bands in a range where di-ubiquitnated FLS2CD would have been expected (~ 60 kDa).
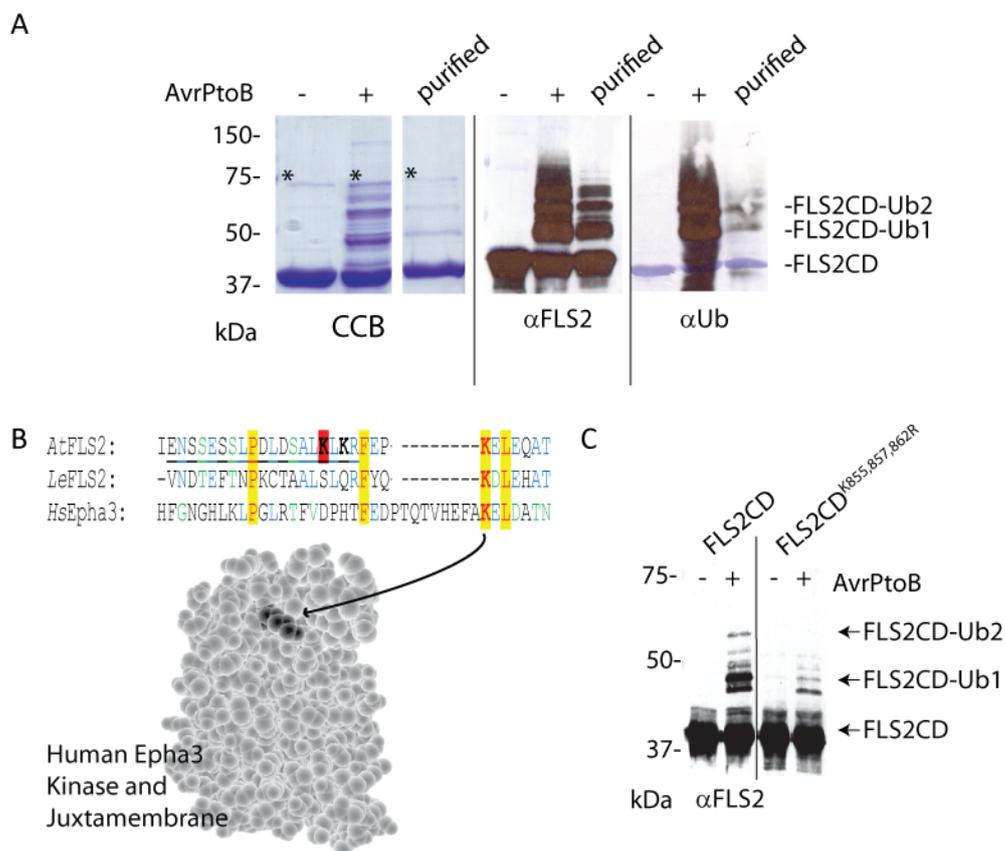
Figure 4   FLS2 is ubiquitinated in the juxtamembrane by AvrPtoB. (A) Purified recombinant proteins of histidin-tagged cytosolic domains (CD) of FLS2 were incubated with (+) or without (-) AvrPtoB, E2, E1 and Ub^{noK}. FLS2CD and ubiquitinated conjugated were purified from the assay. AvrPtoB-mediated ubiquitination of FLS2CD could be observed as a ladder of bands separated by 10 kDa of a single non-lysine containing ubiquitin by Commassie staining (blue), anti-FLS2 and anti-Ubiquitin immunoblotting. Cross-reacting bands are marked by asterisks. (B) Juxtamembrane regions of *Arabidopsis (At)* and tomato (*Le*) were aliened by using Clustal W. Residues identical in all three juxtamembranes are depicted in red and highlighted in yellow. Identical amino acids in two juxtamembranes regions are shown in blue, similar ones in green. MS/MS identified peptide is underlined and di-glycine modified lysine is highlighted in red. Substituted lysines in *At*FLS2 are shown in bold and proposed projection on the crystal structure of human (*Hs*) Epha3 receptor is indicated. (C) Ubiquitination assay was carried out as described in (A).

In order to analyzes the effect of putative FLS2 ubiquitination mutant variants *in planta*, a full-length FLS^{K854,856,861R} referred to as FLS2$^{3K->R}$ fused to GREEN FLUORESCENT PROTEIN (GFP) under the control of a native *FLS2* promoter fragment was transferred into Col-0 *fls2* mutant plants. In total 30 plants transformed with FLS2$^{3K->R}$-GFP mutant variants and 30 plants with FLS2-GFP wild-type (wt) constructs were analyzed by flg22 induced ROS production in T$_1$ (Suppl. Fig. 1). No significant differences were found in average ROS production between FLS2$^{3K->R}$-GFP T$_1$ populations and wt FLS2-GFP T$_1$ populations. T$_2$ families with a segregation of 3:1 were further analyzed.

Previously described ubiquitination site mutants of two *Arabidopsis* metal transporters showed altered endocytosis or endosomal trafficking (Kasai et al., 2010; Barberon et al., 2011). We quantified FLS2-GPF and FLS2$^{3K->R}$-GFP endosome numbers by automated confocal imaging (Figure 5). One low and one high expressing line per construct were analyzed to avoid misleading results due to different FLS2-GFP protein levels (Figure 5 A). In average between 40 and 50 endosomes-like structures per image area were detected in the absence of flg22 and represent therefore the baseline of our measurements (Figure 5 B). Significantly more FLS2-GFP endosomes were detected after flg22 treatment. Depending on the line between 150 and 300 endosomes were measured (Figure 5 B). Low expressing FLS2-GFP line 3 generated significantly less endosomes than other lines tested. No significant differences were observed between high expressing FLS2-GFP line 4 and both high and low expressing FLS2$^{3K->R}$–GFP lines 1 and 4.

Next we tested, whether expressed FLS2 variants complement disease phenotypes of *fls2* mutants. Therefore we quantified *Pto* DC3000 growth three days after spray inoculations (Figure 5 C). All tested lines except low expressing FLS2-GFP wt line 3 restored *Pto* DC3000 resistance of *fls2* mutants to at least Col-0 wt levels. Bacteria grew to significant higher numbers in low expressing FLS2-GFP line 3 and reached the susceptibility of untransformed *fls2* mutants. Even though FLS2$^{3K->R}$–GFP line 1 accumulated less FLS2-GFP levels than FLS2–GFP line 4, both conferred a similar level of resistance to *Pto* DC3000 infections. High expressing FLS2$^{3K->R}$–GFP line 4 displayed significantly less growth of *Pto* DC3000 than Col-0 wt plants.
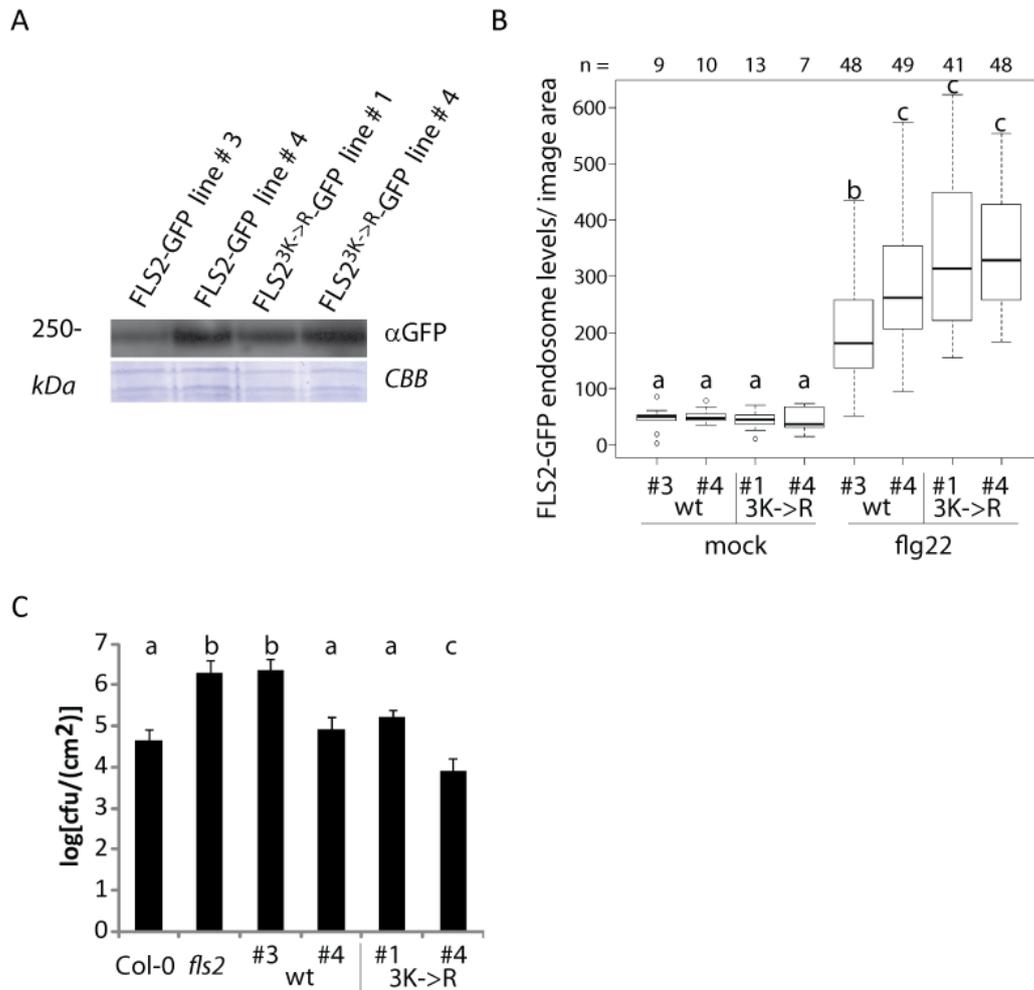
Figure 5 **FLS2 ubiquitination pattern contributes to immunity.** (A) FLS2-GFP protein levels of indicated lines were revealed by Western blot with anti-GFP antibody (upper panel). Coomassie staining (CBB) is included as loading control. (B) FLS2-GFP endosome were quantified in independent transgenic lines representing levels of lower and higher FLS2-GFP accumulation. Number of analyzed pictures are given by n. Similar results were obtained in two independent experiments (C) *Pto* DC3000 growth were quantified in four-week-old plants three days after spray inoculation with *Pto* DC3000. Error bars indicate standard deviations from eight plants. (B + C) Small letters indicate significant levels based on $P < 0.05$ calculated by multiple pairwise comparisons according to standard posthoc ANOVA analysis.

36

3.2.   FLS2 UNDERGOES ESCRT-MEDIATED SORTING

Ubiquitinated plasma membrane proteins are subjected to ESCRT-mediated protein sorting in animals and yeast (Raiborg and Stenmark, 2009). We studied ESCRT-1 mutants *vps28-2* and *vps37-1* in order to investigate, whether FLS2 endosomal trafficking involves ESCRT complexes. Both single T-DNA insertion lines accumulate no full-length transcripts (Suppl. Fig. 2) and showed previously increased disease development in *Pto* DC3000 infections (Salomon, 2009).

Interactions between ELC, VPS28-2 and VPS37-1 were previously shown in yeast-two hybrid assays and by bi-molecular fluorescence complementation (Shahriari et al., 2011). To test if ESCRT-1 components also localize to same subcellular compartment in plants, *VPS28-2, VPS37-1* and *ELC* was cloned from Col-0 cDNA and expressed as fluorescent-labeled fusion proteins under the control of the 35S promotor transiently in *N. benthamiana.* Three days after infiltration in leaves of five-week-old *N. benthamiana* plants*,* fluorescence-labeled vesicles were monitored by confocal microscopy (Figure 6). Fluorescent signals were mainly found in small vesicular structures, but occasionally also in the cytosolic and nucleus. A similar cellular distribution of ESCRT-3 subunit YFP-VPS4 was reported in *Arabidopsis* (Haas et al., 2007). In plant cells expressing all three constructs, ESCRT-1 subunits labeled the same vesicular compartment (Figure 6). ESCRT-1 vesicles were mobile and moved in a stop-and-go fashion with a velocity of approximately 0.5 µm/ seconds. This is in the range for previously described velocities of endosomal and pre-vacuolar vesicle movements in tobacco BY-2 cells (Ruthardt et al., 2005).
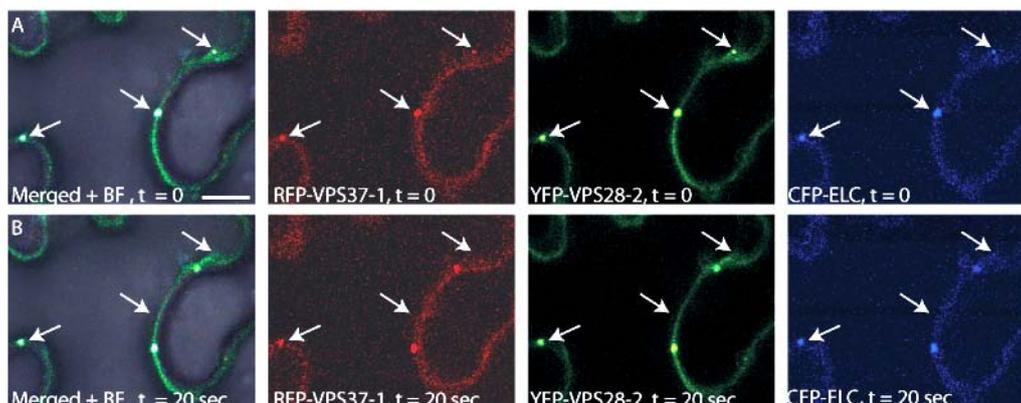
Figure 6   *Arabidopsis* **ESCRT-1 subunits co-localize to mobile vesicles in *N. benthamiana.*** (A) Representative confocal images show RFP-VPS37-1, YFP-VPS28-2 and CFP-ELC three days after transient co-expression in five-week-old *N. benthamiana* leaves at time point 0 (A) and in 20 seconds later (B). Arrows mark localization at time point 0. Bar presents 10 µm.

To monitor FLS2 endosomal trafficking in *Arabidopsis*, *VPS37-1* and *VPS28-2* constructs fused with *RFP* under the control of the *35S* promoter were stably introduced in *FLS2-GFP* plants. Although 30 T_1 transformed plants per line were recovered, only one single line could be further propagated due to sterility. ESCRT-associated genes play a curial role in embryogenesis (Spitzer et al., 2009). Constitutive over-expression of *VPS37-1* and *VPS28-2* could potentially interfere with embryogenesis. We are currently re-transforming Col-0 *pfls2::FLS2-GFP* as well as *vps28-2* and *vps37-1* T-DNA insertion lines to test this possibility. Noteworthy, T-DNA insertions in *VPS37-1* and *VPS28-2* cause no obvious growth or fertility phenotype as well as FLS2-GFP RFP-VPS28-2 double transgenic plants.

We analyzed FLS2-GFP RFP-VPS28-2 plants by sequential confocal imaging (Figure 7). RFP signals were exclusively observed at vesicular structures. Incubation of FLS2-GFP RFP-VPS28-2 plants for 35 min in 10 µM flg22 induced FLS2-GFP endocytosis. A sub-population of FLS2-GFP containing endosomes co-localized thereby with RFP-VPS28-2 labeled vesicles (Figure 7). This suggests that endosomal sorting of plasma membrane receptors involves ESCRT containing compartments not only in yeast and animals, but also in plants.
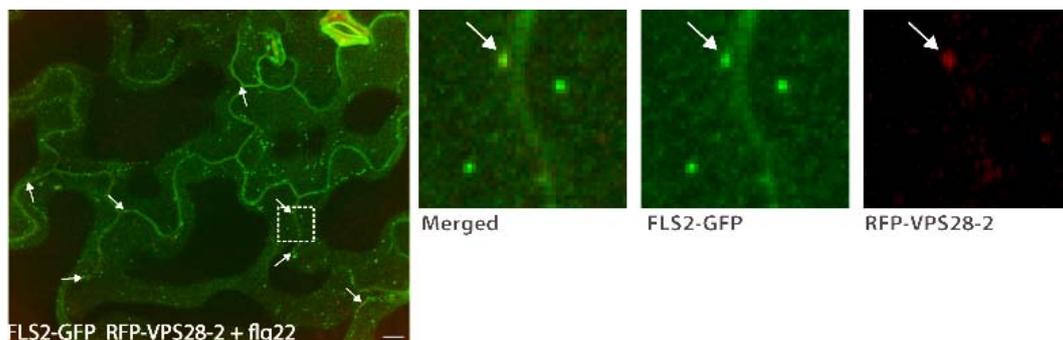
Figure 7   FLS2-GFP and VPS28-2 co-localization in response to flg22. Detached cotyledons of two-week-old FLS2-GFP RFP-VPS28-2 plants were incubated in 10 µM flg22 for 35 min and imaged by sequential automated confocal microscopy. Representative GFP and RFP fluorescence micrographs of optical cross-sections of epidermal cells are merged in the left panel and shown in detail (dashed box) in right panels. Arrows indicate overlapping FLS2-GPF and RFP-VPS28-2 signals. Bars: 10 µm.

Next FLS2-GFP was crossed into *vps28-2* and *vps37-1* mutants to test if ESCRT-1 genes could regulate FLS2 endosome levels. We investigated FLS2-GFP protein levels in homozygous F_3 progeny and evaluated FLS2-GFP protein levels by Western blots. FLS2-GFP accumulated to similar levels in wt and *vps37-1* mutants, but protein levels of FLS2-GFP was reduced in *vps28-2* mutant backgrounds (Figure 8 A). Similar results were observed in a second independent *vps28-2* FLS2-GFP line. Notably, endogenous FLS2 protein accumulated to wt levels in *vps28-2* mutants non-transgenic for FLS2-GFP (Figure 9 B). Since transgene expression can influence FLS2-GFP endosome quantifications (Figure 5), FLS2-GFP endosome quantification in *vps28-2* FLS2-GFP plants has to be taken with care.

After triggering FLS2 endocytosis with flg22, both *ESCRT-1* mutants displayed significant lower numbers of FLS2-GFP endosomes compared to wt FLS2-GFP plants (Figure 8 B). Due to lower FLS2-GFP levels, fewer images could be analyzed for *vps28-2*. In average we observed a reduction of FLS2-GFP endosomes of about 23 % in *vps37-1* and 47 % in *vps28-2,* respectively. In addition, we frequently observed a more peripheral localization of FLS2-GFP endosomes in *ESCRT-1* mutants even 45 min after flg22 treatment, when FLS2-GFP vesicles appeared to be randomly distributed in wt cells (Figure 8 C). Peripheral localization of FLS2-GFP endosomes was more pronounced in *vps28-2*, but also occurred in *vps37-1* mutants (Figure 8 C).
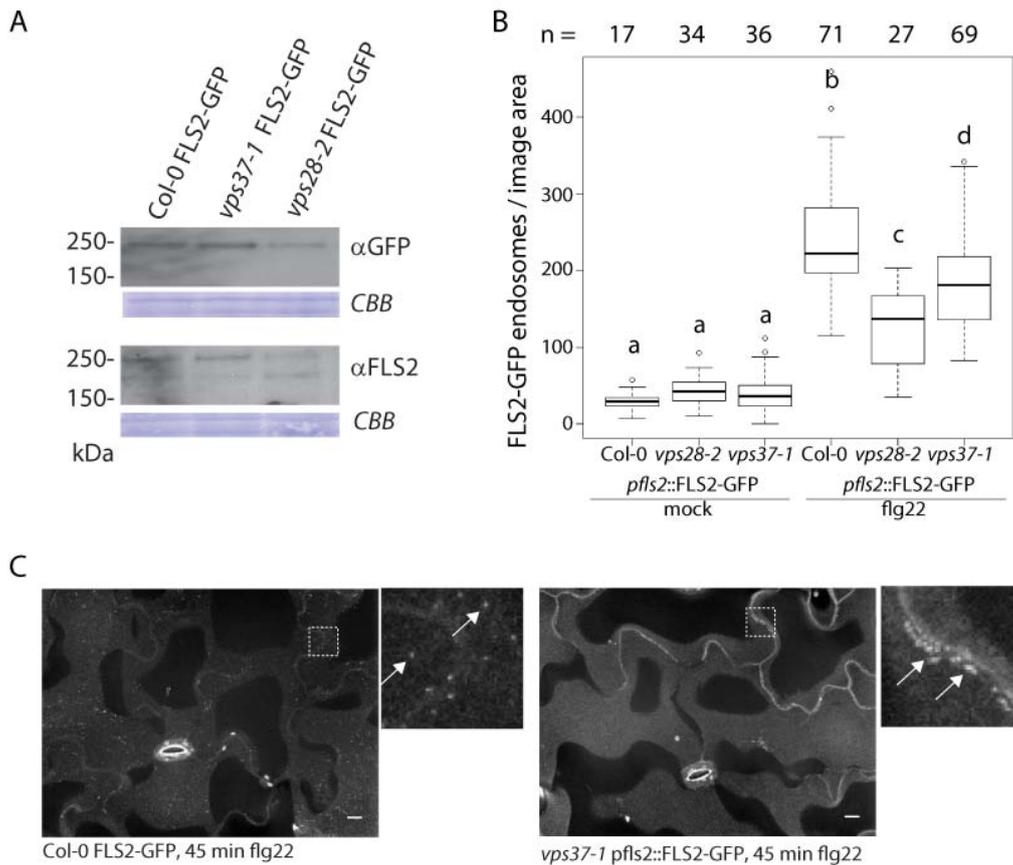
Figure 8 **ESCRT-1 regulates FLS2 endosome levels.** (A) FLS2-GFP protein levels of the indicated genotypes revealed by Western blot with anti-GFP antibody (upper panel) and anti-FLS2 antibody (lower panel). Coomassie staining (CBB) is included as loading control. (B) FLS2-GFP endosomal numbers of indicated genotypes after mock treatment and in the presence of 10 µM flg22 were quantified by automated confocal microscopy. Endosomal numbers of n-analyzed Z-projections from three independent experiments are illustrated by boxplots. Letters indicate significant differences at the level of $P < 0.05$ as revealed by multiple pairwise comparisons according to standard posthoc ANOVA analysis. (C) Representative image show endosome distributions in Col-0 FLS2-GFP and *vps37-1* FLS2-GFP after 45 min of flg22 treatment. Bars: 10 µm.

We studied *vps37-1* and *vps28-2* mutants in more detail to determine the contribution of ESCRT-1 genes in PAMP signaling. Flg22-induced ROS production is one of the earliest measurable PAMP responses. Both mutants showed no significant differences in flg22-induced ROS production (Figure 9 A). Notably, endocytosis-deficient FLS2$^{\Delta PEST}$ mutant is also not impaired in flg22-induced ROS burst (Salomon and Robatzek, 2006). Interestingly, *vps37-1* or *vps28-2* mutants displayed a slightly elevated ROS accumulation compared to Col-0 wt plants, when plants were challenged with flg22 four hours after an initial flg22-induced ROS burst (Suppl. Fig. 5)*.*

It has been reported that the endosome trafficking inhibitor wortmanin reduces flg22-induced MAPK activation (Lambris, 2007). We compared therefore kinetics of MAPK phosphorylation in response to flg22 by Western blots with anti-pERK antibodies. In Col-0, *vps28-2* and *vps37-1* anti-pERK labelling was strongest after 15 min of flg22 treatment and decreased in samples treated for 60 min with flg22 (Figure 9 B). No obvious differences in intensities were observed between Col-0 and *vps28-2* or *vps37-1,* respectively.
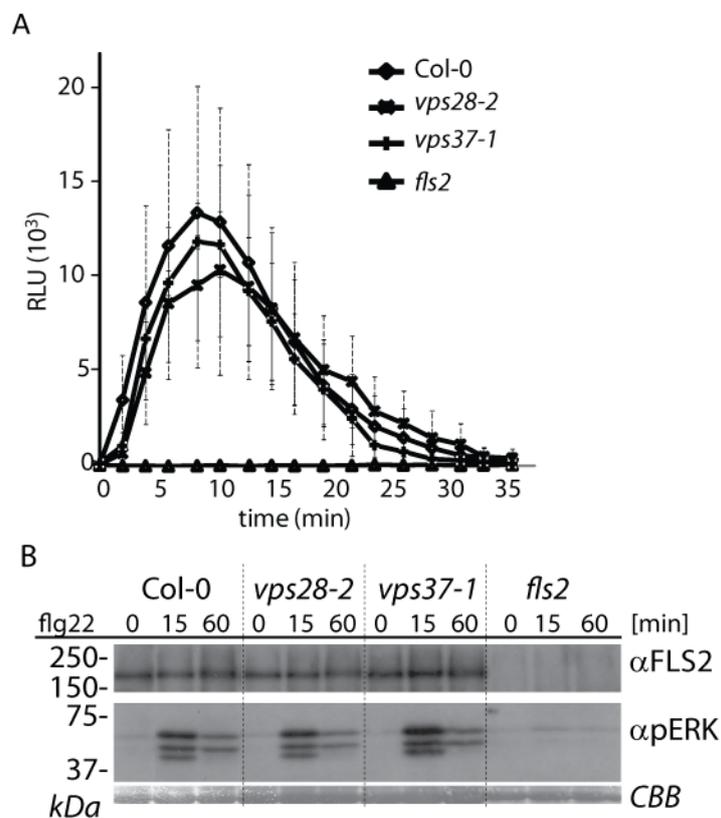
Figure 9 **flg22-triggered ROS burst and MAPK activation is unaltered in ESCRT-1 mutants.** (A) Flg22-triggered ROS production was measured in 16 leaf discs of eight independent four-week-old plants of indicated genotypes. Graphs present mean values +/- SD. Similar results were obtained in three independent results. RLU: relative light units. (B) Total FLS2 protein levels of indicated genotypes are revealed by Western blot with anti-FLS2 antibody (upper panel) and phosphorylation of MAPKs by anti-pERK antibody (middle panel). Proteins were extracted from two-week-old seedlings 0, 15 and 60 min after flg22 treatment. Coomassie staining (CBB) is included as loading control (lower panel).

Transcriptional reprogramming by flg22 or other PAMPs is generally assessed 30 min to 60 min after treatment (Zipfel et al., 2006) and coincides temporal with FLS2 endosome maturation (Robatzek et al., 2006). To test whether *vps28-2* and *vps37-1* mutants are impaired in flg22-dependent gene induction, we analyzed *FLS2, FLG22-INDUCED RECEPTOR-LIKE KINASE 1* (*FRK1*), and *WRKY22* transcripts abundance after 60 min of flg22 treatment (Figure 10 A). We observed no significant differences in *FLS2, FRK1* and *WRKY22* steady-state transcript levels between Col-0 wt, *vps28-2* and *vps37-1* mutants at time point 0. Flg22 induced the expression of all three marker genes in Col-0 wt, *vps28-2* and *vps37-1* mutants. In contrast to Col-0 wt plants, *vps28-2* and *vps37-1* mutants accumulated significantly less *FLS2* and *FRK1* transcripts 60 min after flg22 induction. Only minor differences were observed in *WRKY22* induction. A slight up-regulation of *WRKY22* transcript was also measured in *fls2* mutants, presumably due to non-flg22 related stresses as previously reported (Lee et al., 2005).

Reduced flg22-induced marker gene expression points at impaired immunity. One of the first layers in anti-bacterial immunity is stomatal closure (Melotto et al., 2006). We analyzed flg22-induced stomatal closure in *vps28-2* and *vps37-1* mutants (in collaboration with Dr. Gildas Bourdais, The Sainsbury Laboratory Norwich, UK). In Col-0 wt plants as well as in *vps28-2* and *vps37-1* mutants stomatal apertures were open under control conditions with an average width-to-length ratio of approximately 0.5 (Figure 10 B). In presence of flg22 the population of stomata with open apertures shifted significantly to apertures with lower width-to-length ratios, indicative of closing apertures in Col-0 wt plants, but not in *vps28-2* and *vps37-1* mutants (Figure 10 B). We also tested stomata response to ABA and observed no significant differences between wt and *vps28-2* or *vps37-1* mutants, respectively (Suppl. Fig. 3).
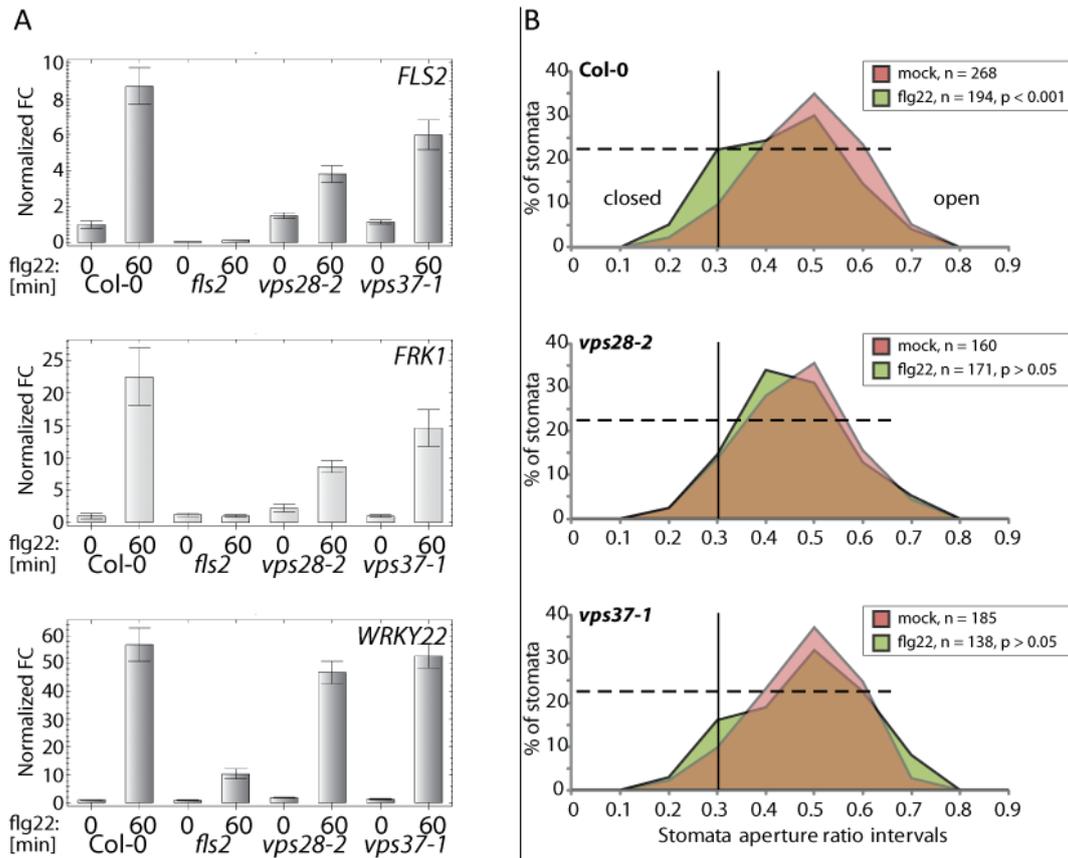
Figure 10 *ESCRT-1* **mutants** *vps28-2* **and** *vps37-1* **are impaired in flg22-responses.** (A) Transcript levels of *FLS2, FRK1* and *WRKY22* were measured by quantitative real-time PCR. Actin2 was used as control. Bars illustrate transcript levels before (0) and after 60 min incubation in 5 µM flg22 solution. Error bars indicate standard deviations based on n = 3 samples. Similar results were obtained in three independent experiments. (B) Relative distributions of stomata related to their aperture were measured in indicated genotypes without flg22 (red) and in the presence of 5 µM flg22 (green). Number of total stomata are given by n. P values were calculated by multiple pairwise comparisons according to standard posthoc ANOVA analysis.

Reduced defense responses in *vps28-2* and *vps37-1* might increase susceptibility to pathogens as both *ESCRT-1* mutant were reported previously to develop more disease symptoms in *Pto* DC3000 spray infections than wt plants (Salomon, 2009). To determine if enhanced disease development and decreased flg22 responses correlated with increased pathogen growth, four-week-old *vps28-2*, *vps37-1* mutants and control plants were spray inoculated with *Pto* DC3000. Growth was quantified four days after infection. Both *ESCRT-1* mutants allowed significant higher *Pto* DC3000 multiplication than wild-type plants (Figure 11 A). *Vps28-2* and *vps37-1* displayed similar levels of susceptibility to *Pto* DC3000, which was below bacterial growth observed in *fls2* mutants.

Other *Arabidopsis*-pathogen interactions were investigated to determine if increased susceptibility of *vps28-2* and *vps37-1* is restricted to *Pto* DC3000. *Hyaloperonospora arabidopsidis* (*Hpa*) is a well-studied obligate-biotrophic oomycete, which specifically infects certain *Arabidopsis thaliana* ecotypes (Coates and Beynon, 2010). Two-week-old wt plants, *vps28-2* and *vps37-1* and super-susceptible *eds1* mutants (Aarts et al., 1998) were inoculated with *Hpa* strain Waco9. Pathogen reproduction was assessed by counting spores seven days after infection. Compared to Col-0 wt plants, significantly more spores were isolated from *vps28-2* and *vps37-1* mutants (Figure 11 B). Susceptibility of *vps28-2* and *vps37-1* mutants did not reach the level of *eds1* mutants, indicating that immunity in *vps28-2* and *vps37-1* is only partially affected.
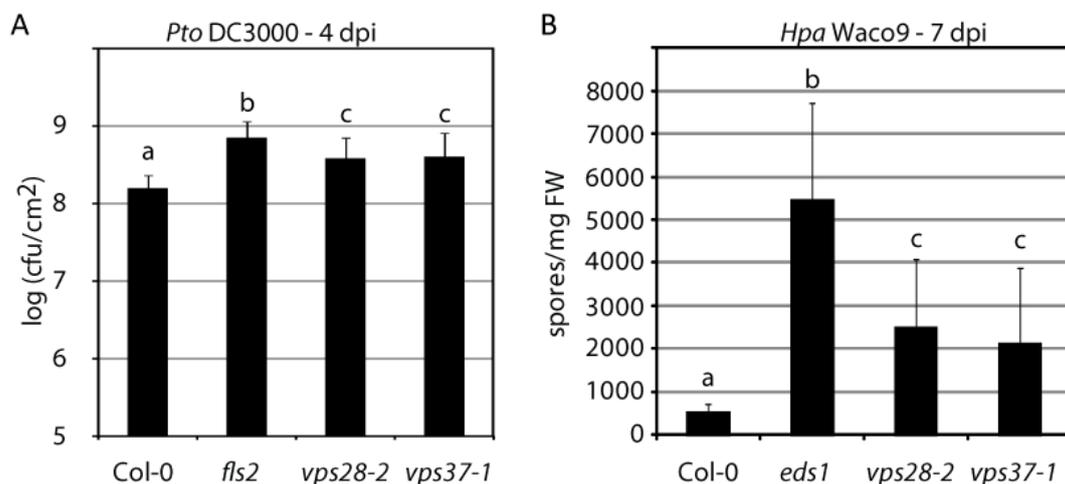
Figure 11   ESCRT-1 mutants are more susceptible to biotrophic pathogens. (A) Average bacterial growth was analyzed four days post infection in eight four-week-old plants per genotype. (B) Spores of *Hpa* Waco9 were quantified seven days post infection on eight two-week-old seedlings. (A + B) Both experiments were repeated twice with similar results. Different letters indicate statistically significant of P < 0.05 calculated by multiple pairwise comparisons according to standard posthoc ANOVA analysis. Error bars show SD.

We used FLS2-GFP RFP-VPS28-2 plants (Figure 7) to study the sub-cellular localization and dynamics of RFP-VPS28 containing vesicles during infection with *Hpa* Waco9. Plants were analyzed by confocal microscopy four days after inoculation. At that time point, several *Hpa* hyphae and haustoria were formed in infected plants, but no sporangia were yet developed (Figure 12). RFP signal were retrieved from small vesicles, which clustered around haustorial projections (Figure 12). Vesicles showed relatively low motility compared to analysis of RFP-VPS28-2 in not infected plants (Figure 6).
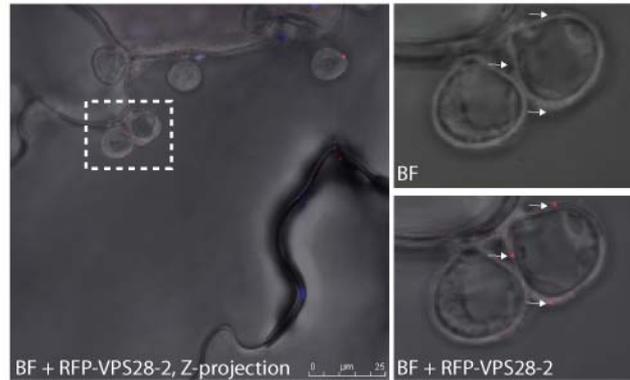
Figure 12 VPS28-2 resides close to *Hpa* infection sites. Representative confocal images of RFP-VPS28-2 expressing plants infected with *Hpa* Waco9 were taken 4 days after inoculation. RFP and bright field (BF) Z-projections of five confocal images spaced by 1 µm are shown in the left panel. Single confocal planes of haustria projection (dashed white box) in bright field (upper left panel) merged with RFP signals (lower right panel) are shown in detail. Localization of RFP signal is highlighted by white arrows. Scale bar indicates 25 µm.

In summary, our data revealed that two *ESCRT-1* mutants, *vps28-2* and *vps37-1*, were impaired in immunity to *Pto* DC3000 and *Hpa* Waco9. Higher susceptibility to *Pto* DC3000 correlated with partially reduced flg22-triggered gene induction and loss of flg22-induced stomatal closure. Other tested flg22-responses were not significantly different from wild-type plants. We furthermore observed, that FLS2-GFP endosomes co-localized to RFP-VPS28-2 labeled vesicles in an flg22-dependent manner. Late endosomal sorting of ubiquitinated plasma membrane proteins by ESCRT complexes has been shown in yeast and animals (Wegner et al., 2011), but so far not in plants.

Higher susceptibility of *vps37-1* correlated with reduced FLS2 endosome numbers in response to flg22. Reduced FLS2 endosome numbers were also observed in *vps28-2*, but this could be a result of lower FLS2-GFP protein accumulation in *vps28-2* FLS2-GFP plants. Likewise, enhanced resistance to *Pto* DC3000 infections of a putative FLS2 ubiquitination mutant (FLS2$^{3K->R}$) correlated with slightly higher FLS2-GFP endosome numbers.

3.3.   *FLI1* REGULATES LATE FLG22 RESPONSES

Temporal control of early and late PAMP responses is genetically poorly understood. In order to identify specific late PAMP response regulator, a gamma-irradiated *Arabidopsis* L*er* population was screened for reduced seedling growth arrest in presence of flg22 (Salomon, 2009). Candidates with reduced ROS production were excluded from further analysis to counterselect for receptor mutants and early signaling regulators. These resulted in the isolation of six *flagellin insensitive* mutants *(fli1-6)* (Salomon, 2009). *Fli1* mutant line displayed the most severe phenotypes and was chosen for further analysis.

Flg22-indiced seedling growth arrest is a commonly used read out for late PAMP-responses (Boller and Felix, 2009). We assessed flg22-induced growth arrest in one-week-old etiolated seedlings by measuring primary root length in the absence and presence of flg22 (Figure 13 A). Seedlings grown in the absence of flg22 showed similar root length in wt plants, *fls2* and *fli1* mutants. With increasing flg22 concentrations wt and *fli1* plants displayed decreasing root length. Root length reduction was thereby approximately 30 % less affected in *fli1* mutants compared to L*er* wt plants. Reduced flg22 responsiveness in *fli1* appeared in a dose-dependent manner as similar root growth inhibition to L*er* wt in the presence of 100 nM flg22 could be observed, when *fli1* was treated with 500 nM flg22. Significant differences in flg22 responsiveness were also measured between *fli1* and Col-0 wt plants, although less pronounced.

Inhibition of root growth is a common stress response and also observed under high NaCl (Cazale et al., 2009) or high glucose conditions (Baena-Gonzalez et al., 2007). To test whether *fli1* mutants exhibit reduced sensitivity to other stresses than flg22, we measured root growth in presence of increasing concentrations of NaCl (Figure 13 B) and glucose (Figure 13 C). Roots of L*er* wt plants, *fls2-17* and *fli1* showed no significant differences in dose-dependent root growth inhibition on NaCl and glucose containing media. We therefore concluded that reduced flg22 sensitivity is unlikely to be caused by a general stress dysfunction.
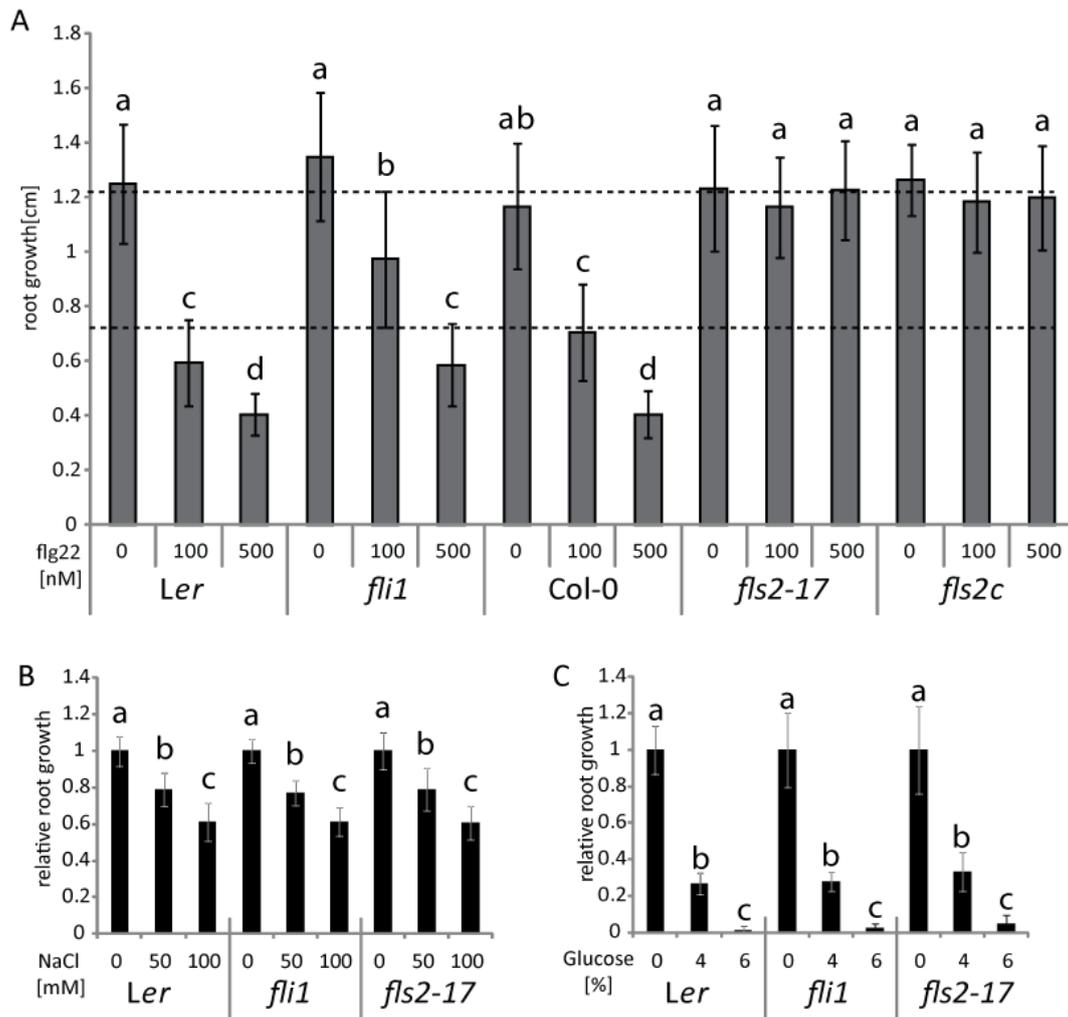
Figure 13 Root growth phenotypes of *fli1*. (A) Seedlings of indicated genotypes were grown in the dark on plates containing different flg22 concentrations. Primary root length of 20 seedlings per condition was measured one week after germination. Col-0 *fls2* mutant is depicted as *fls2c.* Dashed lines illustrate +/- SD of *fli1* grown on 100 nM flg22. (B + C) Indicated genotypes were grown for one week on MS plates and then transferred on plates with increasing concentrations of NaCl (B) or glucose (C). Primary roots of 20 seedlings per genotype and condition were measured after one week. Root growth in (B) and (C) is related to root growth under control conditions of indicated genotypes. (A+B+C) Bars present mean values +/- SD and different letters show statistically significance of P < 0.05, calculated by multiple pairwise comparisons according to standard posthoc ANOVA analysis. Experiments were repeated at least once with similar results.

Four-week-old *fli1* mutants were previously reported to be severely impaired in flg22-callose depositions (Salomon, 2009). Because we carried out most of our studies on two-week-old seedlings, we investigated flg22-triggered callose deposition accordingly. Two-week-old seedlings of L*er* wt, *fls2-17* and *fli1* mutants were incubated in flg22 solution and stained for callose (Figure 14). Compared to mock treated seedlings, a strong accumulation of stained callose deposits were detected in wt seedlings, to lesser extent in *fli1* mutants and not in *fls2-17* mutants.
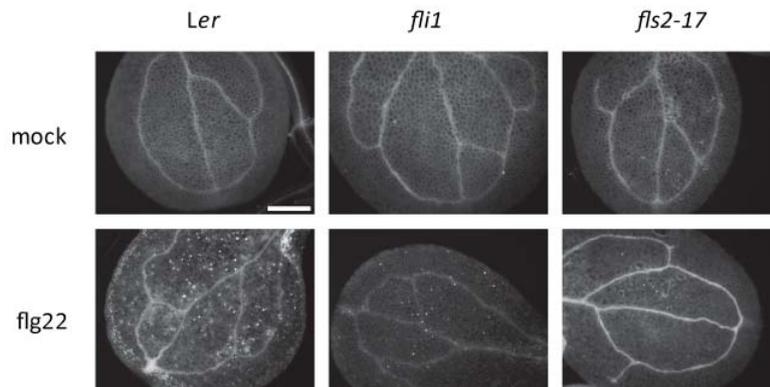
Figure 14 *fli1* **is impaired in flg22-triggered callose deposition.** (A) Two-week-old seedlings were incubated for 12 hours in the absence (upper panel) or in the presence of 1 µM flg22 (lower panel). Representative images of aniline blue stained callose deposits in cotyledons from ten analyzed seedlings per indicated genotype and condition are shown. Scale bar presents 100 µm.

Quantifying flg22-induced resistance is an often used method to assess PTI function (Zipfel et al., 2004; Tsuda et al., 2009). To test whether impaired late PAMP responses in *fli1* mutants are associated with reduced flg22-induced resistance, we pre-treated wt plants, *fls2-17* and *fli1* mutants with or without flg22 prior to syringe infiltration with *Pto* DC3000 (Figure 15). As shown previously (Zipfel et al., 2004), no significant differences in bacterial growth was observed between L*er* and *fls2-17* plants in mock infiltrated plants. Notably, bacteria grew to similar levels in mock treated *fli1* mutants than in mock treated L*er* wt plants, indicating that *fli1* mutants were not generally affected in post-invasive immunity (Figure 15 A). By contrast, in flg22 pre-treated plants significantly less *Pto* DC3000 growth was quantified in L*er* wt plants than in *fli1* and *fls2-17* mutants (Figure 15 B). These results point at impaired flg22-induced resistance in *fli1* and suggest a pivotal role of *FLI1* in the pre-invasive infection phase as previously reported for *FLS2* (Zipfel et al., 2004).
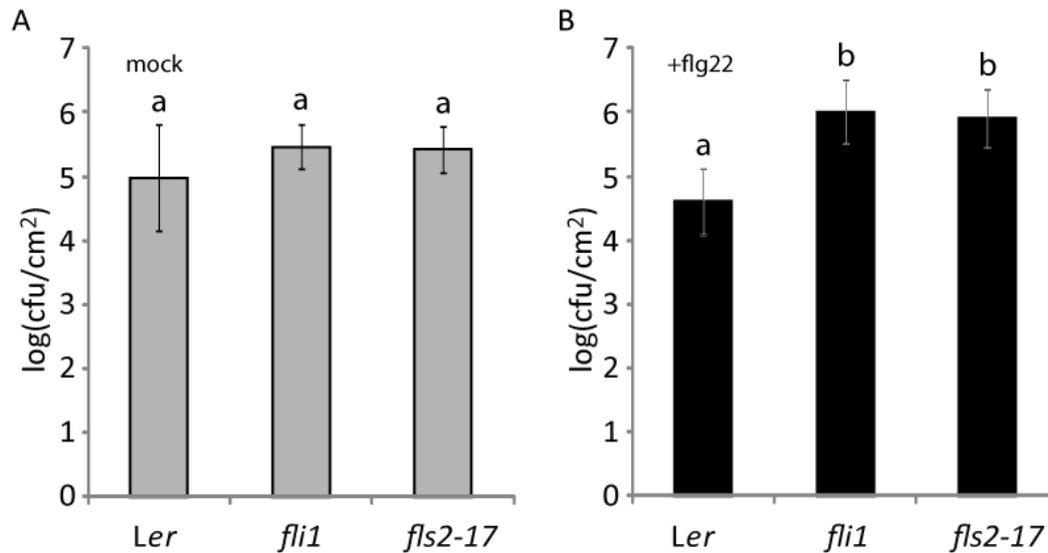
Figure 15 **Flg22-induced resistance is impaired in *fli1* plants.** Four-week-old plants were infiltrated with 10 mM MgCl$_2$ (A) or 1 µM flg22 in 10 mM MgCl$_2$ solution (B). 24 hours after pre-treatment plants were syringe-infiltrated with *Pto* DC3000 and bacterial replication was assessed in eight plants per indicated genotype and condition two days post infection. Bars show mean values +/- SD. Different letters indicate statistically significance of P < 0.05, calculated by multiple pairwise comparisons according to standard posthoc ANOVA analysis. Experiments were repeated twice with similar results.

Flg22-triggered stomatal closure is discussed to account for the important role of FLS2 in pre-invasive immunity (Melotto et al., 2006; Zhang and Zhou, 2010). We studied stomatal closure in response to flg22 in *fli1*, wt and *fls2-17* (Figure 16). Width-length ratios of stomatal apertures in wt, *fli1,* and *fls2-17* showed no significant differences under control conditions (Figure 16). Incubation in flg22 solution triggered significant lowered width-length ratios in wt and *fli1* mutants, but not in *fls2-17.* This indicates that higher susceptibility in *fli1* is not caused by impaired flg22-induced stomatal closure.
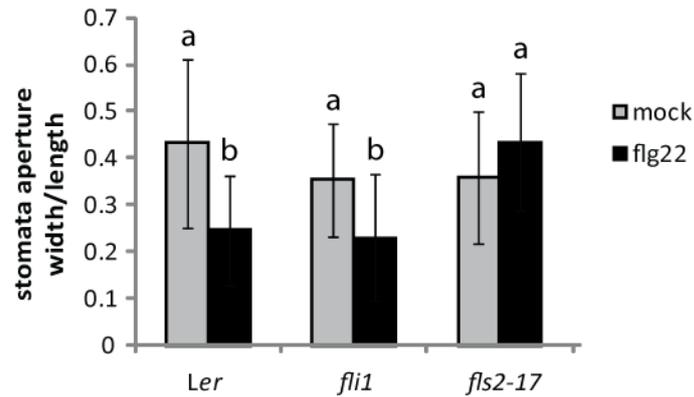
Figure 16 Flg22-induced stomatal closure is not impaired in *fli1* plants. Two-week-old seedlings of indicated genotypes were vacuum infiltrated with (black bars) or without flg22 (grey bars). Images of cotyledons were taken with Zeiss Axiophot microscope. 20 stomata apertures per genotype and condition were measured in ImageJ. Results shown are means +/- SD. Different letters indicate statistically significance of P < 0.05, calculated by multiple pairwise comparisons according to standard posthoc ANOVA analysis.

Mutants, previously reported to be impaired in flg22-induced resistance, PAMP induced seedling growth inhibition or callose deposition, but not in early PAMP responses are mainly linked to hormone homeostasis or gene silencing and exhibit sever developmental phenotypes (Navarro et al., 2006; Navarro et al., 2008; Li et al., 2010). In addition, reduced flg22-triggered callose deposition in callose synthase mutant *pmr4* is associated with elevated salicylic acid levels and increased resistance to biotrophic pathogens (Ham et al., 2007). *Fli1* did not resemble any of these phenotypes. To gain insight into the molecular events underlying the susceptibility phenotype of *fli1*, we analyzed transcriptomes of *fli1,* wt and *fls2-17* mutants during bacterial infection. Infections were carried out by spray-inoculation of two-week-old seedlings with virulent *Pto* DC3000 and RNA samples were collected at 0, 3 and 24 hours post infection and subjected to microarray hybridization (Dr. Bruno Huettel, MPIZP, ADIS, Cologne, Germany).

Transcriptome profiles of wt plants, *fli1* and *fls2-17* mutants at different infection time points were hierarchical clustered (Figure 17). This revealed that profiles can be grouped in three major classes representing the progression of infection. Between these classes, three hours post infection transcriptome profiles differed most compared to profiles of uninfected and the 24 hours infection time point. In all three genotypes 700 genes were more than two-fold higher expressed 3 hpi compared to uninfected plants (Table 8). Up-regulated genes were significantly enriched in genes associated with defense responses. 209 genes showed two-fold less transcript abundance after

three hours of infection compared to uninfected plants. Down regulated genes contained significantly more genes associated with plant metabolism. During transition from 3 to 24 hours post infection a total of 745 genes showed significantly different expression levels in all three genotypes. 234 of these genes were at least two-fold higher expressed at 24 hpi and overrepresented in genes regulated to biotic stimuli. The remaining 511 genes were at least two-fold lower expressed in all three genotypes and significantly enriched in abiotic stress responsive genes and genes with a predicted function in starch metabolism. Comparison between 0 hpi and 24 hpi showed an overrepresentation of defense genes. 98 less abundant genes at 24 hours were mainly enriched in transcription and nucleic acid metabolism.
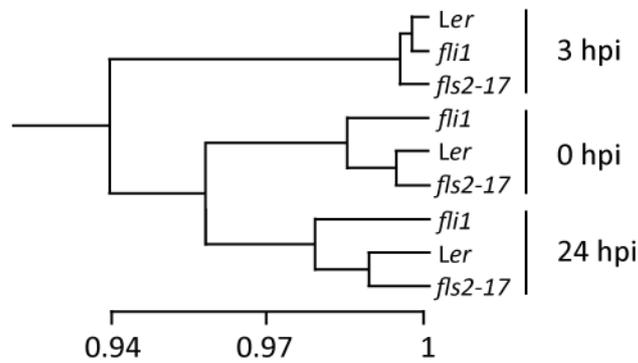
Figure 17   Transcriptional profiling of *fli1* and *fls2-17* during infection. Whole genome transcript array (Ath1, Affymetrix) of RNA collected from 21 two-week-old seedlings infected with *Pto* DC3000 for 0, 3 and 24 hours was used to detect changes in transcript abundances between L*er* wt, *fli1* and *fls2-17*. Transcript profiles were hierarchical clustered accordingly to expression levels.

**Table 8** Transcriptional changes in L*er wt, fli1* and *fls2-17* during infection with *Pto* DC3000.

Transition (hpi)	regulation	Number of genes[a]	GO enrichment[b]	P value
0->3	up	700	response to stimulus	3.40E-12
			defense response	3.61E-11
	down	209	regulation of cellular process	6.99E-09
			regulation of metabolic processes	6.99E-09
3->24	up	234	response to biotic stimulus	0.0108
			response to other organism	0.0155
	down	511	response to abiotic stimulus	8.07E-07
			Starch metabolism	4.16E-06
0->24	up	272	response to stimulus	3.41E-06
			defense response	8.52E-06
	down	98	regulation of transcription	0.000545
			nucleotide and nucleic acid metabolic process	0.000545

[a] Transcriptional changes were determined from whole genome transcript arrays of L*er*, *fli1* and *fls2-17* at 0, 3 and 24 hpi. Numbers represent genes with transcriptional up or down-regulation of at least two-fold with an adjusted P value of < 0.05 in all three genotypes.

[b,c] Two most significant Gene Ontology classes and corresponding P values were obtained from GO Stat (Beissbarth and Speed, 2004).

The smallest variation within in the three major transcriptome clusters was observed at three hours post infection profiles *(*Figure 17). Only two transcripts were significantly altered by two-fold in L*er* and *fli1*, and six genes were specifically at least two-fold lower or higher expressed in *fls2-17* (Figure 18). A complete list of genes with significantly altered transcript levels in *fls2-17* is given in Table 9. Several genes implicated in plant defense or oxidative stress were found to be lower expressed in *fls2-17* mutants, including *1-AMINOCYCLOPROPANE-1-CARBOXYLATE OXIDASE 2* (*ACO2*). ACOs catalyze the last step of ethylene biogenesis and could therefore play an important role in ethylene-mediated defense responses. We studied *ACO2* transcripts abundances at 3 hpi in a Col-0 *fls2* T-DNA insertion line (*fls2c)*, which in contrast to *fls2-17* mutant accumulates no *FLS2* transcripts (Zipfel et al., 2004). We infected plants with virulent *Pto* DC3000 and non-virulent *Pto* DC3000 *hrcC* mutants and analyzed transcript levels by quantitative RT-PCR (Figure 19 A). Col-0 wt plants up-regulated *ACO2* transcripts upon infection with both pathogens, whereas *ACO2* transcript levels remained unaltered in Col-0 *fls2* as previously observed in L*er fls2-17* mutants*.* Ethylene was reported to promote *FLS2* transcript accumulation (Boutrot et al., 2010; Mersmann et al., 2010). Therefore, we also quantified *FLS2* expression in the same experiment, but did not observe a correlation between up-regulation of *AC02* and *FLS2* transcript levels (Figure 19 A).

The largest variation within in the three major transcriptome classes was observed 24 hours post infection (Figure 17). Wt plant showed at least two-fold higher transcript abundances of 48 genes, which did not cluster into any gene ontology pathway (Figure 18). 135 genes were at least two-fold higher expressed in *fls2-17* mutants and overrepresented in nucleasome assembly and chromatin remodeling associated genes. *Fli1* mutants displayed the most distinct expression profile at 24 hours post infection (Figure 17). A list of the ten lowest and highest expressed genes in *fli1* at 24 hpi is given in (Table 10). The total numbers of uniquely two-fold higher or lower expressed genes in *fli1* did not exceed those observed in L*er* and *fls2-17* plants (Figure 18). Higher expressed genes in *fli1* were significantly enriched in genes with a known function in photosynthesis. Several of higher expressed genes in *fli1* were previously also linked to sugar starvation, including *DARK INDUCIBLE 2* (*DIN2*) and sucrose invertase *AT3G06500* (Fujiki et al., 2000; Buchanan-Wollaston et al., 2005; Baena-Gonzalez et al., 2007; Veyres et al., 2008).
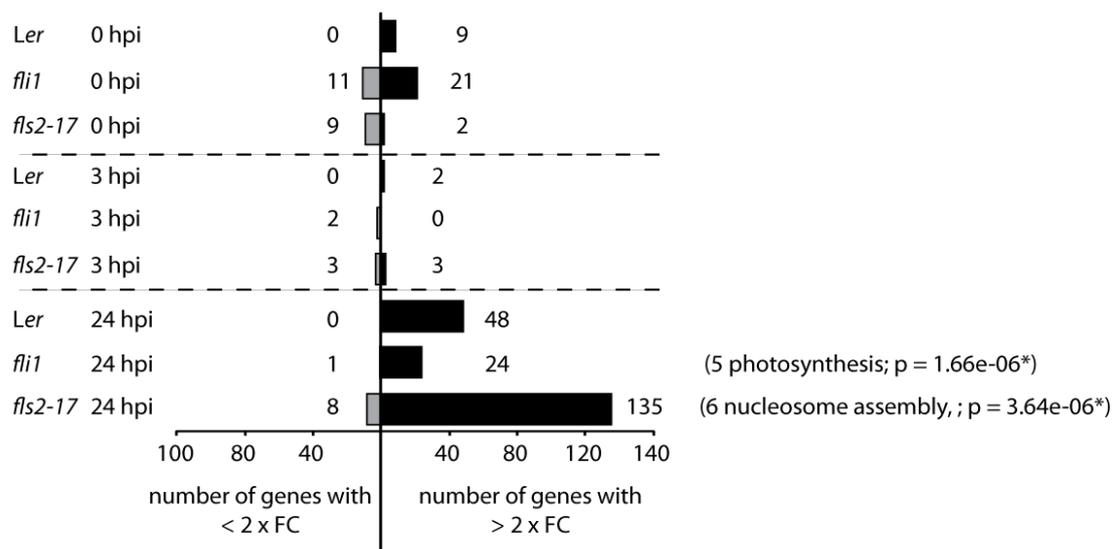
Figure 18 **Number of differently expressed genes between L*er, fli1* and *fls2-17.* Genes with an adjusted P value of < 0.05 and at least two-fold (FC) lower (left panel) or higher (right panel) abundance in indicated genotypes are listed according to different time points after *Pto* DC3000 infection. Enrichment of genes associated with gene ontology pathways include numbers of identified genes and corresponding P value according to Beissbarth and Speed (2004).

Table 9   **Genes differently expressed in *fls2-17* after 3 hours of infection with *Pto* DC3000**

Gene	Encoded protein	Fold change *wt* vs. *fls2*	Fold change *fli1* vs. *fls2*
Significantly **lower** expressed genes (adjusted P value < 0.05)			
AT5G42540	XRN2 (EXORIBONUCLEASE 2)	-3.1	-3.3
AT3G49360	glucosamine/galactosamine-6-phosphate isomerase	-2.7	-2.8
AT2G28630	beta-ketoacyl-CoA synthase family protein	-2.1	-2.1
AT1G78460	SOUL heme-binding family protein	-2.0	-2.3
AT1G63430	leucine-rich repeat transmembrane protein kinase	-1.9	-1.2
AT1G63770	peptidase M1 family protein	-1.8	-1.2
AT1G63810	Unknown protein	-1.8	-1.2
AT2G44790	UCC2 (UCLACYANIN 2); copper ion binding	-1.8	-1.7
AT1G63700	YDA (YODA); kinase	-1.8	-1.2
AT1G73330	ATDR4 (Arabidopsis thaliana drought-repressed 4)	-1.8	-1.3
AT1G69720	HO3 (HEME OXYGENASE 3);	-1.7	-1.5
AT4G38080	hydroxyproline-rich glycoprotein family protein	-1.7	-1.4
AT1G63460	glutathione peroxidase, putative	-1.7	-1.1
AT5G44910	TIR-NBS-LRR protein	-1.7	-2.2
AT1G68600	similar to unknown protein	-1.6	-1.2
AT1G62380	ACO2 (ACC OXIDASE 2)	-1.4	-1.3
AT2G25350	phox (PX) domain-containing protein	-1.4	-1.3
AT1G52870	peroxisomal membrane protein-related	-1.4	-1.3
Significantly **higher** expressed genes (adjusted P value < 0.05)			
AT4G21100	DDB1B (DAMAGED DNA BINDING PROTEIN 1 B)	4.7	5.5
AT5G50360	unknown protein	2.0	2.1
AT1G61580	ARP2/RPL3B (ARABIDOPSIS RIBOSOMAL PROTEIN 2)	1.7	1.3
AT4G24450	ATGWD2/GWD3/PWD	1.5	1.4
AT2G19990	PATHOGENESIS-RELATED PROTEIN-1-LIKE	1.5	1.1
AT2G33620	DNA-binding family protein	1.4	1.2
AT2G38195	protein binding / zinc ion binding	1.4	1.3

**Table 10   Ten most differentially expresses genes in *fli1* after 24 hours of infection with *Pto* DC3000**

Gene [a]	Encoded protein	Fold change *wt* vs. *fli1*	Fold change *fls2* vs. *fli1*
Top ten significantly **higher** expressed genes (adjusted P value < 0.05)			
AT3G60140	**DIN2 (DARK INDUCIBLE 2);**	**6.5**	**2.0**
ATCG00350	**PsaA (photosystem I)**	**4.5**	**3.2**
ATCG00270	**PsbD (photosystem II)**	**4.3**	**3.0**
AT1G61810	BGLU45; hydrolase, hydrolyzing	3.9	3.2
AT4G16990	disease resistance protein (TIR-NBS class), putative	3.9	1.7
AT3G06500	**Sucrose invertase, putative / saccharase, putative**	**3.8**	**2.4**
ATCG00500	beta subunit of the Acetyl-CoA carboxylase (ACCase)	3.6	2.5
ATCG00770	chloroplast 30S ribosomal protein S8	3.4	2.1
ATCG00180	RNA polymerase beta' subunit-1	3.0	1.9
ATCG00120	alpha subunit of ATP synthase and part of the CF1 portion	3.0	2.9
Top ten significantly **lower** expressed genes (adjusted P value < 0.05)			
AT2G42560	LEA domain-containing protein	-2.8	-2.2
AT5G07530	GRP17 (Glycine rich protein 17)	-2.7	-2.8
AT1G32290	unknown protein	-2.7	-2.1
AT1G24620	polcalcin, putative	-2.6	-2.1
AT3G22121	other RNA	-2.6	-3.0
AT4G29340	PRF4 (PROFILIN 4); actin binding	-2.6	-2.1
AT2G14700	unknown protein	-2.5	-1.7
AT4G02660	WD-40 repeat family protein / beige-related	-2.5	-1.5
AT4G19770	glycosyl hydrolase family 18 protein	-2.5	-2.2
AT5G09970	cytochrome P450, family 78,	-2.5	-1.4

[a]   Transcripts of highlighted genes were quantified by qRT-PCR in independent infections.

We tested transcriptional responses in wt plants, *fli1* and *fls2-17* mutants in independent *Pto* DC3000 infections by quantitative RT-PCR of selected genes (Figure 19 B). Enhanced expression of *DIN2* and *AT3G06500* encoding a putative sucrose invertase was repeatedly detected in *fli1* but not in wt plants. Up-regulation was also observed in *fls2-17* mutants. Expression of *PHOTOSYSTEM I APOPROTEIN A* (*PsaA*) was not significantly different expressed in *fli1* and L*er* wt or *fls2-17* in independent infections. In all three genotypes, expression of *PsaA* was lower at late stages of infection. This stands in contrast to data obtained from microarray experiments, where high expression of *PsaA* was maintained in *fli1* during infection. *PHOTOSYSTEM II APOPROTEIN D* (*PsbD*) was higher expressed in *fli1* when compared to L*er* wt, but lower when compared to *fls2-17* mutants

at 48 hpi. Relative transcript levels of both genes varied significantly between different infections (Figure 21).

No significant enrichment of cellular pathways was found to be linked with genes lower expressed in *fli1* or *fls2-17,* respectively (Figure 18 and Table 10). In summary, our transcription profiling did not clearly point at any cellular pathway, which was robustly and specifically impaired in *fli1* mutants during infection with *Pto* DC3000. By contrast, *fli1* plants showed a remarkable similar early transcriptional response to wt plants. This is in line with previous experiments showing wt-like early flg22-repsonses. Transcriptional profiles of *fli1* at late stages were most different from wt plants. This further strengthens the hypothesis for a role of *fli1* in late immune responses.
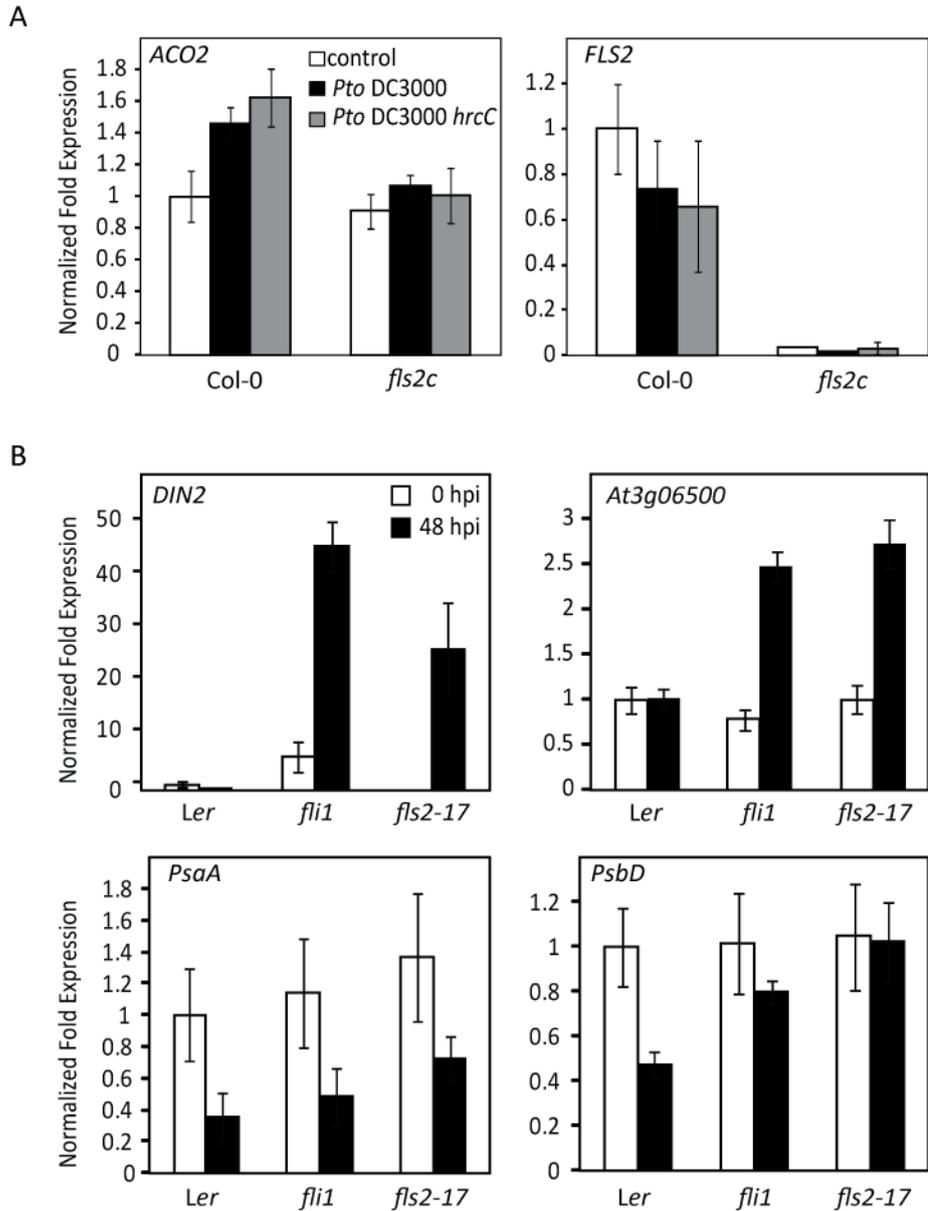
Figure 19 Differential gene expression in wt, *fli1* and *fls2* mutants during bacterial infections. (A) Transcript levels of *ACO2* and *FLS2* in Col-0 wt and *fls2* (*fls2c*) mutants were measured by quantitative RT-PCR in mock treated plants (white bars), or 3 hours after spray inoculation with virulent *Pto* DC3000 (black bars) or non-virulent *Pto* DC3000 *hrcC* mutants. (B) Indicated genes were quantified by qRT-PC in non-infected plants (white bars) or 48 hpi with *Pto* DC3000 (black bars) in L*er*, *fli1* and *fls2-17* mutants. (A + B) Bars present mean relative expression values +/- SD of three technical samples. *Actin2* was used as reference. Experiments were repeated with similar results in independent infections.

To identify the genetic mutation responsible for the *fli1* mutant phenotype, we combined classical map-based cloning with whole-genome sequencing analysis. Previous *fli1* map-based cloning approaches using flg22-induced seedling growth inhibition as phenotypical readout were hampered by small differences between *fli1* and Col-0 wt plants, which favored detection of false positives. We therefore used the most severe *fli1* phenotype, which is enhanced disease development in *Pto* DC3000 infections (Salomon, 2009). Two-week-old seedlings were spray inoculated with *Pto* DC3000 and disease symptoms visually evaluated after five days. Most *fls2-17* and *fli1* seedlings developed chlorosis and necrosis within this time. Necrotic and chlortic spots were in contrast only rarely observed on L*er* or Col-0 wt seedlings (Figure 20 A). In order to quantify *Pto* DC3000 susceptibility, disease symptoms were grouped in four classes, with macroscopic healthy plants in class 0 and severely diseased plants in class 3. We first tested, whether the enhanced disease phenotype of *fli1* is inherited in a recessive manner by crossing *fli1* mutants to L*er* wt plants. Disease development was assessed in bi-directional F_1 progeny. *Fli1* plants showed significant higher disease symptoms then L*er* wt plants and were indistinguishable from *fls2-17* mutant plant populations (Figure 20 B). Disease development in *fli1* x L*er* crosses was restored to wt levels, independent of the direction of analyzed crosses (Figure 20 B).

Fli1 was isolated from a mutagenized L*er* population along with five other *fli* mutants (Salomon, 2009). We analyzed F_1 crosses of *fli1* to other *fli* mutants to test potential allelic interactions between *fli1* and other *fli* mutations (Figure 20 B). *Fli2-6* showed no significant increase in disease development, when infected with *Pto* DC3000. This is in line with previous studies showing that susceptibility to *Pto* DC3000 of different *fli* mutants is most severely affected in *fli1* (Salomon, 2009). Notably *fli2*, *fli5* and *fli6* showed slightly elevated susceptibly and *fli6* was previously shown to allow higher multiplication of *Pto* DC3000 in bacterial counting assays compared to wt, but not compared to *fli1* mutants (Salomon, 2009). F_1 progeny of *fli1* crossed to *fli1*, *fli3* and *fli6* showed wt-like disease symptoms, indicating that underlying mutations are not allelic (Figure 20 B). Slightly higher disease symptoms were observed in *fli1* x *fli4* and *fli1* x *fli5* crosses, but did not reached the level of *fli1* susceptibility. Also L*er* x *fli4* and L*er* x *fli5* crosses were slightly more susceptible than L*er* wt plants (Figure 20 B).
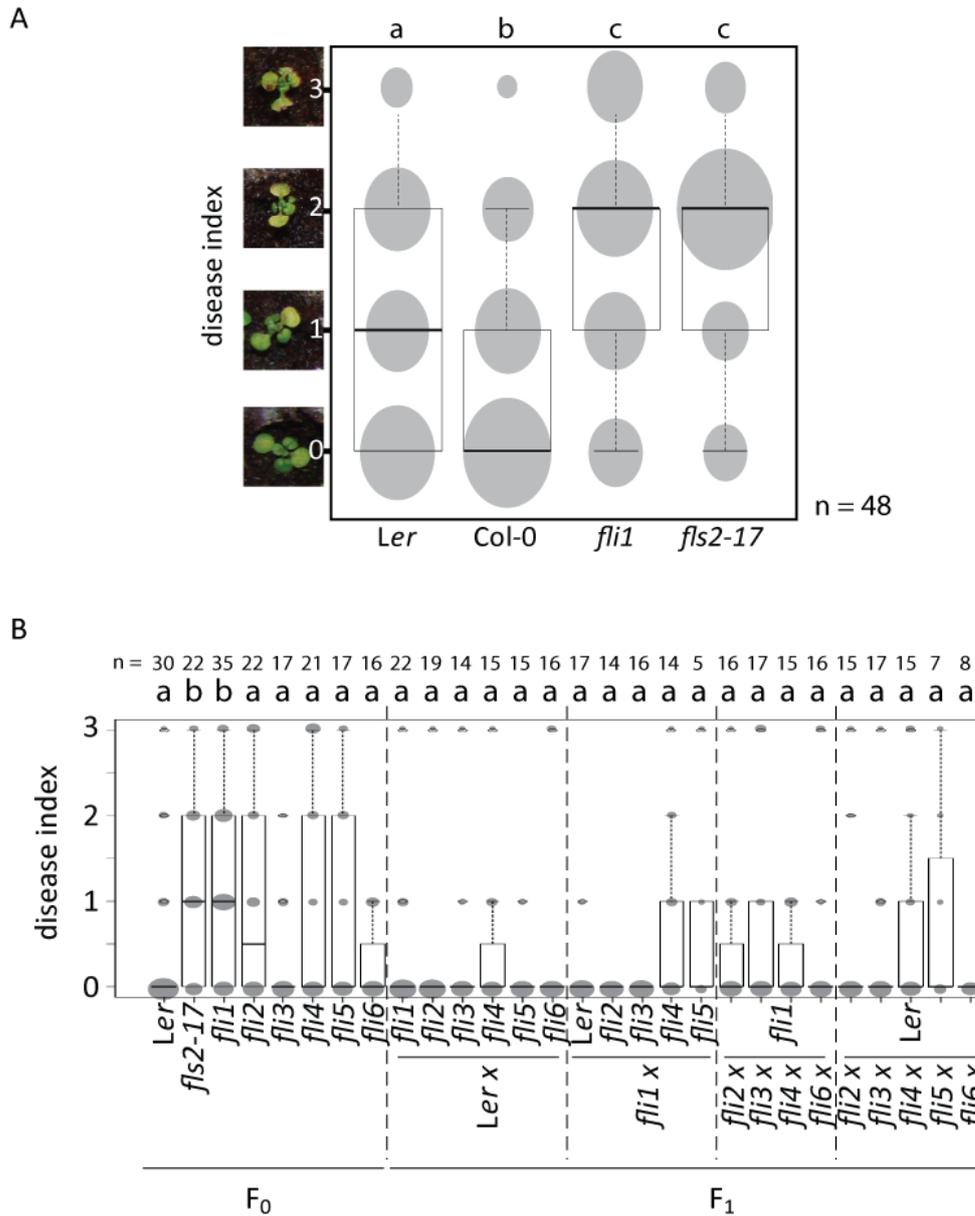
Figure 20 **Genetic analysis of** *fli1.* (A). 48 two-week-old seedlings were spray inoculated with *Pto* DC3000 and disease development categorized from healthy plants, class 0, to severely infected plants in class 3. Graphs show distributions of individuals per indicated genotype according to disease class. Grey circles represent proportions of plants grouped in one class. Different letters indicate statistically significance of $P < 0.05$, calculated according to Fisher's exact test analysis. (B) The same method as an (A) was used to analyze *fli1* and L*er* crosses to indicated genotypes in F_1 progeny. Different letters indicate statistically significance of $P < 0.05$ to L*er* wt plant, calculated by Fisher exact test.

59

Fli1 x L*er* crosses were further analyzed on the level of F_3 families (Table 11). 48 individual plants of 15 different F_3 families were phenotyped for enhanced disease development upon *Pto* DC3000 infections. Four families showed *fli1*-like disease phenotypes (Table 11), whereas 11 families were indistinguishable from wt plants. The observed ratio was statistically insignificant different from a 1:3 ratio underlying recessive inheritance of a single mutant locus. *Fli1* x L*er* back-crosses with *fli1*-like phenotypes showed higher expression of *DIN2*, but not *PsaA* in infections with *Pto* DC3000 (Figure 21), as previously observed in *fli1* parental lines (Figure 19 B). Notably, *DIN2* expression was significant higher compared to L*er* wt, but did not reach the level of *fli1* plants.

Next, we used *fli1* crosses to Col-0 to identify genetic markers co-segregating with *fli1* higher susceptibility in *Pto* DC3000 spray infections. 10 out of 54 F_3 families generated from six independent F_2 populations displayed *fli1*-like disease phenotypes. Chi-square analyzes indicate that the observed distribution is likely to meet a 1:3 segregation ratio of one single recessive locus. Alternatively, a 3:13 segregation with an even lower chi-square value is plausible. Since *fli1* x L*er* crosses segregated with a ratio of 1:3, a potential dominant-epistatic effect of a second L*er* allele might be considered as well as an additive effect of a dominant-inherited L*er* virulence gene (Suppl. Fig. 5). In conclusion, the most likely scenario links the *fli1* phenotype to a single recessive locus and this might require one copy of a second L*er* gene. More phenotyped F_3 families would be required for a detailed genetic analysis.

Table 11   **Genetic analysis of *fli1* mutants**

| Cross	Total number of F_3 family[a]	Number of families with observed phenotypes		Tested segregation	χ^2	P value [b]
		Susceptible	*Resistant*			
fli1 x L*er*	15	4	11	1 : 3	0.02	> 0.8
fli1 x Col-0	54	10	44	1 : 3	1.21	> 0.25
				3 : 13	0.002	> 0.95
				1 : 15	13.87	< 0.001

[a]   48 individual plants per F_3 were phenotyped by according to their disease development in *Pto* DC3000 spray infection assays.

[b]   P values were calculated by F test with degree of freedom =1. P values below 0.05 indicate a significant deviation from tested segregation.
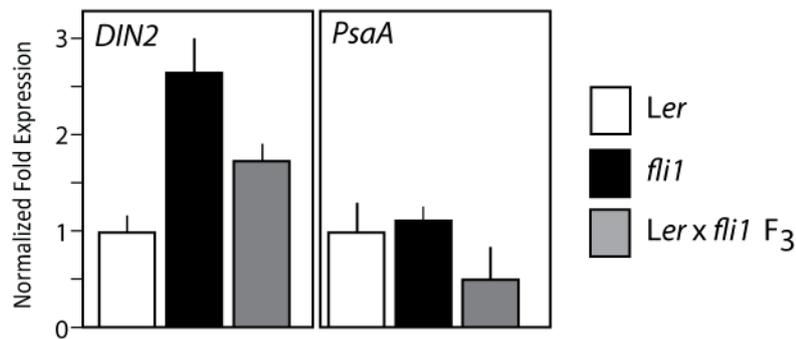
Figure 21 *fli1* **backcrosses to L***er* **show** *DIN2* **up-regulation in infections with** *Pto* **DC3000.** Indicated genes were quantified by qRT-PCR five days after spray-infection with *Pto* DC3000 of two-week-old L*er* (white bars), *fli1* (black bars) parental seedlings and L*er* x *fli1* F$_3$ progeny displaying *fli1*-like disease development (grey bars). Bars present mean relative expression values +/- SD of three technical samples containing four seedlings each. Actin2 was used as reference.

Two L*er* markers on the upper arm of chromosome 5 co-segregated with *fli1* associated disease phenotype in seven out of eight tested F$_3$ families of *fli1* x Col-0 crosses (Figure 22). We defined therefore the region between marker CTR1 and 5-AL3911491762 as rough mapping interval of *fli1*, which likely harbors the *fli1* mutation. This 3.8 Mb long region contained more than 1400 genes.
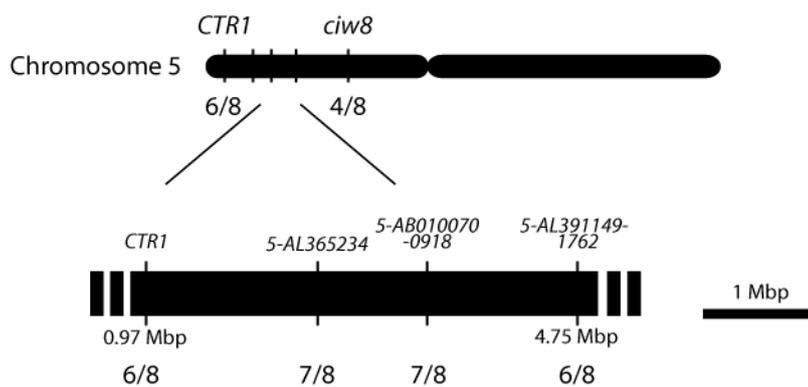
Figure 22 *fli1* **co-segragates with genetic markers on chromosome 5.** Four individual plants for each F$_3$ *Fli1* x Col-0 family showing *fli1*-like disease phenotype were genotyped with simple sequence length polymorphism markers between L*er* and Col-0. Ratios indicate number of F$_3$ families showing only L*er* specific PCR products and corresponding location of used markers on *Arabidopsis thaliana* chromosome 5.

To reduce the mapping interval sufficiently, a classical map-based cloning approach would require an extension of the mapping population to approximately three or four thousand F_2 plants (Jander et al., 2002). We used populations of 48 individuals per F_3 family to limit false-positive phenotying. A classical map-based approach would therefore multiply the amount of required plants substantially and appeared not applicable for our purposes.

Fli1 originated from a gamma-irradiation mutagenized L*er* population. A survey of gamma-irradiation introduced loss of function mutations in *Arabidopsis* detected exclusively deletions of at least 5 kb (Cecchini et al., 1998). Radiation induced deletion in *Drosophila* were previously successfully mapped at kb-resolution using the Illuminina sequencing platform (Daines et al., 2009). Since *Drosophila melanogaster* and *Arabidopsis thaliana* share a similar genome size, a similar approach to detect *fli1* mutations appeared rational. Whole-genome sequencing was done with the Illumina platform (in collaboration with Jodie Pike and Dr. Dan MacLean in the Sainsbury Laboratory Norwich, UK). In total more than 26 million 76 bp paired-end reads were generated from *fli1* M_5 genomic DNA reaching an average coverage of 31.6. Reads were aligned to the Col-0 reference genome. A summary of technical sequencing details are given in Table 12.

Table 12   Whole genome sequencing of *fli1*

Sequencing platform:	Illumina
Read length:	76 bp, paired-end
Raw Paired-Read counts:	26,220,486
Average coverage:	31.6
SNPs identified in mapping range:	23
SNPs confirmed exclusively in *fli1*:	0
Indels identified in mapping range:	5
Indels confirmed exclusively in *fli1*:	0

We searched systematically for deletions in *fli1* rough mapping range, which could potentially affect genes, and identified five putative deletions varying in size from 23 bp to 2175 bp (Table 13). Candidate regions were amplified on *fli1*, *fli2*, L*er* and Col-0 genomic DNA by PCR or sequenced. In all cases, including deletions located outside of *fli1* mapping interval, PCR products of the same size were amplified in *fli1*, *fli2*, L*er* wt, but not in Col-0. This indicates that *in silico* identified deletions represent natural polymorphisms between L*er* and Col-0 accessions and are likely not the cause of *fli1* enhanced susceptibility to *Pto* DC3000.

Table 13   *In silico* prediction of *fli1* deletions and validatio

Del #	Gene	Description	Chr.	Start	Size [bp]	Re.seq.
del_1	*AT5G05657*	Late embryogenesis abundant (LEA)	5	1688990	581	L*er* SNP
del_2	*AT5G06800*	Myb-like	5	2105874	2175	L*er* SNP
del_3	*AT5G09530*	hydroxyproline-rich glycoprotein family protein	5	2960444	23	L*er* SNP
del_4	*AT5G09978*	PEP7 (utr)	5	3120927	224	L*er* SNP
del_5	*AT5G10180*	SULTR2;1	5	3196231	141	L*er* SNP
	<u>Outside rough mapping interval</u>					
del_6	*AT5G02930*	Skp2-like	5	681711	2047	L*er* SNP
del_7	*AT5G17880*	CONSTITUTIVE SHADE-AVOIDANCE1	5	5908874	4225	L*er* SNP

We did not exclude the possibility that one single nucleotide exchange (SNP) might cause the *fli1* phenotype. Mutagenizing irradiation was previously reported to introduce SNPs (Torii et al., 1996). We searched for homozygous, non-synonymous *fli1* SNPs and small Indel relative to the Col-0 reference genome. Schneeberger *et al.* (2011) showed recently that over 50 % of aligned L*er* genes contained at least one non-synonymous polymorphism between L*er* and Col-0 sequences (Schneeberger et al., 2011). We used Illumina reads generated from four other L*er* lines (Yi-Ju Lu, Martina Beck, Silke Robatzek, The Sainsbury Laboratory Norwich, UK) and public available SNPs annotations to limit detection of natural occurring polymorphisms. In total, 23 putative, non-synonymous and homozygous SNPs were retrieved and further analyzed by classical Sanger sequencing. All but two showed the same nucleotide sequence in *fli1* and L*er* wt, and thus are likely L*er* polymorphisms or wrong annotations of the Col-0 reference genome (Table 14). Sequencing of

the two remaining positions revealed the same nucleotide sequence as observed in Col-0 reference genome annotations. We also sequenced ten genes outside *fli1* mapping range and recovered exclusively L*er* polymorphisms or false-positives detected SNPs.

Table 14   *In silico* prediction and validation of *fli1* SNPs and Indels

SNP #	Gene	Description	Chr.	Position	Ref. [a]	SNP	AA level [b]	Re-seq. [c]
1	*AT5G03650*	Starch branching enzyme 2.2	5	936893	G	C	G to A	L*er* SNP
2	*AT5G04853*	unknown protein	5	1410610	T	G	F to V	Ler SNP
3	*AT5G05000*	TOC34	5	1474318	A	T	K to Stop	No SNP
4	*AT5G05060*	Cystatin/monellin	5	1494963	G	C	P to S	L*er* SNP
5	*AT5G05900*	UDP-	5	1776033	G	C	E to D	L*er* SNP
6		Glycosyltransferase		1776047	A	G	Q to R	L*er* SNP
7	*AT5G06140*	SORTING NEXIN 1	5	1856705	C	A	S to Stop	No SNP
8	*AT5G06640*	Proline-rich extensin-like family protein;	5	2041610	A	T	N to Y	L*er* SNP
9	*AT5G06790*	unknown protein	5	2098302	C	A	T to N	L*er* SNP
10	*AT5G07150*	LRR protein kinase	5	2216685	G	C	A to P	Ler SNP
11	*AT5G07170*	microtubule	5	2222903	*	na		L*er* SNP
12		associated protein	5	2222915	*	na		L*er* SNP
13	*AT5G07540*	glycine-rich protein	5	2386249	A	C	E to A	L*er* SNP
14	*AT5G07690*	MYB29	5	2448202	A	G	T to A	L*er* SNP
15			5	2448204	T	C	Silent	L*er* SNP
16			5	2448206	G	A	G to D	L*er* SNP
17			5	2448216	T	A	N to K	L*er* SNP
18	*AT5G10230*	calcium-binding protein annexin	5	3209839	A	T	I to F	L*er* SNP
19	*AT5G10600*	CYP81K2	5	3352211	G	T	V to L	L*er* SNP
20	*AT5G10630*	Translation elongation factor	5	*3362055*	G	A	D to N	L*er* SNP
21	*AT5G11400*	Protein kinase	5	3637096	C	A	T to N	L*er* SNP
22	*AT5G12930*	unknown protein	5	4085156	G	T	A to S	L*er* SNP
23	*AT5G12930*	unknown protein	5	4085173	A	C	H to P	L*er* SNP
		Outside rough mapping position						
24	*AT5G13370*	auxin response factor	5	4288005	C	A	S to K	L*er* SNP
25	*AT5G18180*	ribonucleoprotein	5	6009521	*	na		L*er* SNP
26				6009522	*	na		L*er* SNP
27	*AT5G24950*	P450	5	8596102	G	T	G to Stop	No SNP
28	*AT5G02810*	Pseudo-response regulator 7	5	*639642*	G	A	P to L	L*er* SNP
29	*AT5G03120*	unknown protein	5	734764	*	na	three_prime _UTR	L*er* SNP

Table 14 continued.

SNP #	Gene	Description	Chr.	Position	Ref.[a]	SNP	AA level[b]	Re-seq.[c]
30	*AT5G54650*	FORMIN HOMOLOGY5	5	22198277	T	A	L to stop	L*er* SNP
31	*AT5G64860*	DISPROPORTIONATING ENZYME (DPE1)	5	25926859	G	T	E to stop	No SNP
32	*AT1G48740*	oxygenase superfamily protein	1	18025081	T	A	I to F	L*er* SNP
33	*AT1G52500*	DNA N-glycosylase	1	19562103	T	A	Y to N	L*er* SNP

[a]　Reference according to Col-0 genome. A = Adenine, C = Cytosine, G = Guanine, T =Thymine, * indicates deletions, na not available.

[b]　Amino acid abbreviations according to (JCBN, 1984).

[c]　Primers used to re-sequence (Re-seq.) predicted SNPs by Sanger sequencing can be found in Suppl. table **2**.

In summary, even though gamma-irradiation was previously reported to introduce deletions of several kbs, we did not identity unique deletions in *fli1* whole genome alignments to the Col-0 reference genome. Identified deletions, as well as predicted SNPs were also found in L*er* wt plants, and therefore not linked to the enhanced disease development phenotype in *fli1* mutants. Initial genetic analysis indicated that enhanced disease development upon infection with *Pto* DC3000 co-segregates with genetic markers on chromosome 5 and is likely to be caused by one recessive inherited mutation.

4. DISCUSSION

4.1. UBIQUITINATION AND FLS2 TRAFFICKING

In order to find cellular factors contributing to FLS2 trafficking, we studied the role of ubiquitination in FLS2 endocytosis. Ubiquitination serves as signal for receptor endocytosis and endosomal trafficking across species (Mukhopadhyay and Riezman, 2007). Recently, two ubiquitin E3 ligases PUB12 and PUB13 were shown to be recruited by BAK1 to facilitate flg22-dependent FLS2 ubiquitination and protein turn-over (Lu et al., 2011). Double mutant knock-outs in *pub12* and *pub13* show elevated flg22 responses, favoring a negative regulation of FLS2 signaling by ubiquitination. Slightly enhanced flg22-repsonses were also observed in *pub22 pub23 pub24* triple mutants (Trujillo et al., 2008), but direct interaction or ubiquitination by PUB22, PUB23 or PUB24 could not been shown despite repeated attempts (personal communication by Dr. Vera Göhre, University of Düsseldorf, Germany). The negative regulation of FLS2 function by ubiquitination is exploited by the *Pto* DC3000 effector AvrPtoB (Göhre et al., 2008). Occupation of host ubiquitination processes is not restricted to *Pto* DC3000 and also observed in other host microbe interactions (Spallek et al., 2009).

In order to gain a better understanding of AvrPtoB-mediated ubiquitination, we analyzed FLS2 ubiquitination by different ubiquitin mutants. This revealed that AvrPtoB is able to from poly-ubiquitin chains independent of ubiquitin lysine 48 and lysine 63. Interestingly, ubiquitination was most pronounced with ubiquitin K48R mutant variants. K48-linked ubiquitin chains mark proteins for proteasomal degradation, whereas K48-independent chains are often associated with endocytic processes (Mukhopadhyay and Riezman, 2007). Using an ubiquitin variant mutated in all lysines (Ub^{noK}) enabled us to identify one out of presumably two FLS2 ubiquitination sites. The identified site was located in the juxtamembrane region of FLS2. Juxtamembrane domains play important regulatory roles in Xa21 auto-phosphorylation and protein-protein interactions (Chen et al., 2010c). Our data show that substitutions of all three lysines by arginines reduced FLS2 ubiquitination *in vitro.* Furthermore, complementation of *fls2* mutants with FLS2$^{3K->R}$-GFP variants conferred enhanced resistance to *Pto* DC3000 compared to complementation with wt FLS2-GFP constructs at similar expression levels. This is in line with previous results, showing a negative role of FLS2 ubiquitination in plant immunity (Göhre et al., 2008; Lu et al., 2011). We cannot exclude that identified ubiquitination sites are specific for AvrPtoB function and increased resistance resulted from reduced *Pto* DC3000 virulence. Infection assays with Pto DC3000 deleted in *AvrProB* will provide a clarification. FLS2$^{3K->R}$-GFP variants showed, however, slightly elevated FLS2-GFP endosome number

in response to flg22. This would point at an AvrPtoB independent function of FLS2 putative ubiquitination sites. Similar results were obtained with ubiquitination resistant BOR^{K590A} variants, which accumulate in late endosomal compartments due to impaired trafficking of BOR^{K590A} to lytic vacuoles (Kasai et al., 2010). Further studies are required to determine if lysines located in the juxtamembrane are also targeted by PUB12, 13 and if the observed FLS2$^{3K->R}$ phenotypes are linked to altered FLS2 ubiquitination statuses *in vivo.*

Ubiquitinated receptors trafficking along the endocytic pathway are recognized components of the ESCRT machinery. ESCRT complexes have been extensively studied in yeast and animals, where ESCRT proteins catalyze MVB biogenesis (Henne et al., 2011). It is therefore not surprising, that ESCRTs are involved in various cellular processes like cytokinesis, viral budding, exosome secretion, and autophagy (Henne et al., 2011). Plant genes encoding for ESCRT-1 proteins VPS23, VPS28 and VPS37 were identified based on homology, interaction studies, sub-cellular localization in protoplasts and their ability to bind ubiquitin (Spitzer et al., 2006). Although carrying each a functional homolog *vps28-2* and *vps37-1* were more susceptible to bacterial infections compared to wt plants and T-DNA insertion lines of *vps28-1* and *vps37-2* (Salomon, 2009). Different cellular functions were also reported for the four VPS37 isoforms encoded by the human genome (Carlton et al., 2008; Stefani et al., 2011). Both VPS28-2 and VPS37-1 show in addition different affinities to other ESCRT proteins. Unlike VPS28-1 and VPS37-2, VPS28-2 and VPS37-1 are able to bridge the ESCRT-1 complex to ESCRT-3 subunits in protoplasts and yeast two hybrid assays (Shahriari et al., 2011). It remains to be shown, if this ability is linked to the observed role of *VPS28-2* and *VPS37-1* in plant immunity. Using transient expression of fluorescent-tagged ESCRT-1 proteins in *N. benthamiana*, we observed that CFP-ELC, YFP-VPS28-2 and RFP-VPS37-1 are targeted to the same mobile vesicular compartment. Furthermore, FLS2-GFP endosomes partially co-localized with RFP-VPS28-2 containing vesicles in *Arabidopsis* after flg22 treatment. These results indicate that key endocytic routes are conserved in eukaryotic cells (Husebye et al., 2006; Field and Dacks, 2009).

In mammals and *Drosophila* ESCRT-1 depletion goes along with prolonged MAPK phosphorylation (Babst et al., 2000; Lloyd et al., 2002; Malerod et al., 2007). Our experiments showed no evident differences in flg22 triggered MAPK activation between wt and *vps28-2* or *vps37-1* mutants, respectively. Surprisingly, even though *vps28-2* or *vps37-1* mutants showed wt-like MAPK activation, flg22 induced up-regulation of MAPK-dependent *FRK1* (Boudsocq et al., 2010) and *FLS2* transcripts

was significantly lower in both mutants compared to wt plants. Although *FLS2* transcripts were higher abundant in Col-0 wt plant after 60 min of flg22 treatment, Col-0 wt plants generated less ROS than *vps28-2* and *vps37-1* mutants, when plants were treated a second time with flg22 four hours after an initial ROS burst. Reduced desensitization in *vps37-1* or *vps28-2* mutants could indicate higher availability of FLS2 receptors at the plasma membrane, and thus point at reduced FLS2 endocytosis or enhanced recycling of FLS2 similar to studies on mammalian loss-of-function mutants in *tumor susceptibility gene 101* (*tsg101*, homolog of yeast *VPS23* and *Arabidopsis ELC*). *Tsg101* cells show delayed endosomal trafficking and enhanced recycling of EGFR receptor to the plasma membrane upon EGF stimulation (Babst et al., 2000). Quantification of FLS2 endosomes supported this possibility, since significantly less FLS2-GFP endosomes were generated in *vps37-1* mutants compared to wt plants at similar FLS2-GFP protein levels.

We also observed impaired stomatal closure in *vps28-2* and *vps37-1* mutants after flg22 treatment. A detailed understanding of flg22-induced stomatal closure is still pending, but recent work highlights the importance of flg22-induced MPK3 signaling (Gudesblat et al., 2009). Reduced flg22 responses might not solely rely on MAPK activation, but might dependent on FLS2 trafficking to ESCRT compartments *per se*. Endocytic trafficking and interaction with ESCRT-1 associated proteins is essential for *Drosophila* Toll receptor signaling to fully activate immune responses (Huang et al., 2010). A different study shows that accelerated Toll receptor endocytosis amplifies signaling locally from Rab5-positve vesicles (Lund et al., 2010) and also human TLR4 activates endosomal responses from Rab5-positve vesicles independent of plasma membrane derived signaling (Kagan et al., 2008). *Arabidopsis* ESCRT components were previously shown to localize with Rab5 containing vesicles (Spitzer et al., 2006; Haas et al., 2007). VPS28-2 and VPS37-1 role in plant immunity is likely not restricted to FLS2 function, since *vps28-2* and *vps37-1* mutants were not only higher susceptible to *Pto* DC3000, but also to the oomycete *Hpa* Waco9. It might therefore be possible that immunity against oomycetes employs PRR trafficking. Studies on *bak1-5 serk4* double mutants show an enhanced susceptibility to different *Hpa* strains (Roux et al., 2011). *BAK1* is required to activate most flg22 responses including FLS2 endocytosis (Chinchilla et al., 2007). This could indirectly hint on a contribution of PRR signaling in immunity against *Hpa*.

Taken together, our data revealed flg22 dependent FLS2 localization to ESCRT-1 containing vesicles and the requirement of two ESCRT-1 genes *VPS28-2* and *VPS37-1* for efficient activation of FLS2 responses, immunity to *Pto* DC3000 and *Hpa* Waco9. In parallel, mutations in putative FLS2 ubiquitination sites conferred higher resistance to *Pto* DC3000. FLS2-GFP endosome levels were reduced in *vps37-1*, but slightly elevated for FLS2$^{3K->R}$. It is therefore possible that FLS2 endosomes *per se* contribute to defense signaling. Endosomal signaling was previously shown for BRI1 (Geldner et al., 2007) and several studies in non-plant systems highlight the importance of endocytic signaling (Sadowski et al., 2009; Sorkin and von Zastrow, 2009; Scita and Di Fiore, 2010). The benefit of endosomal signaling appears striking: (1) The small volume in endosomes favors ligand receptor interaction, thus strengthen receptor activation. (2) Passive diffusion is not sufficient for effective signal transduction in cells. Considering that endosomal movement is directed, it will necessarily facilitate detection of activated receptors by intracellular regulators. (3) Compartmentalization provides a platform for receptors to specifically interact with proteins at a given time (Scita and Di Fiore, 2010). Endosomal signaling was proposed for the tomato RLP LeEIX2 (Sharfman et al., 2011). LeEIX2 requires a tyrosine-based motif for endocytosis and function in *N. benthamiana* (Bar and Avni, 2009). This motif is shared with other PRRs like Cf proteins or EFR but absent in FLS2 (Altenbach and Robatzek, 2007). It is therefore possible that different endocytic pathways require different molecular components. Figure 23 provides a model, how late endosomal trafficking could contribute to FLS2 signaling.
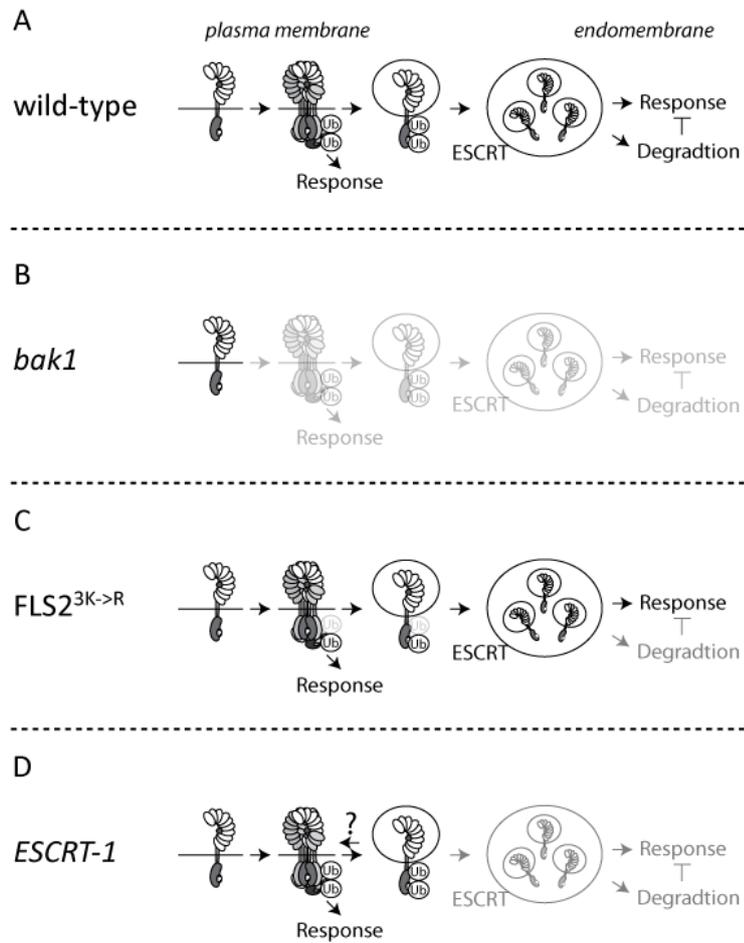
Figure 23 A model for FLS2 endosomal signaling. (A) Plants require plasma membrane derived and endosomal signaling to fully activate FLS2 signaling. (B) Plasma membrane derived and endosomal responses require receptor complex formation with BAK1 to initiate signaling. (C) FLS2 ubiquitination could influences endosomal trafficking and termination of activated receptors, thus lead to sustained signaling if altered. (D) Reduced endosome numbers in ESCRT mutants leads to less endosomal signaling, but does not affect plasma membrane derived signaling. Arrows indicate positive interactions, T-bars negative interactions.

4.2. *FLI1* REGULATES LATE PAMP RESPONSES IN PLANT IMMUNITY

We used whole genome next generation sequencing to detect *fli1* specific mutations in a defined rough mapping region. Earlier attempts to map *fli1* using a classical map-based cloning approach were hampered by variability of *fli1* phenotypes in F_2 mapping populations (Salomon, 2009). To reduce to number of false-positive phenotyped F_2 progeny and increase the chance to find markers linked to the *fli1* phenotype, we analyzed a relatively high number of 48 individual plants in F_3 progeny. This lowered the total number of analyzed F_2 crosses and thus possible recombination events close to the *fli1* locus. One the other hand, stringent phenotyping proofed to be successful: The majority of identified *fli1* x Col-0 progenies displaying *fli1*-like disease development showed linkage with markers on the upper arm of chromosome 5, comprising a 3.8 Mbp region of approximately 1400 genes. Notably, in one out of eight genotyped *fli1* x Col-0 crosses no homozygous L*er* markers were detected in this region. It is thus still possible that false-positive phenotyping occurred even when 48 F_3 plants were phenotyped. Based on known mutation frequencies, a relatively small number of chromosome deletions would have been expected in an interval of this size (Cecchini et al., 1998). Unexpectedly, we did not find any large deletions within or outside the *fli1* mapping range, which were also not found in L*er* wt plants or non-allelic *fli2* mutants, respectively. It is therefore likely that the *fli1* phenotype is not caused by large deletions as result of gamma-irradiation, but rather by small Indels, SNPs or chromosome rearrangement as seen in other systems (Anderson et al., 1995).

We identified several SNPs within the *fli1* mapping range, but none of them was unique to *fli1*. Our approach was based on Col-0 reference guided alignments and this allowed us only to detect mutations at positions homologous to the Col-0 genome (Austin et al., 2011). We can therefore not exclude that potential deletions and SNPs were excluded from analyzes due to high variation or absence in the Col-0 genome. Because so far all tested genetic variations were shared between L*er* wt plants and *fli1* mutants, we could not test if the mapping range identified in crosses to Col-0 corresponds to *fli1* regions in crosses between *fli1* mutants and L*er* wt plants. Our SNP and deletion analyzes were based on the assumption that the *fli1* mutation is homozygous in M_5 progeny. We have no data contradicting this assumption: *Fli1* phenotypes were robustly observed in different progenies and crosses to L*er* or Col-0 wt plants segregated in the expected ratio of a single recessive mutation. Identification of the mutation underlying the *fli1* phenotype is crucial to for a detailed

analysis of *fli1* and could benefit from a newly released L*er* genome assembly (Cao et al., 2011; Schneeberger et al., 2011).

We conducted whole genome transcript profiling of *fli1* plants during infection with virulent *Pto* DC3000 and detected significant differences in *fli1* transcript profiles compared to L*er* wt and *fls2-17* 24 hours post infection. Several genes with predicted functions in sugar starvation and photosynthesis were higher expressed in *fli1* plants at that time point of infection. Such genes are typically down-regulated in wild-type plants upon biotic stresses (Bilgin et al., 2010). Follow-up studies showed that relative expression levels of identified genes coding for photoreaction centres varied significantly between different infections. *Fli1* hyper-susceptibility to *Pto* DC3000 was in contrast to microarray analyzes also observed in infections, where *PsaA* and *PsbD* were similar expressed in *fli1* and wt plants at later stages of infection. Even though variation in disease progression between different infections was frequently observed, a direct negative regulation of genes encoding for proteins with core functions in photosynthesis by *FLI1* during infections appeared questionable. Regulation of chloroplast encoded genes is complex and influenced by multiple environmental factors (Saibo et al., 2009) and in many cases, transcription levels do not correlate with protein levels of photosynthetic genes (Eberhard et al., 2008).

By contrast, genes associated with sugar starvation were reproducibly higher expressed in *fli1* mutants compared to L*er* plants during infection. *DIN2* and sucrose invertase *At3g06500* were previously reported to be up-regulated during infection, but not studied in detail (de Torres-Zabala et al., 2007; Zhang et al., 2007b). Sugar responses are intertwined with abiotic stress signaling (Baena-Gonzalez et al., 2007). Notably, root growth in presence of different NaCl and glucose concentration was similar affected in *fli1* mutants than in wild-type plants. This suggests that *fli1* is not globally impaired in stress responses. It is not clear, whether higher transcription of genes associated with sugar starvation in *fli1* is cause or consequence of higher susceptibility to *Pto* DC3000 infections. Pathogens were shown to actively promote sugar effluxes from host cells, thus directly compete with available sugar resources (Chen et al., 2010a). Higher infection rates in *fli1* could consequently lead to accelerated depletion of energy resources and trigger starvation inducible genes.

Higher infection rates in *fli1* correlated with reduced late flg22-dependent defense responses. Whole genome transcriptome analyzes indicated that *fli1* activated a similar transcriptional program like wt plants three hours after spray inoculation with *Pto* DC3000. Also other early PAMP responses like flg22-mediated stomatal closure, PAMP-induced ROS and ethylene production as well as flg22-induced MAPK activation were indistinguishable from wt plants (Salomon, 2009). By contrast, flg22-induced resistance and late PAMP responses like callose deposition and seedling growth arrest were impaired in *fli1.* It is therefore possible that *Pto* DC3000 virulence is fostered in *fli1* mutants by reduced late PAMP response and deficiencies in flg22-induced immunity. The contribution of late PAMP responses to plant immunity is not well understood. Most identified PTI mutants are impaired in PAMP signal transduction or PRR biogenesis directly (Zhang and Zhou, 2010). Loss of function mutations in callose synthase *pmr4* is accompanied with reduced flg22-induced callose deposits, elevated SA levels and enhanced resistance to pathogens. By contrast, *pmr4* mutants crossed to mutants impaired in SA signaling show slightly more growth of non-host *Pseudomonas syringae* pv. *phaseolicola* 1448a than SA-deficient mutants *per se*, suggesting a role of callose deposition in plant immunity (Ham et al., 2007). In contrast to *pmr4* mutants, *fli1* mutants showed residual callose deposition, but were also impaired in other late PAMP responses and flg22-induced resistance. It is therefore possible, that combined disturbance of several late PAMP responses account for *fli1* hyper-susceptibility to *Pto* DC3000 at levels comparable to *fls2-17* receptor mutants.

Our experiment on transcriptional changes during infection with *Pto* DC3000 showed that three hours after spray inoculation, only a relatively small number of genes was significantly different expressed in wt plants, *fli1* and *fls2-17*, with *fls2-17* displaying the most distinct transcriptional profile. Similar transcript profiles might be explained by partially overlapping transcriptional changes upon perception of different PAMPs (Zipfel et al., 2006; Denoux et al., 2008). It is therefore remarkable that *fls2-17* mutants are severely immuno-compromised in bacterial infections (Zipfel et al., 2004). Among genes significantly less expressed in *fls2-17* mutants three hours post infection, *ACO2* oxidizes aminocyclopropane-1-carboxylic acid (ACC) to finally release ethylene (Wang et al., 2002). *Arabidopsis* ACO2 and homologs in tomato are up-regulated upon pathogen infection, but also by ethylene *per se* (Jia and Martin, 1999; Zhong and Burns, 2003). *FLS2* transcription is under direct positive control of ethylene signaling components (Boutrot et al., 2010; Mersmann et al., 2010), but we did not observed significant differences in *FLS2* transcript levels three hours after infection with virulent *Pto* DC3000 or non-virulent *Pto* DC3000 *hrcC*. Alternatively a role of ethylene in regulating late immune responses has been proposed (Denoux et al., 2008). Further analyzes are

required to test if ethylene levels are indeed altered in *fls2* mutants and if this is mediated by *ACO2* expression during infection.

In summary, our data provide good evidence that late PAMP responses and flg22-induced resistance contribute to plant immunity in infections with virulent *Pto* DC3000. We used *fli1,* a mutant impaired in late, but not early PAMP responses, and compared differences between *fli1,* wt and *fls2,* respectively. Higher susceptibility of *fli1* to *Pto* DC3000 was associated with higher expression of sugar starvation responsive genes. *Fli1* co-segregated with markers on the upper arm of chromosome 5 in *fli1* crosses to Col-0, but remains to be identified. Further studies will implement sequence information from recently released L*er* genome assemblies (Cao et al., 2011; Schneeberger et al., 2011) and broaden analyzes to SNPs in non-protein coding regions and regulatory sequences. Re-sequencing of *fli1* mutants backcrossed multiple times to wt plants might also be considered, since it was successfully used in other studies (Ashelford et al., 2011).

5. REFERENCES

Aarts, N., Metz, M., Holub, E., Staskawicz, B.J., Daniels, M.J., and Parker, J.E. (1998). Different requirements for EDS1 and NDR1 by disease resistance genes define at least two R gene-mediated signaling pathways in Arabidopsis. Proc Natl Acad Sci U S A **95,** 10306-10311.

Achard, P., Cheng, H., De Grauwe, L., Decat, J., Schoutteten, H., Moritz, T., Van Der Straeten, D., Peng, J., and Harberd, N.P. (2006). Integration of Plant Responses to Environmentally Activated Phytohormonal Signals. Science **311,** 91-94.

Albrecht, C., Russinova, E., Kemmerling, B., Kwaaitaal, M., and de Vries, S.C. (2008). Arabidopsis SOMATIC EMBRYOGENESIS RECEPTOR KINASE proteins serve brassinosteroid-dependent and -independent signaling pathways. Plant Physiol **148,** 611-619.

Altenbach, D., and Robatzek, S. (2007). Pattern recognition receptors: from the cell surface to intracellular dynamics. Mol Plant Microbe Interact **20,** 1031-1039.

Anderson, P., Henry, F.E., and Diane, C.S. (1995). Chapter 2 Mutagenesis. In Methods in Cell Biology (Academic Press), pp. 31-58.

Asai, T., Tena, G., Plotnikova, J., Willmann, M.R., Chiu, W.-L., Gomez-Gomez, L., Boller, T., Ausubel, F.M., and Sheen, J. (2002). MAP kinase signaling cascade in Arabidopsis innate immunity. Nature **415,** 977-983.

Ashelford, K., Eriksson, M.E., Allen, C.M., D'Amore, R., Johansson, M., Gould, P., Kay, S., Millar, A.J., Hall, N., and Hall, A. (2011). Full genome re-sequencing reveals a novel circadian clock mutation in Arabidopsis. Genome Biol **12,** R28.

Austin, R.S., Vidaurre, D., Stamatiou, G., Breit, R., Provart, N.J., Bonetta, D., Zhang, J., Fung, P., Gong, Y., Wang, P.W., McCourt, P., and Guttman, D.S. (2011). Next-generation mapping of Arabidopsis genes. Plant J.

Babst, M., Odorizzi, G., Estepa, E.J., and Emr, S.D. (2000). Mammalian tumor susceptibility gene 101 (TSG101) and the yeast homologue, Vps23p, both function in late endosomal trafficking. Traffic **1,** 248-258.

Baena-Gonzalez, E., Rolland, F., Thevelein, J.M., and Sheen, J. (2007). A central integrator of transcription networks in plant stress and energy signaling. Nature **448,** 938-942.

Bar, M., and Avni, A. (2009). EHD2 inhibits ligand-induced endocytosis and signaling of the leucine-rich repeat receptor-like protein LeEix2. Plant J **59,** 600-611.

Barberon, M., Zelazny, E., Robert, S., Conejero, G., Curie, C., Friml, J., and Vert, G. (2011). Monoubiquitin-dependent endocytosis of the IRON-REGULATED TRANSPORTER 1 (IRT1) transporter controls iron uptake in plants. Proc Natl Acad Sci U S A.

Bednarek, P., Piślewska-Bednarek, M., Svatoš, A., Schneider, B., Doubský, J., Mansurova, M., Humphry, M., Consonni, C., Panstruga, R., Sanchez-Vallet, A., Molina, A., and Schulze-Lefert, P. (2009). A Glucosinolate Metabolism Pathway in Living Plant Cells Mediates Broad-Spectrum Antifungal Defense. Science **323,** 101-106.

Beissbarth, T., and Speed, T.P. (2004). GOstat: find statistically overrepresented Gene Ontologies within a group of genes. Bioinformatics **20,** 1464-1465.

Bilgin, D.D., Zavala, J.A., Zhu, J., Clough, S.J., Ort, D.R., and DeLucia, E.H. (2010). Biotic stress globally downregulates photosynthesis genes. Plant Cell Environ **33,** 1597-1613.

Boller, T., and Felix, G. (2009). A renaissance of elicitors: perception of microbe-associated molecular patterns and danger signals by pattern-recognition receptors. Annu Rev Plant Biol **60,** 379-406.

Boudsocq, M., Willmann, M.R., McCormack, M., Lee, H., Shan, L., He, P., Bush, J., Cheng, S.H., and Sheen, J. (2010). Differential innate immune signaling via Ca(2+) sensor protein kinases. Nature **464,** 418-422.

Boutrot, F., Segonzac, C., Chang, K.N., Qiao, H., Ecker, J.R., Zipfel, C., and Rathjen, J.P. (2010). Direct transcriptional control of the Arabidopsis immune receptor FLS2 by the ethylene-dependent transcription factors EIN3 and EIL1. Proc Natl Acad Sci U S A **107,** 14502-14507.

Buchanan-Wollaston, V., Page, T., Harrison, E., Breeze, E., Lim, P.O., Nam, H.G., Lin, J.F., Wu, S.H., Swidzinski, J., Ishizaki, K., and Leaver, C.J. (2005). Comparative transcriptome analysis reveals significant differences in gene expression and signaling pathways between developmental and dark/starvation-induced senescence in Arabidopsis. Plant J **42,** 567-585.

Camborde, L., Planchais, S.v., Tournier, V., Jakubiec, A., Drugeon, G.l., Lacassagne, E., Pflieger, S.p., Chenon, M.l., and Jupin, I. (2010). The Ubiquitin-Proteasome System Regulates the Accumulation of Turnip yellow mosaic virus RNA-Dependent RNA Polymerase during Viral Infection. The Plant Cell Online **22,** 3142-3152.

Cao, J., Schneeberger, K., Ossowski, S., Gunther, T., Bender, S., Fitz, J., Koenig, D., Lanz, C., Stegle, O., Lippert, C., Wang, X., Ott, F., Muller, J., Alonso-Blanco, C., Borgwardt, K., Schmid, K.J., and Weigel, D. (2011). Whole-genome sequencing of multiple Arabidopsis thaliana populations. Nat Genet.

Carlton, J.G., Agromayor, M., and Martin-Serrano, J. (2008). Differential requirements for Alix and ESCRT-III in cytokinesis and HIV-1 release. Proceedings of the National Academy of Sciences **105,** 10541-10546.

Cazale, A.-C., Clement, M., Chiarenza, S., Roncato, M.-A., Pochon, N., Creff, A., Marin, E., Leonhardt, N., and NoÃ«l, L.D. (2009). Altered expression of cytosolic/nuclear HSC70-1 molecular chaperone affects development and abiotic stress tolerance in Arabidopsis thaliana. Journal of Experimental Botany **60,** 2653-2664.

Cecchini, E., Mulligan, B.J., Covey, S.N., and Milner, J.J. (1998). Characterization of gamma irradiation-induced deletion mutations at a selectable locus in Arabidopsis. Mutation Research/Fundamental and Molecular Mechanisms of Mutagenesis **401,** 199-206.

Chen, L.-Q., Hou, B.-H., Lalonde, S., Takanaga, H., Hartung, M.L., Qu, X.-Q., Guo, W.-J., Kim, J.-G., Underwood, W., Chaudhuri, B., Chermak, D., Antony, G., White, F.F., Somerville, S.C., Mudgett, M.B., and Frommer, W.B. (2010a). Sugar transporters for intercellular exchange and nutrition of pathogens. Nature **468,** 527-532.

Chen, X., Chern, M., Canlas, P.E., Ruan, D., Jiang, C., and Ronald, P.C. (2010b). An ATPase promotes autophosphorylation of the pattern recognition receptor XA21 and inhibits XA21-mediated immunity. Proc Natl Acad Sci U S A **107,** 8029-8034.

Chen, X., Chern, M., Canlas, P.E., Jiang, C., Ruan, D., Cao, P., and Ronald, P.C. (2010c). A Conserved Threonine Residue in the Juxtamembrane Domain of the XA21 Pattern Recognition Receptor Is Critical for Kinase Autophosphorylation and XA21-mediated Immunity. Journal of Biological Chemistry **285,** 10454-10463.

Chinchilla, D., Zipfel, C., Robatzek, S., Kemmerling, B., Nurnberger, T., Jones, J.D., Felix, G., and Boller, T. (2007). A flagellin-induced complex of the receptor FLS2 and BAK1 initiates plant defense. Nature **448,** 497-500.

Clay, N.K., Adio, A.M., Denoux, C., Jander, G., and Ausubel, F.M. (2009). Glucosinolate metabolites required for an Arabidopsis innate immune response. Science **323,** 95-101.

Clough, S.J., and Bent, A.F. (1998). Floral dip: a simplified method for Agrobacterium-mediated transformation of Arabidopsis thaliana. Plant J **16,** 735-743.

Coates, M.E., and Beynon, J.L. (2010). Hyaloperonospora Arabidopsidis as a pathogen model. Annu Rev Phytopathol **48,** 329-345.

Collins, N.C., Thordal-Christensen, H., Lipka, V., Bau, S., Kombrink, E., Qiu, J.-L., Huckelhoven, R., Stein, M., Freialdenhoven, A., Somerville, S.C., and Schulze-Lefert, P. (2003). SNARE-protein-mediated disease resistance at the plant cell wall. Nature **425,** 973-977.

Cunnac, S., Lindeberg, M., and Collmer, A. (2009). Pseudomonas syringae type III secretion system effectors: repertoires in search of functions. Current Opinion in Microbiology **12,** 53-60.

Daines, B., Wang, H., Li, Y., Han, Y., Gibbs, R., and Chen, R. (2009). High-Throughput Multiplex Sequencing to Discover Copy Number Variants in Drosophila. Genetics **182,** 935-941.

de Torres-Zabala, M., Truman, W., Bennett, M.H., Lafforgue, G., Mansfield, J.W., Rodriguez Egea, P., Bogre, L., and Grant, M. (2007). Pseudomonas syringae pv. tomato hijacks the Arabidopsis abscisic acid signaling pathway to cause disease. Embo J **26,** 1434-1443.

Denoux, C., Galletti, R., Mammarella, N., Gopalan, S., Werck, D.l., De Lorenzo, G., Ferrari, S., Ausubel, F.M., and Dewdney, J. (2008). Activation of Defense Response Pathways by OGs and Flg22 Elicitors in Arabidopsis Seedlings. Molecular Plant **1,** 423-445.

Dhonukshe, P., Aniento, F., Hwang, I., Robinson, D.G., Mravec, J., Stierhof, Y.-D., and Friml, J. (2007). Clathrin-Mediated Constitutive Endocytosis of PIN Auxin Efflux Carriers in Arabidopsis. Current Biology **17,** 520-527.

Earley, K.W., Haag, J.R., Pontes, O., Opper, K., Juehne, T., Song, K., and Pikaard, C.S. (2006). Gateway-compatible vectors for plant functional genomics and proteomics. Plant J **45,** 616-629.

Eberhard, S., Finazzi, G., and Wollman, F.A. (2008). The dynamics of photosynthesis. Annu Rev Genet **42,** 463-515.

Ebine, K., Fujimoto, M., Okatani, Y., Nishiyama, T., Goh, T., Ito, E., Dainobu, T., Nishitani, A., Uemura, T., Sato, M.H., Thordal-Christensen, H., Tsutsumi, N., Nakano, A., and Ueda, T. (2011). A membrane trafficking pathway regulated by the plant-specific RAB GTPase ARA6. Nat Cell Biol.

Field, M.C., and Dacks, J.B. (2009). First and last ancestors: reconstructing evolution of the endomembrane system with ESCRTs, vesicle coat proteins, and nuclear pore complexes. Curr Opin Cell Biol **21,** 4-13.

Fiume, M., Williams, V., Brook, A., and Brudno, M. (2010). Savant: genome browser for high-throughput sequencing data. Bioinformatics **26,** 1938-1944.

Forsyth, A., Mansfield, J.W., Grabov, N., de Torres, M., Sinapidou, E., and Grant, M.R. (2010). Genetic dissection of basal resistance to Pseudomonas syringae pv. phaseolicola in accessions of Arabidopsis. Mol Plant Microbe Interact **23,** 1545-1552.

Frey, N.F.d., and Robatzek, S. (2009). Trafficking vesicles: pro or contra pathogens? Current Opinion in Plant Biology **12,** 437-443.

Fujiki, Y., Ito, M., Nishida, I., and Watanabe, A. (2000). Multiple Signaling Pathways in Gene Expression during Sugar Starvation. Pharmacological Analysis of din Gene Expression in Suspension-Cultured Cells of Arabidopsis. Plant Physiology **124,** 1139-1148.

Geldner, N., Hyman, D.L., Wang, X., Schumacher, K., and Chory, J. (2007). Endosomal signaling of plant steroid receptor kinase BRI1. Genes Dev **21,** 1598-1602.

Gimenez-Ibanez, S., Hann, D.R., Ntoukakis, V., Petutschnig, E., Lipka, V., and Rathjen, J.P. (2009). AvrPtoB Targets the LysM Receptor Kinase CERK1 to Promote Bacterial Virulence on Plants. Current biology : CB **19,** 423-429.

Göhre, V., Spallek, T., Häweker, H., Mersmann, S., Mentzel, T., Boller, T., de Torres, M., Mansfield, J.W., and Robatzek, S. (2008). Plant Pattern-Recognition Receptor FLS2 Is Directed for Degradation by the Bacterial Ubiquitin Ligase AvrPtoB. Current Biology **18,** 1824-1832.

Gómez-Gómez, L., and Boller, T. (2000). FLS2: An LRR Receptor-like Kinase Involved in the Perception of the Bacterial Elicitor Flagellin in Arabidopsis. Molecular Cell **5,** 1003-1011.

Gudesblat, G.E., Torres, P.S., and Vojnov, A.A. (2009). Xanthomonas campestris overcomes Arabidopsis stomatal innate immunity through a DSF cell-to-cell signal-regulated virulence factor. Plant Physiol **149,** 1017-1027.

Haas, T.J., Sliwinski, M.K., MartÃnez, D.E., Preuss, M., Ebine, K., Ueda, T., Nielsen, E., Odorizzi, G., and Otegui, M.S. (2007). The Arabidopsis AAA ATPase SKD1 Is Involved in Multivesicular Endosome Function and Interacts with Its Positive Regulator LYST-INTERACTING PROTEIN5. The Plant Cell Online **19,** 1295-1312.

Ham, J.H., Kim, M.G., Lee, S.Y., and Mackey, D. (2007). Layered basal defenses underlie non-host resistance of Arabidopsis to Pseudomonas syringae pv. phaseolicola. Plant J **51,** 604-616.

Hann, D.R., and Rathjen, J.P. (2007). Early events in the pathogenicity of Pseudomonas syringae on Nicotiana benthamiana. Plant J **49,** 607-618.

Heese, M., Gansel, X., Sticher, L., Wick, P., Grebe, M., Granier, F., and Juergens, G. (2001). Functional characterization of the KNOLLE-interacting t-SNARE AtSNAP33 and its role in plant cytokinesis. The Journal of Cell Biology **155,** 239-250.

Henne, W.M., Buchkovich, N.J., and Emr, S.D. (2011). The ESCRT Pathway. Dev Cell **21,** 77-91.

Hicks, G.R., and Raikhel, N.V. (2010). Advances in dissecting endomembrane trafficking with small molecules. Current Opinion in Plant Biology **13,** 706-713.

Huang, H.R., Chen, Z.J., Kunes, S., Chang, G.D., and Maniatis, T. (2010). Endocytic pathway is required for Drosophila Toll innate immune signaling. Proc Natl Acad Sci U S A **107,** 8322-8327.

Hurley, J.H., and Hanson, P.I. (2010). Membrane budding and scission by the ESCRT machinery: it's all in the neck. Nat Rev Mol Cell Biol **11,** 556-566.

Husebye, H., Halaas, O., Stenmark, H., Tunheim, G., Sandanger, O., Bogen, B., Brech, A., Latz, E., and Espevik, T. (2006). Endocytic pathways regulate Toll-like receptor 4 signaling and link innate and adaptive immunity. EMBO J **25,** 683-692.

Jander, G., Norris, S.R., Rounsley, S.D., Bush, D.F., Levin, I.M., and Last, R.L. (2002). Arabidopsis Map-Based Cloning in the Post-Genome Era. Plant Physiology **129,** 440-450.

JCBN, I.-I.J.C.o.B.N. (1984). Nomenclature and symbolism for amino acids and peptides. Recommendations 1983. Biochem J **219,** 345-373.

Jeworutzki, E., Roelfsema, M.R.G., Anschütz, U., Krol, E., Elzenga, J.T.M., Felix, G., Boller, T., Hedrich, R., and Becker, D. (2010). Early signaling through the Arabidopsis pattern recognition receptors FLS2 and EFR involves Ca2+-associated opening of plasma membrane anion channels. The Plant Journal **62,** 367-378.

Jia, Y., and Martin, G.B. (1999). Rapid transcript accumulation of pathogenesis-related genes during an incompatible interaction in bacterial speck disease-resistant tomato plants. Plant Molecular Biology **40,** 455-465.

Jones, J.D., and Dangl, J.L. (2006). The plant immune system. Nature **444,** 323-329.

Kagan, J.C., Su, T., Horng, T., Chow, A., Akira, S., and Medzhitov, R. (2008). TRAM couples endocytosis of Toll-like receptor 4 to the induction of interferon-beta. Nat Immunol **9,** 361-368.

Kaku, H., Nishizawa, Y., Ishii-Minami, N., Akimoto-Tomiyama, C., Dohmae, N., Takio, K., Minami, E., and Shibuya, N. (2006). Plant cells recognize chitin fragments for defense signaling through a plasma membrane receptor. Proc Natl Acad Sci U S A **103,** 11086-11091.

Kasai, K., Takano, J., Miwa, K., Toyoda, A., and Fujiwara, T. (2010). High Boron-induced Ubiquitination Regulates Vacuolar Sorting of the BOR1 Borate Transporter in Arabidopsis thaliana. Journal of Biological Chemistry **286,** 6175-6183.

Kunze, G., Zipfel, C., Robatzek, S., Niehaus, K., Boller, T., and Felix, G. (2004). The N terminus of bacterial elongation factor Tu elicits innate immunity in Arabidopsis plants. Plant Cell **16,** 3496-3507.

Kwaaitaal, M., Huisman, R., Maintz, J., Reinstadler, A., and Panstruga, R. (2011). Ionotropic glutamate receptor (iGluR)-like channels mediate MAMP-induced calcium influx in Arabidopsis thaliana. Biochem J.

Kwon, C., Neu, C., Pajonk, S., Yun, H.S., Lipka, U., Humphry, M., Bau, S., Straus, M., Kwaaitaal, M., Rampelt, H., Kasmi, F.E., Jurgens, G., Parker, J., Panstruga, R., Lipka, V., and Schulze-Lefert, P. (2008). Co-option of a default secretory pathway for plant immune responses. Nature **451,** 835-840.

Lacombe, S., Rougon-Cardoso, A., Sherwood, E., Peeters, N., Dahlbeck, D., van Esse, H.P., Smoker, M., Rallapalli, G., Thomma, B.P., Staskawicz, B., Jones, J.D., and Zipfel, C. (2010).

Interfamily transfer of a plant pattern-recognition receptor confers broad-spectrum bacterial resistance. Nat Biotechnol **28,** 365-369.

Lambris, J.D. (2007). Current topics in innate immunity. (Springer).

Lee, D., Polisensky, D.H., and Braam, J. (2005). Genome-wide identification of touch- and darkness-regulated Arabidopsis genes: a focus on calmodulin-like and XTH genes. New Phytol **165,** 429-444.

Li, J., Wen, J., Lease, K.A., Doke, J.T., Tax, F.E., and Walker, J.C. (2002). BAK1, an Arabidopsis LRR receptor-like protein kinase, interacts with BRI1 and modulates brassinosteroid signaling. Cell **110,** 213-222.

Li, Y., Zhang, Q., Zhang, J., Wu, L., Qi, Y., and Zhou, J.M. (2010). Identification of microRNAs involved in pathogen-associated molecular pattern-triggered plant innate immunity. Plant Physiol **152,** 2222-2231.

Lipka, V., Dittgen, J., Bednarek, P., Bhat, R., Wiermer, M., Stein, M., Landtag, J.r., Brandt, W., Rosahl, S., Scheel, D., Llorente, F., Molina, A., Parker, J., Somerville, S., and Schulze-Lefert, P. (2005). Pre- and Postinvasion Defenses Both Contribute to Nonhost Resistance in Arabidopsis. Science **310,** 1180-1183.

Lloyd, T.E., Atkinson, R., Wu, M.N., Zhou, Y., Pennetta, G., and Bellen, H.J. (2002). Hrs regulates endosome membrane invagination and tyrosine kinase receptor signaling in Drosophila. Cell **108,** 261-269.

Lu, D., Lin, W., Gao, X., Wu, S., Cheng, C., Avila, J., Heese, A., Devarenne, T.P., He, P., and Shan, L. (2011). Direct Ubiquitination of Pattern Recognition Receptor FLS2 Attenuates Plant Innate Immunity. Science **332,** 1439-1442.

Lu, X., Tintor, N., Mentzel, T., Kombrink, E., Boller, T., Robatzek, S., Schulze-Lefert, P., and Saijo, Y. (2009). Uncoupling of sustained MAMP receptor signaling from early outputs in an Arabidopsis endoplasmic reticulum glucosidase II allele. Proceedings of the National Academy of Sciences **106,** 22522-22527.

Luna, E., Pastor, V., Robert, J.r.m., Flors, V., Mauch-Mani, B., and Ton, J. (2011). Callose Deposition: A Multifaceted Plant Defense Response. Mol. Plant-Microbe Interact. **24,** 183-193.

Lund, V.K., DeLotto, Y., and DeLotto, R. (2010). Endocytosis is required for Toll signaling and shaping of the Dorsal/NF-kappaB morphogen gradient during Drosophila embryogenesis. Proc Natl Acad Sci U S A **107,** 18028-18033.

Malerod, L., Stuffers, S., Brech, A., and Stenmark, H. (2007). Vps22/EAP30 in ESCRT-II mediates endosomal sorting of growth factor and chemokine receptors destined for lysosomal degradation. Traffic **8,** 1617-1629.

McKinney, E.C., Ali, N., Traut, A., Feldmann, K.A., Belostotsky, D.A., McDowell, J.M., and Meagher, R.B. (1995). Sequence-based identification of T-DNA insertion mutations in Arabidopsis: actin mutants act2-1 and act4-1. Plant J **8,** 613-622.

Melotto, M., Underwood, W., Koczan, J., Nomura, K., and He, S.Y. (2006). Plant Stomata Function in Innate Immunity against Bacterial Invasion. Cell **126,** 969-980.

Mendes, B.M.J., Cardoso, S.C., Boscariol-Camargo, R.L., Cruz, R.B., Mourão Filho, F.A.A., and Bergamin Filho, A. (2009). Reduction in susceptibility to Xanthomonas axonopodis pv. citri in transgenic Citrus sinensis expressing the rice Xa21 gene. Plant Pathology **59,** 68-75.

Mersmann, S., Bourdais, G., Rietz, S., and Robatzek, S. (2010). Ethylene Signaling Regulates Accumulation of the FLS2 Receptor and Is Required for the Oxidative Burst Contributing to Plant Immunity. Plant Physiology **154,** 391-400.

Miya, A., Albert, P., Shinya, T., Desaki, Y., Ichimura, K., Shirasu, K., Narusaka, Y., Kawakami, N., Kaku, H., and Shibuya, N. (2007). CERK1, a LysM receptor kinase, is essential for chitin elicitor signaling in Arabidopsis. Proceedings of the National Academy of Sciences **104,** 19613-19618.

Mukhopadhyay, D., and Riezman, H. (2007). Proteasome-Independent Functions of Ubiquitin in Endocytosis and Signaling. Science **315,** 201-205.

Nakagawa, T., Kurose, T., Hino, T., Tanaka, K., Kawamukai, M., Niwa, Y., Toyooka, K., Matsuoka, K., Jinbo, T., and Kimura, T. (2007). Development of series of gateway binary vectors, pGWBs, for realizing efficient construction of fusion genes for plant transformation. Journal of Bioscience and Bioengineering **104,** 34-41.

Navarro, L., Bari, R., Achard, P., Lison, P., Nemri, A., Harberd, N.P., and Jones, J.D. (2008). DELLAs control plant immune responses by modulating the balance of jasmonic acid and salicylic acid signaling. Curr Biol **18,** 650-655.

Navarro, L., Dunoyer, P., Jay, F., Arnold, B., Dharmasiri, N., Estelle, M., Voinnet, O., and Jones, J.D.G. (2006). A Plant miRNA Contributes to Antibacterial Resistance by Repressing Auxin Signaling. Science **312,** 436-439.

Nekrasov, V., Li, J., Batoux, M., Roux, M., Chu, Z.-H., Lacombe, S., Rougon, A., Bittel, P., Kiss-Papp, M., Chinchilla, D., van Esse, H.P., Jorda, L., Schwessinger, B., Nicaise, V., Thomma, B.P.H.J., Molina, A., Jones, J.D.G., and Zipfel, C. (2009). Control of the pattern-recognition receptor EFR by an ER protein complex in plant immunity. EMBO J **28,** 3428-3438.

Nishimura, M.T., Stein, M.n., Hou, B.-H., Vogel, J.P., Edwards, H., and Somerville, S.C. (2003). Loss of a Callose Synthase Results in Salicylic Acid-Dependent Disease Resistance. Science **301,** 969-972.

Parmigiani, G., Garrett, E., Irizarry, R., Zeger, S., Gautier, L., and Cope, L. (2003). An R Package for Analyzes of Affymetrix Oligonucleotide Arrays. In The Analysis of Gene Expression Data, M. Gail, K. Krickeberg, J.M. Samet, A. Tsiatis, and W. Wong, eds (Springer London), pp. 102-119.

Raiborg, C., and Stenmark, H. (2009). The ESCRT machinery in endosomal sorting of ubiquitylated membrane proteins. Nature **458,** 445-452.

Richter, S., Voss, U., and Jurgens, G. (2009). Post-Golgi traffic in plants. Traffic **10,** 819-828.

Robatzek, S., Chinchilla, D., and Boller, T. (2006). Ligand-induced endocytosis of the pattern recognition receptor FLS2 in Arabidopsis. Genes Dev **20,** 537-542.

Robatzek, S., Bittel, P., Chinchilla, D., Kochner, P., Felix, G., Shiu, S.H., and Boller, T. (2007). Molecular identification and characterization of the tomato flagellin receptor LeFLS2, an orthologue of Arabidopsis FLS2 exhibiting characteristically different perception specificities. Plant Mol Biol **64,** 539-547.

Robinson, D.G., Jiang, L., and Schumacher, K. (2008). The endosomal system of plants: charting new and familiar territories. Plant Physiol **147,** 1482-1492.

Rodriguez, M.C., Petersen, M., and Mundy, J. (2010). Mitogen-activated protein kinase signaling in plants. Annu Rev Plant Biol **61,** 621-649.

Rogers, S., Wells, R., and Rechsteiner, M. (1986). Amino acid sequences common to rapidly degraded proteins: the PEST hypothesis. Science **234,** 364-368.

Ron, M., and Avni, A. (2004). The receptor for the fungal elicitor ethylene-inducing xylanase is a member of a resistance-like gene family in tomato. Plant Cell **16,** 1604-1615.

Rosebrock, T.R., Zeng, L., Brady, J.J., Abramovitch, R.B., Xiao, F., and Martin, G.B. (2007). A bacterial E3 ubiquitin ligase targets a host protein kinase to disrupt plant immunity. Nature **448,** 370-374.

Roux, M., Schwessinger, B., Albrecht, C., Chinchilla, D., Jones, A., Holton, N., Malinovsky, F.G., Tor, M., de Vries, S., and Zipfel, C. (2011). The Arabidopsis Leucine-Rich Repeat Receptor-Like Kinases BAK1/SERK3 and BKK1/SERK4 Are Required for Innate Immunity to Hemibiotrophic and Biotrophic Pathogens. Plant Cell.

Rushton, P.J., Somssich, I.E., Ringler, P., and Shen, Q.J. (2010). WRKY transcription factors. Trends in Plant Science **15,** 247-258.

Russinova, E., Borst, J.-W., Kwaaitaal, M., CaÃ±o-Delgado, A., Yin, Y., Chory, J., and de Vries, S.C. (2004). Heterodimerization and Endocytosis of Arabidopsis Brassinosteroid Receptors BRI1 and AtSERK3 (BAK1). The Plant Cell Online **16,** 3216-3229.

Ruthardt, N., Gulde, N., Spiegel, H., Fischer, R., and Emans, N. (2005). Four-dimensional imaging of transvacuolar strand dynamics in tobacco BY-2 cells. Protoplasma **225,** 205-215.

Sadowski, L., Pilecka, I., and Miaczynska, M. (2009). Signaling from endosomes: location makes a difference. Exp Cell Res **315,** 1601-1609.

Saeed, A.I., Sharov, V., White, J., Li, J., Liang, W., Bhagabati, N., Braisted, J., Klapa, M., Currier, T., Thiagarajan, M., Sturn, A., Snuffin, M., Rezantsev, A., Popov, D., Ryltsov, A., Kostukovich, E., Borisovsky, I., Liu, Z., Vinsavich, A., Trush, V., and Quackenbush, J. (2003). TM4: a free, open-source system for microarray data management and analysis. Biotechniques **34,** 374-378.

Saibo, N.J., Lourenco, T., and Oliveira, M.M. (2009). Transcription factors and regulation of photosynthetic and related metabolism under environmental stresses. Ann Bot **103,** 609-623.

Saijo, Y., Tintor, N., Lu, X., Rauf, P., Pajerowska-Mukhtar, K., Haweker, H., Dong, X., Robatzek, S., and Schulze-Lefert, P. (2009). Receptor quality control in the endoplasmic reticulum for plant innate immunity. EMBO J **28,** 3439-3449.

Salomon, S., and Robatzek, S. (2006). Induced Endocytosis of the Receptor Kinase FLS2. Plant Signal Behav **1,** 293-295.

Salomon, S., Grunewald, D., Stuber, K., Schaaf, S., MacLean, D., Schulze-Lefert, P., and Robatzek, S. (2010). High-throughput confocal imaging of intact live tissue enables quantification of membrane trafficking in Arabidopsis. Plant Physiol **154,** 1096-1104.

Salomon, S.A. (2009). Linking endosomal traffic and PAMP-triggered immuity in plants. In Mathematisch-Naturwissenschaftlichen Fakultät der Universität zu Köln (Cologene: Universität zu Köln), pp. 106.

Sambrook, J., and William Russell, D. (2001). Molecular cloning: a laboratory manual. (NY: CSHL Press).

Sanger, F., Nicklen, S., and Coulson, A.R. (1977). DNA sequencing with chain-terminating inhibitors. Proc Natl Acad Sci U S A **74,** 5463-5467.

Schneeberger, K., Ossowski, S., Ott, F., Klein, J.D., Wang, X., Lanz, C., Smith, L.M., Cao, J., Fitz, J., Warthmann, N., Henz, S.R., Huson, D.H., and Weigel, D. (2011). Reference-guided assembly of four diverse Arabidopsis thaliana genomes. Proc Natl Acad Sci U S A **108,** 10249-10254.

Schulze, B., Mentzel, T., Jehle, A.K., Mueller, K., Beeler, S., Boller, T., Felix, G., and Chinchilla, D. (2010). Rapid Heteromerization and Phosphorylation of Ligand-activated Plant Transmembrane Receptors and Their Associated Kinase BAK1. Journal of Biological Chemistry **285,** 9444-9451.

Schwessinger, B., Roux, M., Kadota, Y., Ntoukakis, V., Sklenar, J., Jones, A., and Zipfel, C. (2011). Phosphorylation-Dependent Differential Regulation of Plant Growth, Cell Death, and Innate Immunity by the Regulatory Receptor-Like Kinase BAK1. PLoS Genet **7,** e1002046.

Scita, G., and Di Fiore, P.P. (2010). The endocytic matrix. Nature **463,** 464-473.

Shahriari, M., Richter, K., Keshavaiah, C., Sabovljevic, A., Huelskamp, M., and Schellmann, S. (2011). The Arabidopsis ESCRT protein-protein interaction network. Plant Mol Biol **76,** 85-96.

Shan, L., He, P., Li, J., Heese, A., Peck, S.C., Nürnberger, T., Martin, G.B., and Sheen, J. (2008). Bacterial Effectors Target the Common Signaling Partner BAK1 to Disrupt Multiple MAMP Receptor-Signaling Complexes and Impede Plant Immunity. Cell Host & Microbe **4,** 17-27.

Sharfman, M., Bar, M., Ehrlich, M., Schuster, S., Melech-Bonfil, S., Ezer, R., Sessa, G., and Avni, A. (2011). Endosomal signaling of the tomato leucine-rich repeat receptor-like protein LeEix2. Plant J.

Song, W.-Y., Wang, G.-L., Chen, L.-L., Kim, H.-S., Pi, L.-Y., Holsten, T., Gardner, J., Wang, B., Zhai, W.-X., Zhu, L.-H., Fauquet, C., and Ronald, P. (1995). A Receptor Kinase-Like Protein Encoded by the Rice Disease Resistance Gene, Xa21. Science **270,** 1804-1806.

Sorkin, A., and von Zastrow, M. (2009). Endocytosis and signaling: intertwining molecular networks. Nat Rev Mol Cell Biol **10,** 609-622.

Spallek, T., Robatzek, S., and Göhre, V. (2009). How microbes utilize host ubiquitination. Cellular Microbiology **11,** 1425-1434.

Spitzer, C., Reyes, F.C., Buono, R., Sliwinski, M.K., Haas, T.J., and Otegui, M.S. (2009). The ESCRT-related CHMP1A and B proteins mediate multivesicular body sorting of auxin carriers in Arabidopsis and are required for plant development. Plant Cell **21,** 749-766.

Spitzer, C., Schellmann, S., Sabovljevic, A., Shahriari, M., Keshavaiah, C., Bechtold, N., Herzog, M., MÃ¼ller, S., Hanisch, F.-G., and HÃ¼lskamp, M. (2006). The Arabidopsis elch mutant reveals functions of an ESCRT component in cytokinesis. Development **133,** 4679-4689.

Stefani, F., Zhang, L., Taylor, S., Donovan, J., Rollinson, S., Doyotte, A., Brownhill, K., Bennion, J., Pickering-Brown, S., and Woodman, P. (2011). UBAP1 Is a Component of an Endosome-Specific ESCRT-I Complex that Is Essential for MVB Sorting. Curr Biol.

Stein, M.n., Dittgen, J., SÃ¡nchez-RodrÃ-guez, C., Hou, B.-H., Molina, A., Schulze-Lefert, P., Lipka, V., and Somerville, S. (2006). Arabidopsis PEN3/PDR8, an ATP Binding Cassette Transporter, Contributes to Nonhost Resistance to Inappropriate Pathogens That Enter by Direct Penetration. The Plant Cell Online **18,** 731-746.

Stenmark, H., and Olkkonen, V.M. (2001). The Rab GTPase family. Genome Biol **2,** REVIEWS3007.

Stergiopoulos, I., and de Wit, P.J. (2009). Fungal effector proteins. Annu Rev Phytopathol **47,** 233-263.

Takai, R., Isogai, A., Takayama, S., and Che, F.S. (2008). Analysis of flagellin perception mediated by flg22 receptor OsFLS2 in rice. Mol Plant Microbe Interact **21,** 1635-1642.

Takano, J., Miwa, K., Yuan, L., von Wiren, N., and Fujiwara, T. (2005). Endocytosis and degradation of BOR1, a boron transporter of Arabidopsis thaliana, regulated by boron availability. Proc Natl Acad Sci U S A **102,** 12276-12281.

Toer, M., Gordon, P., Cuzick, A., Eulgem, T., Sinapidou, E., Mert-Tuerk, F., Can, C., Dangl, J.L., and Holub, E.B. (2002). Arabidopsis SGT1b Is Required for Defense Signaling Conferred by Several Downy Mildew Resistance Genes. The Plant Cell Online **14,** 993-1003.

Torii, K.U., Mitsukawa, N., Oosumi, T., Matsuura, Y., Yokoyama, R., Whittier, R.F., and Komeda, Y. (1996). The Arabidopsis ERECTA Gene Encodes a Putative Receptor Protein Kinase with Extracellular Leucine-Rich Repeats. The Plant Cell Online **8,** 735-746.

Trujillo, M., Ichimura, K., Casais, C., and Shirasu, K. (2008). Negative Regulation of PAMP-Triggered Immunity by an E3 Ubiquitin Ligase Triplet in Arabidopsis. Current biology : CB **18,** 1396-1401.

Tsuda, K., Sato, M., Stoddard, T., Glazebrook, J., and Katagiri, F. (2009). Network properties of robust immunity in plants. PLoS Genet **5,** e1000772.

Veyres, N., Danon, A., Aono, M., Galliot, S., Karibasappa, Y.B., Diet, A., Grandmottet, F., Tamaoki, M., Lesur, D., Pilard, S., Boitel-Conti, M., Sangwan-Norreel, B.S., and Sangwan, R.S. (2008). The Arabidopsis sweetie mutant is affected in carbohydrate metabolism and defective in the control of growth, development and senescence. The Plant Journal **55,** 665-686.

Viotti, C., Bubeck, J., Stierhof, Y.D., Krebs, M., Langhans, M., van den Berg, W., van Dongen, W., Richter, S., Geldner, N., Takano, J., Jurgens, G., de Vries, S.C., Robinson, D.G., and Schumacher, K. (2010). Endocytic and secretory traffic in Arabidopsis merge in the trans-Golgi network/early endosome, an independent and highly dynamic organelle. Plant Cell **22,** 1344-1357.

Wang, D., and Dong, X. (2011). A highway for war and peace: the secretory pathway in plant-microbe interactions. Mol Plant **4,** 581-587.

Wang, K.L., Li, H., and Ecker, J.R. (2002). Ethylene biosynthesis and signaling networks. Plant Cell **14 Suppl,** S131-151.

Wang, Y., Geer, L.Y., Chappey, C., Kans, J.A., and Bryant, S.H. (2000). Cn3D: sequence and structure views for Entrez. Trends in Biochemical Sciences **25,** 300-302.

Wegner, C.S., Rodahl, L.M.W., and Stenmark, H. (2011). ESCRT Proteins and Cell Signaling. Traffic**, no-no.**

Weigel, D., and Glazebrook, J. (2002). Arabidopsis: A Laboratory Manual (NY: Cold Spring Harbor Laboratory Press).

Weinl, C., Marquardt, S., Kuijt, S.J.H., Nowack, M.K., Jakoby, M.J., Huelskamp, M., and Schnittger, A. (2005). Novel Functions of Plant Cyclin-Dependent Kinase Inhibitors, ICK1/KRP1, Can Act Non-Cell-Autonomously and Inhibit Entry into Mitosis. The Plant Cell Online **17,** 1704-1722.

Xiang, T., Zong, N., Zhang, J., Chen, J., Chen, M., and Zhou, J.-M. (2011). BAK1 Is Not a Target of the Pseudomonas syringae Effector AvrPto. Mol. Plant-Microbe Interact. **24,** 100-107.

Yuan, J., and He, S.Y. (1996). The Pseudomonas syringae Hrp regulation and secretion system controls the production and secretion of multiple extracellular proteins. J. Bacteriol. **178,** 6399-6402.

Zhang, J., and Zhou, J.M. (2010). Plant immunity triggered by microbial molecular signatures. Mol Plant **3,** 783-793.

Zhang, J., Shao, F., Li, Y., Cui, H., Chen, L., Li, H., Zou, Y., Long, C., Lan, L., Chai, J., Chen, S., Tang, X., and Zhou, J.-M. (2007a). A Pseudomonas syringae Effector Inactivates MAPKs to Suppress PAMP-Induced Immunity in Plants. Cell Host & Microbe **1,** 175-185.

Zhang, J., Li, W., Xiang, T., Liu, Z., Laluk, K., Ding, X., Zou, Y., Gao, M., Zhang, X., Chen, S., Mengiste, T., Zhang, Y., and Zhou, J.M. (2010). Receptor-like cytoplasmic kinases integrate signaling from multiple plant immune receptors and are targeted by a Pseudomonas syringae effector. Cell Host Microbe **7,** 290-301.

Zhang, Z., Li, Q., Li, Z., Staswick, P.E., Wang, M., Zhu, Y., and He, Z. (2007b). Dual regulation role of GH3.5 in salicylic acid and auxin signaling during Arabidopsis-Pseudomonas syringae interaction. Plant Physiol **145,** 450-464.

Zhong, G.Y., and Burns, J.K. (2003). Profiling ethylene-regulated gene expression in Arabidopsis thaliana by microarray analysis. Plant Mol Biol **53,** 117-131.

Zhou, L., Jang, J.C., Jones, T.L., and Sheen, J. (1998). Glucose and ethylene signal transduction crosstalk revealed by an Arabidopsis glucose-insensitive mutant. Proc Natl Acad Sci U S A **95,** 10294-10299.

Zipfel, C., Robatzek, S., Navarro, L., Oakeley, E.J., Jones, J.D., Felix, G., and Boller, T. (2004). Bacterial disease resistance in Arabidopsis through flagellin perception. Nature **428,** 764-767.

Zipfel, C., Kunze, G., Chinchilla, D., Caniard, A., Jones, J.D.G., Boller, T., and Felix, G. (2006). Perception of the Bacterial PAMP EF-Tu by the Receptor EFR Restricts Agrobacterium-Mediated Transformation. Cell **125,** 749-760.

APPENDIX

APPENDIX A – SUPPLEMENT DATA
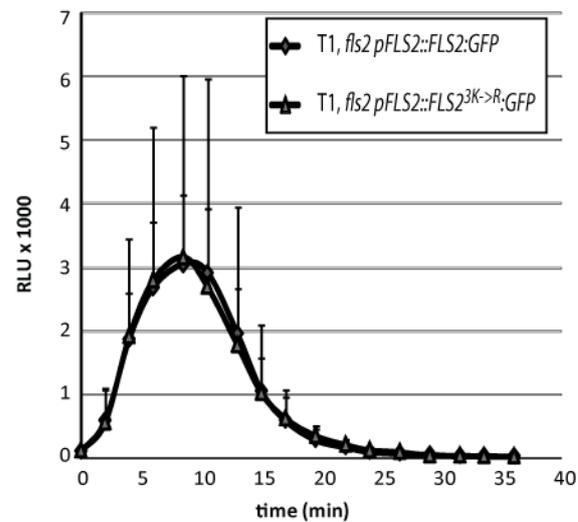
Suppl. Fig. 1   **ROS in T$_1$ *fls2* complemented lines.** Leaf disks of 15 individual eight-week-old T$_1$ plants were tested for flg22-sensitiviety in ROS measurements. Error bars show +/- SD.
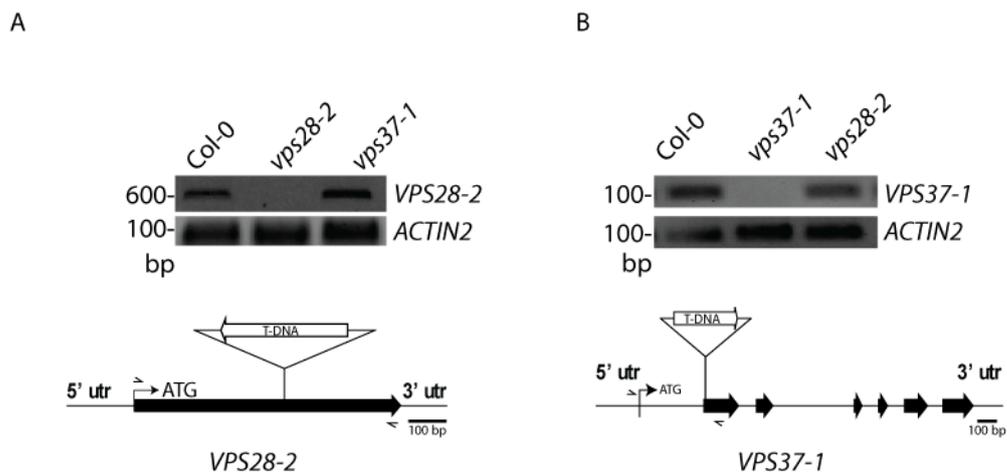
Suppl. Fig. 2   **Analyzes of T-DNA insertion lines *vps28-2* and *vps37-1*.** (A) *VPS28-2* and a fragment of *VPS37-1* including translation start site (B) were amplified from cDNA of Col-0 wt, *vps28-2* and *vps37-1* T-DNA mutants. Actin2 was used as a control. Lower panels indicate position and orientation of T-DNA and used primers. Bars present 100 bp.
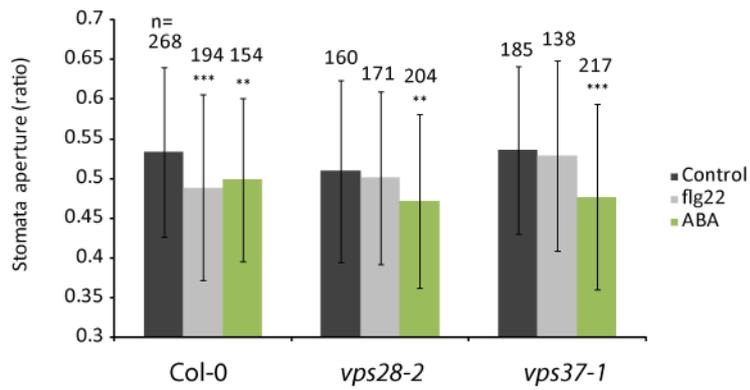
Suppl. Fig. 3   ***ESCRT-1* mutatns *vps28-2* and *vps37-1* are not impaired in ABA mediated stomatal closure.** Stomatal aperture measurements of n two-week-old seedlings were done after incubation in 5 µM flg22 (grey) and 10 µM ABA (green). Significance was calculated by multiple pairwise comparisons according to standard posthoc ANOVA analysis (collaboration with Dr. Gildas Bourdais, The Sainsbury Laboratory, Norwich, UK).
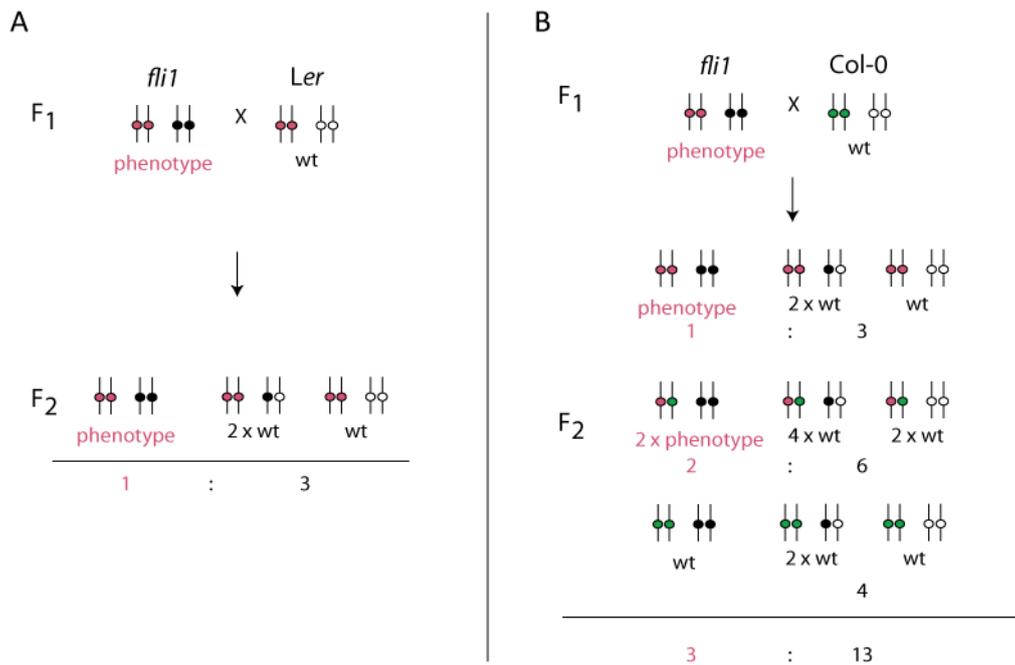
Suppl. Fig. 4   **Models of *fli1* genetics.** A) 1:3 ration in *fli1* x L*er* backcrosses indicates recessive inheritance of one single *fli1* locus. (B) 3:13 can be explained by the requirement of a second dominant L*er* allele (pink) for *fli1* phenotype development in Col-0 crosses.
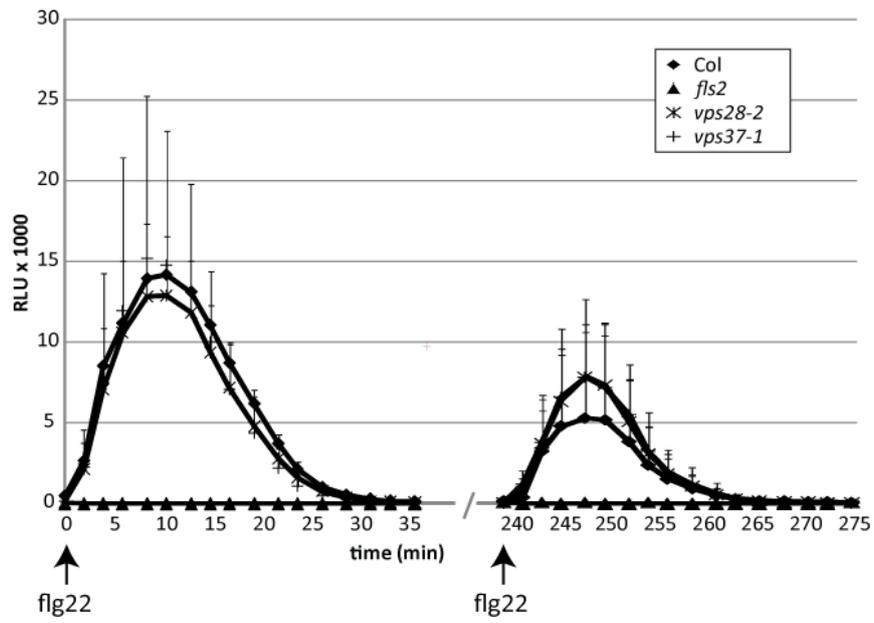
Suppl. Fig. 5   **ESCRT-1 mutants are less desensitised for subsequent ROS burst.** ROS measurements were done of eight biological replicates in two independent experiments on four-week-old plants. Leaf disks were washed twice with ddH_2O after first measurements were completed. Error bars indicate +/- SD.

Suppl. table 1   MASCOT analysis of ubiquitinated FLS2CD

1. <u>FLS2-CD-His</u>   Mass: 41569   Score: 1038   Queries matched: 29   emPAI: 4.64
    FLS2-CD-His
    ☐ Check to include this hit in error tolerant search or archive report

	Query	Observed	Mr(expt)	Mr(calc)	Delta	Miss	Score	Expect	Rank	Peptide
☑	86	424.24	846.47	846.44	0.02	0	40	0.00011	1	R.LQASSVDK.L
☑	197	554.30	1106.59	1106.58	0.01	0	56	2.4e-006	1	K.ILGFAWESGK.T
☑	213	580.32	1158.63	1158.58	0.05	0	34	0.00038	1	R.VAHVSDFGTAR.I
☑	227	611.34	1220.67	1220.59	0.07	0	(32)	0.0006	1	K.QEEAIEDFLK.L
☑	228	611.36	1220.71	1220.59	0.11	0	41	8e-005	1	K.QEEAIEDFLK.L
☑	231	615.40	1228.79	1228.67	0.12	0	77	2.2e-008	1	K.GQLEDGTVIAVK.V
☑	274	503.57	1507.69	1507.68	0.01	2	8	0.14	1	K.ANSFREDRNEDR.E
☑	278	759.95	1517.89	1517.80	0.08	0	(74)	3.6e-008	1	R.VLDMELGDSIVSLK.Q
☑	283	767.92	1533.83	1533.80	0.03	0	97	2.2e-010	1	R.VLDMELGDSIVSLK.Q + Oxidation (M)
☑	284	767.94	1533.87	1533.80	0.07	0	(61)	8.1e-007	1	R.VLDMELGDSIVSLK.Q + Oxidation (M)
☑	289	792.42	1582.83	1582.80	0.03	0	(93)	5.5e-010	1	R.EVDIGDPNSVQALAR.L
☑	290	528.62	1582.84	1582.80	0.04	0	(38)	0.00016	1	R.EVDIGDPNSVQALAR.L
☑	291	792.43	1582.85	1582.80	0.05	0	104	4.4e-011	1	R.EVDIGDPNSVQALAR.L
☑	348	613.30	1836.88	1836.82	0.06	1	8	0.16	1	K.EFSAESDKWFYTEAK.T
☑	362	940.98	1879.95	1879.88	0.07	0	61	7.2e-007	1	K.ADVFSFGIIMMELMTK.Q + 3 Oxidation (M)
☑	375	976.43	1950.85	1950.91	-0.06	0	103	4.6e-011	1	-.MIENSSESSLPDLDSALK.L + Oxidation (M)
☑	376	651.30	1950.88	1950.91	-0.03	0	(22)	0.0068	1	-.MIENSSESSLPDLDSALK.L + Oxidation (M)
☑	377	651.36	1951.06	1950.91	0.15	0	(23)	0.0054	1	-.MIENSSESSLPDLDSALK.L + Oxidation (M)
☑	387	989.98	1977.95	1977.92	0.03	0	(45)	2.9e-005	1	-.MIENSSESSLPDLDSALK.L + Carbamyl (N-term)
☑	396	997.98	1993.95	1993.91	0.03	0	(40)	9.4e-005	1	-.MIENSSESSLPDLDSALK.L + Carbamyl (N-term); Oxidation (M)
☑	397	998.00	1993.99	1993.91	0.07	0	(76)	2.8e-008	1	-.MIENSSESSLPDLDSALK.L + Carbamyl (N-term); Oxidation (M)
☑	398	665.67	1993.99	1993.91	0.07	0	(30)	0.00095	1	-.MIENSSESSLPDLDSALK.L + Carbamyl (N-term); Oxidation (M)
☑	447	1049.48	2096.95	2097.01	-0.06	1	(8)	0.14	1	R.NEDREVDIGDPNSVQALAR.L
☑	448	700.03	2097.07	2097.01	0.06	1	52	5.7e-006	1	R.NEDREVDIGDPNSVQALAR.L
☑	449	1049.55	2097.09	2097.01	0.08	1	(13)	0.048	1	R.NEDREVDIGDPNSVQALAR.L
☑	557	1175.49	2348.97	2349.14	-0.17	1	54	3.8e-006	1	-.MIENSSESSLPDLDSALKLK.R + Carbamyl (N-term); GlyGly (K); Ox
☑	588	833.45	2497.33	2497.18	0.15	2	(6)	0.27	1	R.EDRNEDREVDIGDPNSVQALAR.L
☑	589	625.34	2497.33	2497.18	0.15	2	23	0.0048	1	R.EDRNEDREVDIGDPNSVQALAR.L
☑	611	887.78	2660.32	2660.28	0.04	0	61	8.2e-007	1	K.ELEQATDSFNSANIIGSSSLSTVYK.G

2. <u>Human_UbNoLys</u>   Mass: 8756   Score: 244   Queries matched: 8   emPAI: 5.74
    Human_UbNoLys
    ☐ Check to include this hit in error tolerant search or archive report

	Query	Observed	Mr(expt)	Mr(calc)	Delta	Miss	Score	Expect	Rank	Peptide
☑	175	520.25	1038.49	1038.51	-0.02	0	(31)	0.00085	1	R.EGIPPDQQR.L
☑	176	520.26	1038.51	1038.51	-0.00	0	32	0.00068	1	R.EGIPPDQQR.L
☑	186	534.32	1066.63	1066.61	0.01	0	44	3.6e-005	1	R.ESTLHLVLR.L
☑	198	1109.50	1108.49	1108.55	-0.06	0	(10)	0.11	1	R.TLSDYNIQR.E
☑	200	555.29	1108.57	1108.55	0.01	0	48	1.5e-005	1	R.TLSDYNIQR.E
☑	343	908.47	1814.93	1814.93	-0.00	0	65	2.9e-007	1	R.TITLEVEPSDTIENVR.A
☑	344	606.00	1814.98	1814.93	0.05	0	(43)	5.5e-005	1	R.TITLEVEPSDTIENVR.A
☑	345	908.50	1814.99	1814.93	0.06	0	(59)	1.2e-006	1	R.TITLEVEPSDTIENVR.A

Suppl. table 2   **Sequencing primer used to validate *fli1* SNPs and Indels**

#	Forward	Reverse	2nd reverse
indel_01	GGTAACACAGACGCGTCCCCG	GACTTGAGGCCGACGCGGAG	
indel_02	ACGGTGCGATAACGGAGGCG	GCTCAGTACCAGTGTACGAATTCCC	
indel_03	GGTCTCAGTTGCTGCCGTTGGT	ACGTCTTGGAAGATAAAGCGTGGT	AAGGCGTGGACGGGGTCAGG
indel_04	TCCGGCGGAATGGAGTCCGT	ACGGGATGTACTCTGTATGCGTGC	CGGTTGAGCTGACAAAGGTTTCGG
indel_05	GCCTGAGTTGCCAAAGATCCCGG	AGCTGGGCCTTCTCTTCGCT	
indel_06	GGTACACGACGCTGAAGCCC	CCGGAGACGAAGAAGACCGGTGA	CTGGCGTTCCTGGTGCGGTT
indel_07	GCATCCCTTTTAACTCCATCCGCGA	TTCGCGCTGCAACGTTCCCC	
indel_08	CATACGGGGTGGGTCAGGGC	AGTGAAGTGGTTATGCCACAGCCAA	
indel_09	CGATTTGGTTGAGAGGCTCGT	TCTGATGGTTGCTTCTGATATACCA	
indel_10	AGTCTATGCAGATCGTGGCGCC	TTCCCTCTCAGCGATCCACTTTCCA	GGGCGAGAACCCTTCATTCACGG
snp_01	CTCAAGTTTGTCGGCTACTCCGAG	CGCTTCTATTCAGGGTTCCTTGGG	
snp_02	CCGTCGTTTCGTAACCGCGC	TCTGAGACGGGTTTAGGGATCTCAA	
snp_03,07	ACGAGTCGTAACCCGGTCTGGG	ACACAGCATCTCCCTCACAAGCA	
snp_05,06,08,11	TCCTTGAGCTCCAAGAAACGTTGTT	CCACGGCATCACAAGGTTCTCTAAC	
snp_09	ACTGGTCAACTGTGGGGCAGGT	TCCCAACGCCTTTGGAAATGGCA	
snp_10	TGGAATCGGGCAACGAGGCG	TGGAAGATGGAAGCCAAAACTGGC	
snp_12	TGACGTTAGCTAGGTCCGAGGCT	ACCAAGTTGCAAGTCCAACCACA	
snp_13,18	CGCGGGGTCAATGAGAGTGA	GCCACACTGAACGCAGGCC	
snp_14,15	ACCTTCTCATAGCTACTTCCCAGGC	TTTCCATCCTCTCTCGGATCGCT	
snp_16	TTGGGGCTTGTGAGGGTGAACC	TGTCTGAACGTGTGAGCATGAGTT	
snp_17	AGCTCCCCGCCCCCACAATA	TGGTGGTGGGGGAGACTTGTAGT	
snp_19	ACTGAAGGTGTAAGAGCGGCTCG	CGCGCACAATCACAAACAAACGC	
snp_20	CAACACCCCTTGTTCTTGTTGCAGT	TGGCGTCTGAGGATGTGGAGC	
snp_21	TGTGAAGCTTTGCACACATCCA	ATCACCCACATTATAACAGTGCCT	
snp_22	TCTGGCAAGAAAGATGAGGTCCAGT	TGGAACAGCTCAAGGTCTCGCG	
snp_23,25	CGTGGCTTCAATGTAGACCCAGAC	CTTCTTCGACTGAGCGGCGGC	
snp_24	TGGGAAACGAATTCGGACATCCAGG	ACTCTGCCTTGCGATCGAGCC	
snp_26	ACCCCGAGTCCGATGTTGTTACT	TGTACTGTGCCATGGTGCCTG	
snp_29	TGTGAACACGTAGAATCTGGTTAGG	GCTCCACACTCTTCAGGGAAGA	
snp_30	ATACCTCCGCCGCTGGGCTC	AGACCGGACATGACATCAGGAGAG	
snp_31	GGAAGACTGTATGCGTCGTCCA	TGTCGCATCGCCGCGAATCT	
snp_32	CCACGTTCTCTTTTTCTCGCGT	AACTGCAGCGGTTACTTTTACCATT	
snp_33	TCGTAGTAAACGTGAAAAGCCCTTT	AGATGAACAGCTCCGCGACCA	

APPENDIX B – FIGURE AND TABLE LISTS

List of figures

List of tables

List of supplement figures

List of supplement tables

ACKNOWLEDGEMENTS

ERKLÄRUNG

„Ich versichere, dass ich die von mir vorgelegte Dissertation selbstständig angefertigt, die benutzten Quellen und Hilfsmittel vollständig angegeben und die Stellen der Arbeit – einschließlich Tabellen, Karten und Abbildungen –, die anderen Werken im Wortlaut oder dem Sinn nach entnommen sind, in jedem Einzelfall als Entlehnung kenntlich gemacht habe; dass diese Dissertation noch keiner anderen Fakultät oder Universität zur Prüfung vorgelegen hat; dass sie – abgesehen von den auf Seite IX angegebenen Teilpublikationen – noch nicht veröffentlicht worden ist sowie, dass ich eine solche Veröffentlichung vor Abschluss des Promotionsverfahrens nicht vornehmen werde. Die Bestimmungen dieser Promotionsordnung sind mir bekannt. Die von mir vorgelegte Dissertation ist von Prof. Dr. Paul Schulze-Lefert betreut worden.“

Köln, im September 2011 \underline{\hspace{4cm}}

Thomas Spallek

LEBENSLAUF

Angaben zur Person

Name:	Thomas Spallek
Anschrift:	Heckenfeldstraße 4 76726 Germersheim
Telefon:	07274- 8334
Geburtsdatum:	07. Juli 1982
Geburtsort:	Germersheim
Staatsangehörigkeit:	Deutsch
Familienstand:	Ledig

Ausbildung

Seit 03/2008	**Promotionsstudium** an der Universität zu Köln am Max-Planck-Institut für Züchtungsforschung, unter der Leitung von Prof. Dr. Paul Schulze-Lefert;
07/2007 – 03/2008	**Diplomarbeit** am Lehrstuhl für Pflanzenphysiologie der Universität Konstanz, unter der Leitung von Prof. Dr. Iwona Adamska und dem Max-Planck-Institut für Züchtungsforschung, unter der Leitung von Prof. Dr. Paul Schulze-Lefert zum Thema "Posttranslational Modification of Arabidopsis Pattern Recognition Receptors"
10/2002 – 03/2008	**Diplom-Studium Biologie** an der Universität Konstanz, Deutschland Abschluss: sehr gut (1.35)
03/2002	**Abitur** am Goethe Gymnasium Germersheim, Deutschland Abschluss: sehr gut (2.1)
08/1993- 03/2002	**Goethe Gymnasium** Germersheim, Deutschland

Köln, im September 2011

Thomas Spallek